

## Jury Member Report – Doctor of Philosophy thesis.

**Name of Candidate:** Timur Bulatov

**PhD Program:** Petroleum Engineering

**Title of Thesis:** Lithological and Geochemical Study of Type I Kerogen in the Bazhenov Formation in Application to Exploration and Production of Hydrocarbons

**Supervisor:** Professor Dr. Mikhail Spasennykh

**Name of the Reviewer:** Professor Nikolai Pedentchouk

I confirm the absence of any conflict of interest

**Date:** 20-10-2022

*The purpose of this report is to obtain an independent review from the members of PhD defense Jury before the thesis defense. The members of PhD defense Jury are asked to submit signed copy of the report at least 30 days prior the thesis defense. The Reviewers are asked to bring a copy of the completed report to the thesis defense and to discuss the contents of each report with each other before the thesis defense.*

*If the reviewers have any queries about the thesis which they wish to raise in advance, please contact the Chair of the Jury.*

### Reviewer's Report

Reviewers report should contain the following items:

- Brief evaluation of the thesis quality and overall structure of the dissertation.
- The relevance of the topic of dissertation work to its actual content
- The relevance of the methods used in the dissertation
- The scientific significance of the results obtained and their compliance with the international level and current state of the art
- The relevance of the obtained results to applications (if applicable)
- The quality of publications

The summary of issues to be addressed before/during the thesis defense

The PhD thesis titled "Lithological and Geochemical Study of Type I Kerogen in the Bazhenov Formation in Application to Exploration and Production of Hydrocarbons" by Timur Bulatov is a very well-written document that contains high-quality data with significant implications in the area of exploration and development of conventional and unconventional hydrocarbon resources in the Russian Federation.

The thesis provides a detailed literature review, gives a clear justification for studying type I kerogen deposits in the Bazhenov Formation as one of the key targets for potentially improving the quality and quantity of hydrocarbons extracted from the West Siberian petroleum basin. The research methods are well chosen. The author provides a thorough analysis of the results from multiple core samples used in this study.

As part of his PhD program, the candidate was involved as an author and co-author in a number of high-quality publications in Q1 and Q2 international journals. The publications are directly relevant to the PhD thesis under consideration. Additionally, there is an impressive list of conference national and international presentations.

As mentioned above, the thesis is well written and well structured. However, there are a number of mostly minor comments and suggestions that I would like to be addressed in the final version of the thesis. Please refer to the original thesis with my comments/suggestions.

I found the section 5.10 "Depositional environments and origin" discussing possible mechanisms for the origin of type I kerogen in the Bazhenov Formation particularly interesting. However, there was not much of a discussion comparing the mechanisms proposed for the Bazhenov Formation with those that were possibly offered in the previously published literature to explain the origin of type I kerogen deposits in the other sedimentary basins, i.e., in the Section 2.3 "Deposits containing type I kerogen". I suggest adding a paragraph or two at the end of Section 5.10 to cover this point.

Overall, I found the thesis to be of high quality, well written and well presented. The candidate should be given the opportunity to defend his thesis as scheduled.

#### **Provisional Recommendation**

*I recommend that the candidate should defend the thesis by means of a formal thesis defense*

*I recommend that the candidate should defend the thesis by means of a formal thesis defense only after appropriate changes would be introduced in candidate's thesis according to the recommendations of the present report*

*The thesis is not acceptable, and I recommend that the candidate be exempt from the formal thesis defense*

Skolkovo Institute of Science and Technology

LITHOLOGICAL AND GEOCHEMICAL STUDY OF TYPE I KEROGEN IN THE  
BAZHENOV FORMATION IN APPLICATION TO EXPLORATION AND PRODUCTION  
OF HYDROCARBONS

*Doctoral Thesis*

by

TIMUR BULATOV

DOCTORAL PROGRAM IN PETROLEUM ENGINEERING

Supervisor  
Professor Dr. Mikhail Spasennykh

Co-supervisor  
Dr. Elena Kozlova

Moscow - 2022

© Timur Bulatov 2022

I hereby declare that the work presented in this thesis was carried out by myself at Skolkovo Institute of Science and Technology, Moscow, except where due acknowledgment is made and has not been submitted for any other degree.

Timur Bulatov

Professor Dr. Mikhail Spasennykh

Dr. Elena Kozlova

## ABSTRACT

Most of the world's petroleum comes from fossilized organic matter (marine organisms or terrestrial plants) deposited under anoxic conditions. Petroleum generation occurs in sedimentary basins due to the thermal alteration of organic geopolymer – kerogen. Traditionally there are three types of kerogen. From type I and type II kerogens predominantly liquid hydrocarbons are formed. Type III kerogen generates gaseous hydrocarbons. The majority of petroleum source rocks for oil fields. The source of hydrocarbons for the majority of oil fields is type II kerogen (mixed terrestrial and marine source material). However, type I kerogen (sapropelic organic matter) has the best petroleum generation potential due to the most hydrogen-rich organic matter. The majority of sedimentary rocks containing type I kerogen were formed during lacustrine and marine deposition with a significant accumulation of algal material that had undergone extensive bacterial reworking in oxygen-poor conditions. Despite the fact that oil-source deposits containing type I kerogen are rarely found, they are of interest not only in terms of hydrocarbon exploration but also in order to reconstruct the depositional environment, the processes of diagenesis and catagenesis of sedimentary strata, to solve the problems of rock stratification, and to assess their hydrocarbon generation potential.

The Upper Jurassic–Lower Cretaceous Bazhenov Formation is the most important unconventional reservoir in Western Siberia and produces hydrocarbons in many fields. The Bazhenov Formation organic-rich rocks contain oil-prone type II kerogen deposited predominantly in marine anoxic environments. However, questions still remain about the presence of other kerogen types in the Bazhenov Formation. The hydrocarbon generation potential of the Bazhenov organic matter is very high. The admixture of type I kerogen in the Bazhenov organic matter has been mentioned previously, but a detailed characterization has never been presented. We were the first to discover and study in detail the thin Bazhenov Formation layers containing pure type I kerogen. The study began with the problem of identifying luminescent marker layers in the upper part of the Bazhenov Formation, which were originally identified as "tuff interlayers".

In this study, the luminescent layers containing a significant amount of alginite in the Bazhenov Formation named “the alginite-rich layers”, were identified in several wells drilled in West Siberian Petroleum Basin. Lithological and geochemical methods, including thin section petrography, organic petrography, Rock-Eval pyrolysis, kinetics, elemental analysis, GC-GC-MS, isotope analysis and others, were used to determine distinctive features of these layers and to evaluate their impact on the total petroleum generation potential of the Bazhenov Formation.

Artificial maturation of the alginite-rich layer and host rock reveals different maturation pathways for type I and type II kerogens. Extraordinarily high  $\delta^{15}\text{N}_{\text{tot}}$  and low  $\delta^{13}\text{C}_{\text{org}}$  values prove the unusual origin of organic matter. Due to widespread distribution over the central part of

Western Siberia and isochronous behavior, luminescent alginite-rich layers can be good regional stratigraphic markers of the Bazhenov Formation. The intensity and color of luminescence of the alginite-rich layers can be used as a thermal maturity indicator providing a Ro equivalent up to the peak of the oil window (within PC3-MC1-2 stage). These findings further our understanding of depositional environments and have basin modeling interest.

## PUBLICATIONS

### *Peer-Reviewed Articles*

1. **Bulatov T.**, Kozlova, Pronina N., Korobova I., Leushina E., Voropaev A., Panchenko I., Morozov N., Spasennykh M. (2022) Type I kerogen in the Bazhenov Formation rocks of the West Siberian Petroleum Basin, *Moscow University Geology Bulletin*, Vol. 77, No. 1, P. 114-123. DOI: 10.3103/S0145875222010033.
2. **Bulatov T.**, Kozlova E., Leushina E., Panchenko I., Pronina N., Voropaev A., Morozov N., Spasennykh M. (2021) Alginite-rich layers in the Bazhenov deposits of Western Siberia, *Geosciences*, Vol. 11, No. 6. DOI: 10.3390/geosciences11060252.
3. Leushina E., **Bulatov T.**, Kozlova E., Panchenko I.; Voropaev A.; Karamov T., Yermakov Y., Bogdanovich N., Spasennykh M. (2021) Upper Jurassic–Lower Cretaceous source rocks in the North of Western Siberia: Comprehensive geochemical characterization and reconstruction of paleo-sedimentation conditions, *Geosciences*, Vol. 11, No. 8. DOI: 10.3390/geosciences11080320.
4. Spasennykh M., Maglevannaia P., Kozlova E., **Bulatov T.**, Leushina E., Morozov N. (2021) Geochemical trends reflecting hydrocarbon generation, migration and accumulation in unconventional reservoirs based on pyrolysis data (on the example of the Bazhenov Formation), *Geosciences*, Vol. 11, No. 8. DOI: 10.3390/geosciences11080307.

### *Side Topic Articles*

1. Vtorushina E., **Bulatov T.**, Kozlova E., Kul'kov M. (2022) Pyrolysis criteria for assessing thermal maturity of organic matter in the Bazhenov Formation, *Russian oil and gas geology*, No. 4, P. 45-55. DOI: 10.31087/0016-7894-2022-4-53-63. (In Russian)
2. Vtorushina E., **Bulatov T.**, Kul'kov M., Povzhik P., Eroshenko A., Tsygankov A. (2020) Geochemistry of organic matter in between-the-salt deposits: northern block of Pripyatsky Petroleum Basin, *Russian oil and gas geology*, No. 5, P. 83-94. DOI: 10.31087/0016-7894-2020-5-83-94. (In Russian)
3. Gutman I., Potemkin G., Baturin A., Maslyanko M., Kozlova E., Spasennykh M., **Bulatov T.** (2019) Study of the West Siberian Bazhenov formation at multiple levels according to pyrolysis data as the basis for the unbiased assessment of petroleum potential. *Nedropolzovanie XXI vek*, 3. (In Russian)

### *Extended Abstracts in Conference Proceedings*

1. Kozlova E., **Bulatov T.**, Leushina E., Matseva A., Bazhanova A., Ermakov Y., Gutman I., Bondina A., Kochikyants V., Mollaev Z., Spasennykh M. Geochemical model of an

- unconventional reservoir in the Paleogene deposits of Ciscaucasia. *In Proceedings of the Geomodel 2022: 24st Conference on Oil and Gas Geological Exploration and Development*, Gelendzhik, Russia, 5-8 September 2022. (In Russian)
2. Vtorushina E., Kozlova E., **Bulatov T.**, Vtorushin M. Evaluation of organic matter catagenesis in the Bazhenov Formation based on triangular diagram of pyrolytic parameters. *In Proceedings of the Geomodel 2022: 24st Conference on Oil and Gas Geological Exploration and Development*, Gelendzhik, Russia, 5-8 September 2022. (In Russian)
  3. Ermakov Y., Bazhanova A., Maltseva A., Leushina E., Kozlova E., **Bulatov T.**, Spasennykh M. Isotope-geochemical characteristics of organic matter in the Paleogene kerogen-rich deposits of Ciscaucasia. *In Proceedings of the Practice GeoChemistry 2022*, Kazan, Russia, 4-5 August 2022. (In Russian)
  4. Kozlova E., **Bulatov T.**, Leushina E., Spasennykh M. Unconventional reservoirs in kerogen-rich deposits. Modified OM study methods and terminology. *In Proceedings of the 6th Sevastopol International Scientific and Practical Conference*, Sevastopol, Crimea, 6-8 June 2022.
  5. Kozlova E., **Bulatov T.**, Leushina E., Spasennykh M. Improved technique of programmed temperature pyrolysis for unconventional reservoir rocks and criteria for oil saturation. *In Proceedings of the 2nd Russian Scientific Conference with International Participation "Advances in Organic Geochemistry"*, Novosibirsk, Russia, 5-6 April 2022. DOI 10.25205/978-5-4437-1312-0-128-131. (In Russian)
  6. Manasyan A., Skachek K., Papukhin S., Saakyan M., Potemkin G., Subbotina I., Rakhimova E., Biktagirov V., Gaponenko E., Mett D., Belyaev M., Spasennykh M., Kozlova E., **Bulatov T.** 2022. Volgo-Ural petroleum province. *In: Gutman I. (ed.). Correlation of well sections of complex petroleum objects and geological interpretation of results*. ESOEN, p. 71-113. (In Russian)
  7. Kochikyants V., Molaev Z., Bidilo I., Shpurov I., Pisarnitskiy A., Kolova A., Bondina A., Spasennykh M., Kozlova E., **Bulatov T.** 2022. Paleogene deposits of East Ciscaucasia. *In: Gutman I. (ed.). Correlation of well sections of complex petroleum objects and geological interpretation of results*. ESOEN, p. 114-144. (In Russian)
  8. Arefiev S., Semyanov A., Skachek K., Saakyan M., Aaturin A., Kachina E., Kuzhetsova G., Mitina A., Obgolts A., Fedoseeva E., Shevchenko D., Vologods D., Shalupina A., Spasennykh M., Kozlova E., **Bulatov T.** 2022. West Siberian petroleum province. *In: Gutman I. (ed.). Correlation of well sections of complex petroleum objects and geological interpretation of results*. ESOEN, p. 145-271. (In Russian)

9. **Bulatov T.**, Kozlova E., Leushina E., Vtorushina E., Morozov N., Spasennykh M. Study of type I kerogen: Origin, characterization and hydrocarbon generation. *In Proceedings of the XXV Scientific and Practical Conference ““Ways of Realization of Oil and Gas Potential of West Siberia”*, Khanty- Mansiysk, Russia, 23-26 November 2021. (In Russian)
10. Karamov T., Leushina E., Kozlova E., **Bulatov T.**, Spasennykh M. Development of organic matter porosity during thermal maturation: study on the example of the Bazhenov Formation source rocks. *In Proceedings of the 30th International Meeting on Organic Geochemistry (IMOG)*, Montpellier, France, 12–17 September 2021. DOI: 10.3997/2214-4609.202134225.
11. **Bulatov T.**, Kozlova E., Leushina E., Panchenko I., Voropaev A., Pronina N., Morozov N., Kostina Y., Spasennykh M. Characterization of the luminescent layers of the Bazhenov Formation. *In Proceedings of the 35th IAS Meeting of Sedimentology*, Prague, Czech Republic, 21–25 June 2021.
12. **Bulatov T.**, Kozlova E., Spasennykh M. Source rock characteristics of the Eocene-Oligocene deposits of the East Caucasian petroleum basin: assessment of the generation potential and identification of reservoir horizons. *In Proceedings of the 6th Sevastopol International Scientific and Practical Conference*, Sevastopol, Crimea, 6-8 June 2021.
13. Kozlova E., **Bulatov T.**, Leushina E., Spasennykh M., Thi S., Lubnina N., Krylov O., Bychkov A. Oil fields and mud volcanoes of the Kerch Peninsula: From antiquity to the present day. *In Proceedings of the 6th Sevastopol International Scientific and Practical Conference*, Sevastopol, Crimea, 6-8 June 2021.
14. Karamov T., Leushina E., Kozlova E., **Bulatov T.**, Spasennykh M. Void space formation in the Bazhenov Formation kerogen during isothermal treatment in an open system. *In Proceedings of the EAGE/SPE Workshop on Shale Science*, Moscow, Russia, 5–6 April 2021. DOI: 10.3997/2214-4609.202151024. (In Russian)
15. Kozlova E., Leushina E., **Bulatov T.**, Thi S., Bogdanovich N., Spasennykh M., Vtorushina E., Gutman I. Terms and categories in the study of the Bazhenov Formation organic matter. *In Proceedings of the XXIV Scientific and Practical Conference ““Ways of Realization of Oil and Gas Potential of West Siberia”*, Khanty- Mansiysk, Russia, 26 November 2020. (In Russian)
16. Kozlova E., Bogdanovich N., Stenin V., Leushina E., Karamov T., **Bulatov T.**, Spasennykh M., Malyavin S. Estimation of the residual petroleum potential and bitumoid composition of subsalt deposits of the Astrakhan Arch. *In Proceedings of the 3d international conference on Geology of the Caspian Sea and Adjacent Areas*, Baku, Azerbaijan, 16-18 October 2019. DOI: 10.3997/2214-4609.201952019. (In Russian)

17. **Bulatov T.**, Kozlova E., Spasennykh M., Leushina E. Geochemical characteristics of sapropelites in the Bazhenov Formation. *In Proceedings of the Geomodel 2019: 21st Conference on Oil and Gas Geological Exploration and Development*, Gelendzhik, Russia, 9-13 September 2019. DOI: 10.3997/2214-4609.201950156. (In Russian)
18. Kozlova E., **Bulatov T.**, Leushina E., Spasennykh M., Gutman I., Potemkin G., Baturin A. Estimation of the organic matter maturity level in the Bazhenov Formation deposits. *In Proceedings of the Geomodel 2019: 21st Conference on Oil and Gas Geological Exploration and Development*, Gelendzhik, Russia, 9-13 September 2019. DOI: 10.3997/2214-4609.201950155. (In Russian)
19. Vtorushina E., Vtorushin M., **Bulatov T.** Using pyrolysis for the reservoir properties assessment of low-permeability carbonate formation. *In Proceedings of the Geomodel 2019: 21st Conference on Oil and Gas Geological Exploration and Development*, Gelendzhik, Russia, 9-13 September 2019. DOI: 10.3997/2214-4609.201950121. (In Russian)
20. Gutman I., Potemkin G., Baturin A., Maslyanko M., Kozlova E., Spasennykh M., **Bulatov T.** Pyrolysis studies as the basis for an objective assessment of the petroleum potential for the Bazhenov Formation (West Siberia). *In Proceedings of the Geomodel 2019: 21st Conference on Oil and Gas Geological Exploration and Development*, Gelendzhik, Russia, 9-13 September 2019. DOI: 10.3997/2214-4609.201950076. (In Russian)
21. **Bulatov T.**, Kozlova E., Leushina E., Pronina N., Panchenko I., Kostina Y., Spasennykh M. Specific layers containing highly oil-prone organic matter in the Bazhenov Formation. *In Proceedings of the 29th International Meeting on Organic Geochemistry (IMOG)*, Gothenburg, Sweden, 1-6 September 2019. DOI: 10.3997/2214-4609.201902828.
22. Kozlova E., Spasennykh M., **Bulatov T.**, Leushina E., Bogdanovich N., Voropaev A. Characteristics of the Bazhenov Horizon from peripheral area based on geochemical study of the organic matter. *In Proceedings of the EAGE/SPE Workshop on Shale Science*, Moscow, Russia, 1-5 April 2019. DOI: 10.3997/2214-4609.201900481. (In Russian)

## ACKNOWLEDGMENTS

I first wish to sincerely thank my supervisor, Professor Dr. Mikhail Spasennykh, through whom I received tireless support and trust during the course of this research. I would like to extend my deep appreciation and gratitude to my co-supervisor Dr. Elena Kozlova, whose positive energy, enthusiasm and continuous support and advice have been invaluable assets in this project and a precious source of motivation for me.

I am also very thankful to Dr. Evgeniya Leushina for help with GC-GC-MS analysis and compositional kinetic analysis. I thank to Dr. Natalia Pronina for the organic petrography analysis. I would like to express my thanks to Dr. Andrey Voropaev and Dr. Anna Maltseva for the preparation, measurement and discussion of isotope composition data. Special thanks to Ivan Panchenko for his stratigraphic data, the great company and valuable discussions. I thank Dr. Yulia Kostina for carrying out FTIR spectroscopy analysis and Dr. Tagir Karamov for electron microscopy analysis.

I also extend my acknowledgment to Nikita Morozov (LLC Gazprom-Neft), Professor Dr. Igor Gutman (IPNE) for rock samples, Dr. Ella Vtorushina and Mikhail Kul'kov (V.I. Shpilman Research and Analytical Centre for Rational Use of the Subsoil) for CSIA measurements.

This research was supported by the Ministry of Science and Higher Education of the Russian Federation under agreement No. 075-10-2020-119 within the framework of the development program for a world-class research center. This financial support enabled me to undertake my PhD research and is highly appreciated.

Finally, I would like to express my sincere appreciation to my family for their kind wishes, unconditional support and love.

## TABLE OF CONTENT

|   |    |
|---|----|
| ABSTRACT .....  | 3  |
| PUBLICATIONS .....  | 5  |
| ACKNOWLEDGMENTS .....   | 9  |
| TABLE OF CONTENT .....  | 10 |
| ABBREVIATIONS AND SYMBOLS.....  | 13 |
| LIST OF FIGURES .....   | 14 |
| LIST OF TABLES.....   | 16 |
| CHAPTER 1. INTRODUCTION .....   | 17 |
| 1.1 General overview.....   | 17 |
| 1.2 Aims and objectives .....   | 18 |
| 1.3 Structure of the Thesis.....  | 19 |
| CHAPTER 2. TYPE I KEROGEN: ORIGIN, CHARACTERIZATION AND<br>HYDROCARBON GENERATION ..... | 20 |
| 2.1 Source of organic matter.....   | 20 |
| 2.2 General classification of kerogen types.....  | 22 |
| 2.3 Deposits containing type I kerogen .....  | 24 |
| 2.3.1 Green River Formation.....  | 24 |
| 2.3.2 Kukersite.....  | 27 |
| 2.3.3 Stellarites .....   | 28 |
| 2.3.4 Lacustrine deposits of East China .....   | 28 |
| 2.3.5 Pyropissite .....   | 30 |
| 2.3.6 Australian tasmanites.....  | 31 |
| 2.3.7 Catalan oil shales .....  | 31 |
| 2.4 Summary.....  | 32 |
| CHAPTER 3. MATERIALS AND METHODS .....  | 34 |
| 3.1 Samples.....  | 34 |
| 3.2 Analysis .....  | 35 |
| 3.2.1 Thin section petrography.....   | 35 |
| 3.2.2 Organic petrography .....   | 35 |

|        |  |    |
|--------|--|----|
| 3.2.3  | Scanning electron microscopy .....                 | 35 |
| 3.2.4  | X-Ray diffraction.....                             | 35 |
| 3.2.5  | X-Ray fluorescence .....                           | 36 |
| 3.2.6  | Inductively coupled plasma mass spectrometry ..... | 36 |
| 3.2.7  | Bitumen extraction .....                           | 36 |
| 3.2.8  | Kerogen isolation.....                             | 36 |
| 3.2.9  | CHNS/O elemental analysis .....                    | 36 |
| 3.2.10 | Rock-Eval pyrolysis .....                          | 37 |
| 3.2.11 | Kinetic analysis .....                             | 39 |
| 3.2.12 | Fourier transform infrared spectroscopy .....      | 39 |
| 3.2.13 | GC×GC-TOFMS and Py-GC×GC-TOFMS.....                | 40 |
| 3.2.14 | Stable isotope composition.....                    | 40 |
| 3.2.15 | Compound-specific isotope analysis .....           | 40 |
| 3.3    | Accepted classifications .....                     | 43 |
| 3.3.1  | Tectonic units .....                               | 43 |
| 3.3.2  | Thermal maturity of organic matter .....           | 43 |
| 3.3.3  | Stratification of the Bazhenov sequence .....      | 44 |

**CHAPTER 4. LITHOLOGICAL CHARACTERIZATION OF THE ALGINITE-RICH LAYERS 45**

|     |                                    |    |
|-----|------------------------------------|----|
| 4.1 | Visual description.....            | 45 |
| 4.2 | Thin section petrography .....     | 47 |
| 4.3 | Mineralogy .....                   | 48 |
| 4.4 | Chemical composition .....         | 49 |
| 4.5 | Morphological characteristic ..... | 53 |
| 4.6 | Stratigraphic occurrence .....     | 54 |
| 4.7 | Summary.....                       | 56 |

**CHAPTER 5. ORGANIC GEOCHEMISTRY, PETROGRAPHY, ISOTOPE CHARACTERIZATION AND DEPOSITION ENVIRONMENT OF THE ALGINITE-RICH LAYERS 57**

|     |  |    |
|-----|--|----|
| 5.1 | Source rock richness.....                  | 57 |
| 5.2 | Type of kerogen and thermal maturity ..... | 61 |
| 5.3 | Maceral composition .....                  | 64 |

|      |   |    |
|------|---|----|
| 5.4  | Structural characteristics of kerogen .....   | 65 |
| 5.5  | Bulk kinetics .....   | 66 |
| 5.6  | Biomarker analysis .....  | 67 |
| 5.7  | Pyrolysis products .....  | 70 |
| 5.8  | C, N and S isotope composition of whole rock samples .....  | 72 |
| 5.9  | CSIA of individual n-alkanes .....  | 74 |
| 5.10 | Depositional environment and origin .....   | 76 |
| 5.11 | Summary.....  | 78 |
|      |   |    |
|      | CHAPTER 6. MODELING OF THERMAL MATURATION AND HYDROCARBON<br>GENERATION OF THE TYPE I KEROGEN ..... | 79 |
| 6.1  | Artificial maturation in open system .....  | 79 |
| 6.2  | The amount of generated hydrocarbons .....  | 84 |
| 6.3  | Summary.....  | 85 |
|      |   |    |
|      | CONCLUSIONS .....   | 87 |
|      | REFERENCES .....  | 90 |

## ABBREVIATIONS AND SYMBOLS

- A – frequency factor,  $s^{-1}$
- CPI – carbon preference index
- E<sub>a</sub> – activation energy, kcal/mol
- GI – gammacerane index
- GOC – generative (pyrolyzable) organic carbon, wt. %
- HI – hydrogen index, mg HC/g TOC
- HC – hydrocarbons
- K<sub>goc</sub> – proportion of pyrolyzable organic carbon, %
- MC – mesocatagenesis
- NGOC – non-generative organic carbon, wt. %
- OEP – odd-even predominance index
- OI – oxygen index, mg CO<sub>2</sub>/g TOC
- OSI – oil saturation index, mg HC/g TOC
- PC – protocatagenesis
- REE – rare earth elements
- PI – production index
- Ph – phytane
- Pr – pristane
- S<sub>0</sub> – gaseous HC, mg HC/g rock
- S<sub>1</sub> – amount of free HCs volatilized at 300 °C, mg HC/g rock
- S<sub>2</sub> – HC generated from kerogen and heavy HC cracking between 300 and 650 °C, mg HC/g rock
- T<sub>max</sub> – temperature of the maximum generation of HCs during the cracking of kerogen, °C
- TOC – total organic carbon, wt. %
- UV – ultraviolet
- XRF – x-ray fluorescence
- XRD – x-ray diffraction
- δ<sup>13</sup>C – a measure of the ratio of stable isotopes <sup>13</sup>C/<sup>12</sup>C relative to the PDB standard, ‰
- δ<sup>15</sup>N – a measure of the ratio of stable isotopes <sup>15</sup>N/<sup>14</sup>N relative to the AIR, ‰
- δ<sup>34</sup>S – a measure of the ratio of stable isotopes <sup>34</sup>S/<sup>32</sup>S relative to the CDT standard, ‰

## LIST OF FIGURES

|   |    |
|---|----|
| Figure 1.1.1. Map of organic-rich shales in Russia, modified from (Kisilev, 2020).....  | 17 |
| Figure 2.2.1. A van Krevelen diagram showing main types of kerogen and their evolution pathways (Killops and Killops, 2005) .....   | 22 |
| Figure 2.2.2. Kerogen classification based on hydrogen and oxygen indices (a) and hydrogen index and $T_{max}$ (b) (Espitalié et al., 1977; Espitalié et al., 1984) .....   | 23 |
| Figure 2.3.1. The cross plot of HI vs. $T_{max}$ (a) and H/C vs. O/C (b) for deposits containing type I kerogen (Espitalié et al., 1984) (based on own and published data) .....  | 25 |
| Figure 2.3.2. The $E_a$ distribution for type I kerogen from different deposits (based on own data) .....   | 26 |
| Figure 2.3.3. Gas chromatogram of kukersite extract from the Kohtla, Estonia (Burdelnaya et al., 2013).....   | 27 |
| Figure 2.3.4. Gas chromatogram of the oil shale extracts from the Qingshankou Formation (He et al., 2019).....  | 29 |
| Figure 2.3.5. Saturate gas chromatogram of the Shahejie source rock (Li et al., 2005) .....   | 30 |
| Figure 2.3.6. Gas chromatogram of the aliphatic fractions of tasmanite extracts from sample taken from Douglas River (Revill et al., 1994).....   | 31 |
| Figure 2.3.7. Total ion current trace of the flash pyrolysate (Curie temperature 610 °C) of the kerogen of the oil shale (Sinninghe et al., 1993).....  | 32 |
| Figure 3.1.1. Map of the Bazhenov Horizon showing the location of studied wells contained luminescent alginite layers (left) and stratigraphy of Mesozoic deposits of Western Siberia (right), modified from [Amon et al., 2010]..... | 34 |
| Figure 3.2.1. Example of HAWK pyrogram .....  | 37 |
| Figure 3.2.2. S2 peaks at different heating rates .....   | 39 |
| Figure 3.2.3. A simplified schematic of a GC-IRMS system for $\delta^{13}C$ measurements (Pedentchouk and Turich, 2018) .....   | 42 |
| Figure 3.2.2. A chromatogram showing an m/z 44, 45 and 46 trace corresponding to CO <sub>2</sub> produced from the combustion of individual n-alkanes .....   | 42 |
| Figure 3.3.1. Example of the Bazhenov Formation succession. ....  | 44 |
| Figure 4.1.1. Core layout showing typical appearance of the Bazhenov Formation organic-rich siliceous rocks with presence of the luminescent alginite-rich layers (marked in red) and luminescent tuffs (marked in light green) ..... | 45 |
| Figure 4.1.2. Photographs of the alginite-rich layers under white (a, c) and UV light (b, d) showing normal grading.....  | 46 |
| Figure 4.2.1. Typical thin section photomicrographs of the alginite-rich layers with and without analyzer.....  | 47 |
| Figure 4.2.2. Typical thin section photomicrographs of the host rocks with and without analyzer .....   | 48 |
| Figure 4.4.1. NASC-normalized REE (Taylor and McLennan, 1985) distribution pattern (a) and NASC-normalized trace element diagram (b) for the alginite-rich layers and host rocks .....  | 52 |
| Figure 4.4.2. Correlations between $\Sigma REE$ and TOC of the alginite-rich layers and host rocks....  | 53 |
| Figure 4.5.1. Back-scattered scanning electron micrographs showing organic and mineral grain morphology of the alginite-rich layers .....   | 54 |
| Figure 4.6.1. Correlation of the Bazhenov sequence with the luminescent alginite-rich layers. ...   | 55 |
| Figure 5.1.1. The S0+S1+S2 vs TOC plot (a) and TOC vs S2 plot (b) for the alginite-rich layers and host rocks .....   | 57 |
| Figure 5.1.2. Geochemical log of well S5. ....  | 60 |

|  |    |
|--|----|
| Figure 5.2.1. The HI to $T_{max}$ plot (a) and H/C to O/C plot (b) showing different type of kerogen for the alginite-rich layers and host rocks .....   | 61 |
| Figure 5.2.2. Detailed (layer-by-layer) Rock-Eval pyrolysis for core sample with interbedding of the alginite-rich layer and hosting organic-rich siliceous rock from well V-K 81.....                         | 62 |
| Figure 5.2.3. The location of wells with alginite-rich layers finds (blue stars), mapped on the map of the thermal maturity of the Bazhenov Formation (based on Rock-Eval pyrolysis data Table 3.3.1).....     | 63 |
| Figure 5.2.4. Color of the luminescent alginite-rich layers in the Bazhenov deposits of different thermal maturity (based on Rock-Eval pyrolysis data Table 3.3.1) .....                                       | 63 |
| Figure 5.3.1. Photomicrographs illustrating a typical maceral composition of the alginite-rich layers.....   | 64 |
| Figure 5.3.2. Photomicrographs illustrating a maceral composition of the host rock.....  | 65 |
| Figure 5.4.1. FTIR spectra of the alginite-rich layers and host rocks .....  | 65 |
| Figure 5.5.1. The distribution of Ea for kerogen of (a, c, e) the alginite-rich layers and (b, d, f) the host rocks.....   | 66 |
| Figure 5.6.1. Distribution pattern of n-alkanes for the alginite-rich layers and host rock .....   | 67 |
| Figure 5.6.2. A cross-plot diagram of (a) Pr/n-C <sub>17</sub> vs. Ph/n-C <sub>18</sub> ; (b) DBT/Phen vs. Pr/Ph for the studied samples and extracts of the Bazhenov rocks.....                               | 69 |
| Figure 5.6.3. Relationships between different thermal maturity parameters in the studied samples and extracts of the Bazhenov Formation rocks .....  | 70 |
| Figure 5.7.1. Two-dimensional total ion chromatograms (TIC) of kerogen cracking products (500°C) for the alginite-rich layers (a) and host rocks (b).....  | 71 |
| Figure 5.8.1. Plots of (a) $\delta^{13}C_{org-C_{org}}$ , (b) $\delta^{15}N_{tot-C_{org}/N_{tot}}$ , (c) $\delta^{34}S_{tot-C_{org}/N_{tot}}$ , and (d) $\delta^{34}S_{tot-S_{tot}}$ for studied samples ..... | 73 |
| Figure 5.8.2. Ranges of measured $\delta^{15}N$ values for a different shale samples .....   | 74 |
| Figure 5.9.1. Curves of n-alkane carbon isotopes .....   | 75 |
| Figure 5.10.1. Paleogeography of West Siberia in the Tithonian (Kontorovich et al., 2013).....   | 77 |
| Figure 6.1.1. The distribution of Ea for studied initial samples. ....   | 79 |
| Figure 6.1.2. Change in the ratio of GOC and NGOC during artificial maturation .....   | 80 |
| Figure 6.1.3. The HI- $T_{max}$ plot for the initial and matured samples .....   | 81 |
| Figure 6.1.4. The Ea distribution for matured samples in open system. ....   | 82 |
| Figure 6.1.5. The bulk and compositional kinetic spectra of the type I kerogen in the Bazhenov Formation .....   | 83 |

## LIST OF TABLES

|  |    |
|--|----|
| Table 2.1.1. General chemical composition of the major organic matter producers (Bazhenova, 2000; Tissot and Welte, 1984)..... | 20 |
| Table 2.4.1. Comparison of geochemical characteristics of deposits containing type I kerogen...33                              |    |
| Table 3.2.1. Values of pyrolysis parameters for the WT standard .....  | 38 |
| Table 3.3.1. Thermal maturity assessment based on Rock-Eval pyrolysis data.....  | 43 |
| Table 4.3.1. Mineralogical composition of the alginite-rich layers and host rocks .....  | 48 |
| Table 4.4.1. Major oxides composition of the alginite-rich layers and host rocks.....  | 49 |
| Table 4.4.2. Trace elements and REE concentration of the alginite-rich layers and host rocks ...                               | 50 |
| Table 5.1.1. Rock-Eval pyrolysis data for the alginite-rich layers and host rocks.....   | 58 |
| Table 5.6.1. Selected biomarker ratios and indices for extracts of the alginite-rich layers and....                            | 68 |
| Table 5.7.1. Distribution of HC classes from Pyro-GC×GC-TOF MS/FID for the alginite-rich layers and host rocks .....           | 71 |
| Table 5.8.1. Bulk C, N and S elemental and isotope composition for the alginite-rich layers and host rocks.....                | 72 |
| Table 5.9.1. Individual carbon isotopic compositions and standard deviation of n-alkanes for extracts and oil.....             | 75 |
| Table 6.1.1. Rock-Eval pyrolysis data for initial samples.....   | 79 |
| Table 6.1.2. Rock-Eval pyrolysis data for matured samples in open system .....   | 80 |
| Table 6.2.1. Estimation of the total mass of generated hydrocarbons.....   | 85 |

## CHAPTER 1. INTRODUCTION

### 1.1 General overview

Recent additions to global unconventional reserves have been discovered by the application of increasingly sophisticated petroleum exploration methods. The Bazhenov Formation of the West Siberian Petroleum Basin is one of the biggest unconventional reservoir (Figure 1.1.1). Petroleum geoscientists in their effort to locate commercial accumulations of hydrocarbons, now ask specific questions concerning source rocks of the Bazhenov Formation and their related crude oils. Major issues are the stratigraphic correlation of the Bazhenov sequence in the West Siberian Petroleum Basin, source rocks characteristics, their potential to generate hydrocarbons, distribution of the productive intervals and likely migration pathways of the expelled hydrocarbons. Moreover, knowledge of the type of kerogen provides insights on depositional environments and thermal history.

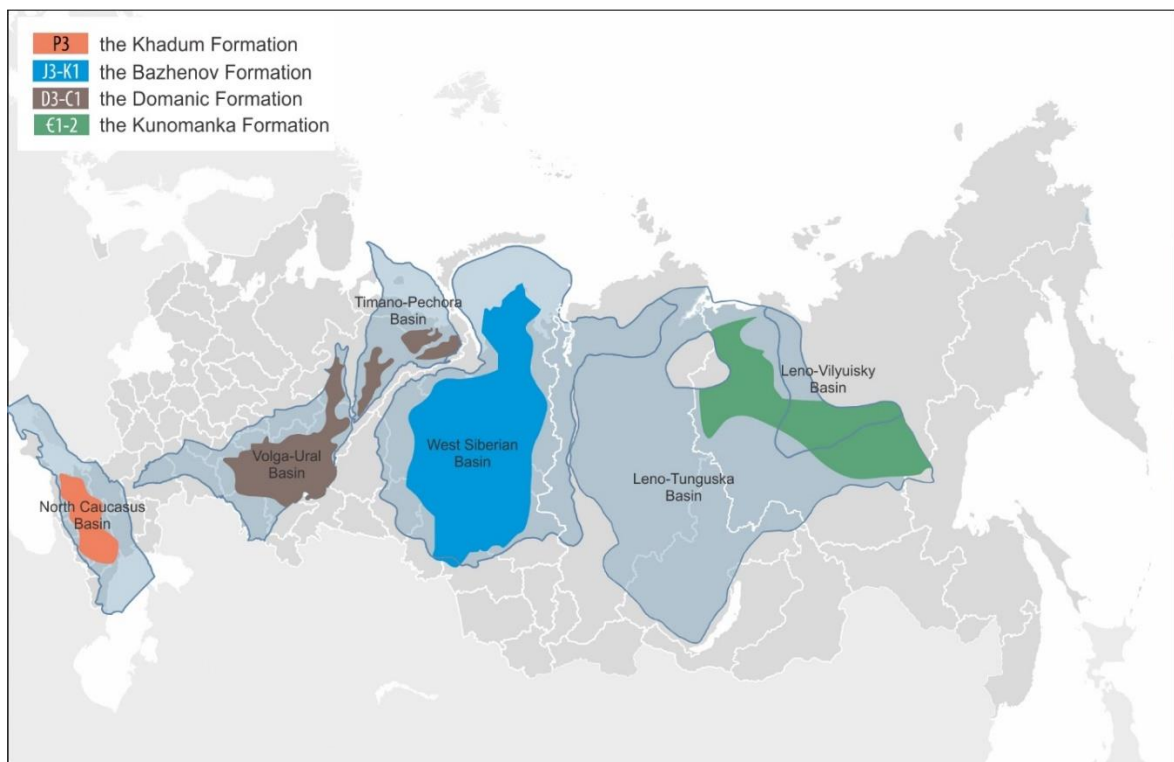


Figure 1.1.1. Map of organic-rich shales in Russia, modified from (Kisilev, 2020)

The West Siberian Petroleum Basin has a long research history and it is now the focus of a regional petroleum prospective assessment of the Upper Jurassic – Lower Cretaceous Bazhenov Formation. It is poised to become Russia's next major unconventional shale oil province. The oil discoveries of commercial productive unconventional reservoirs at the Salym area gave rise to the big interest of petroleum geoscientists in this unique object. However, visual lithological

homogeneity and wide regional distribution erroneously formed an idea of the overall productivity of the Bazhenov Formation. Despite the fact that the Bazhenov Formation almost everywhere has high generation potential, productivity is highly sporadic. In a more detailed study, the Bazhenov Formation is characterized by a various source rock characteristics, including content of organic matter, type of kerogen and thermal maturity.

Since the Bazhenov Formation is a promising unconventional reservoir for the Western Siberia, a detailed geochemical study of the composition of its organic matter is required. Particular attention must be paid to the type of kerogen, since organic matter with different generation kinetics could result in non-synchronous timing of onset of the earliest petroleum generation. Therefore, it is important to study the organic matter type, thermal maturity and depositional environmental.

Many previous works are devoted to the study of the types, composition, structure, and transformation processes of organic matter in the Bazhenov Formation, e.g., (Galimov, 1968; Goncharov, 1987; Kalmykov et al., 2019; Kontorovich et al., 1975; Lopatin and Emec, 1987). Kerogen of the Bazhenov Formation is traditionally characterized as type II. However, questions remain about the presence of other kerogen types in the Bazhenov Formation rocks. Admixture of type I kerogen in the Bazhenov deposits has been mentioned previously in recent studies, but a detailed characterization has never been presented (Goncharov et al., 2016; Kontorovich et al., 2019; Oksenoyd et al., 2017).

Most deposits containing type I kerogen were formed under conditions of significant accumulation of algal material that had undergone extensive bacterial reworking in a reducing environment (Peters et al., 2005; Tissot and Welte, 1984). Despite the fact that deposits containing type I kerogen are rarely found, they are of interest not only in terms of hydrocarbon exploration but also in order to reconstruct the depositional conditions.

## 1.2 Aims and objectives

The main aims are the detail study of rocks containing type I kerogen in the Bazhenov Formation sequence, the evaluation of the depositional environment and the potential application to the exploration and production of hydrocarbons.

To achieve the stated aim following objectives have been accomplished:

- To identify type I kerogen in the Bazhenov Formation (based on Rock-Eval pyrolysis and lithological study of more than 60 wells within the central part of the West Siberian Petroleum Basin).

- To analyze the distribution of deposits containing type I kerogen over the world. Special attention was paid to the geochemical characterization of organic matter and assessment of the main factors controlling their formation.
- To perform geochemical and lithological analysis of the alginite-rich layers, to confirm the predominance of type I kerogen.
- To reconstruct the paleoenvironmental conditions of the alginite-rich layers formation process.
- To assess the influence of type I kerogen on the total hydrocarbon generation potential of the Bazhenov Formation.

### 1.3 Structure of the Thesis

This thesis is divided into six chapters. Chapter 1 includes an introduction, the main aim and the objectives of the research. The literature review on type I kerogen of world-known deposits is presented in Chapter 2. This chapter introduces the geochemical characterization of organic matter and summarizes the main factors controlling the formation of organic-rich deposits. Chapter 3 shows the description of the samples, methods and techniques used in this research. The studied area and wells location are presented in this chapter, too. Chapter 4 surveys lithological characterization and an inorganic geochemistry of the alginite-rich layers. Chapters 5 concentrate on the organic geochemistry, maceral analysis and stable isotope composition of the studied layers. The obtained data are used to determine the origin of the layers and depositional environments. Artificial maturation experiments and a quantities assessment of generated hydrocarbons by type I kerogen are put in Chapter 6. Finally, after Chapter 6 the main conclusions and the significant findings of the Thesis are summarized and given recommendations for future work.

## CHAPTER 2. TYPE I KEROGEN: ORIGIN, CHARACTERIZATION AND HYDROCARBON GENERATION

### 2.1 Source of organic matter

The accumulation and decomposition of biomass in sea basins affect all processes of sedimentation and diagenesis and largely predetermine the chemical characteristics of petroleum source rocks. Therefore, the type of initial (or original) organic matter of the source rock, depositional environments and its thermal maturation determine the composition and properties of the generated hydrocarbons.

The chemical composition of all organisms can be divided into several groups of chemical constituents: lipids, proteins, carbohydrates and lignin, which is part of higher plants (Table 2.1.1). The active decomposition of organic matter in marine and lacustrine environments occurs in the surface sediment layer. The most resistant to degradation are lipids and lignin. Proteins and carbohydrates are broken down into amino acids and sugars. The resistance to decomposition increases in the series: proteins < carbohydrates < lignin < lipids. Lipids play a major role in the formation of kerogen and in the subsequent formation of petroleum.

There are four major source of original organic matter: phytoplankton, zooplankton, bacteria and higher plants.

Table 2.1.1. General chemical composition of the major organic matter producers (Bazhenova, 2000; Tissot and Welte, 1984)

| Producers     | Lipids, wt. % | Proteins, wt. % | Carbohydrates, wt. % | Lignin, wt. % |
|---------------|---------------|-----------------|----------------------|---------------|
| Green plants  | <5            | 5-10            | >50                  | >25           |
| Phytoplankton | 5-20          | 24-48           | 30-65                | —             |
| Zooplankton   | 10-22         | 65-75           | 5-20                 | —             |
| Bacteria      | 20            | 50-60           | 20                   | —             |
| Spores        | 50            | 8               | 42                   | —             |

*Phytoplankton.* The major producer of organic matter is phytoplankton. The amount of phytoplankton in the sea primarily depends on the amount of nutrients in the water. The main places of high productivity of phytoplankton are the areas of surface runoff and coastal upwelling regions. Also, nutrients can be brought by volcanic ash from volcanic eruptions and eolian material carried by air currents. The productivity of phytoplankton is also affected by the presence of sunlight, the depth of the thermocline and the zooplankton grazing (Drits et al., 2018; Romankevich, 1977).

Phytoplankton production started in the Precambrian and then has several maxima and lows during geological history. At the present time, the main primary producers in the ocean include

diatoms, green algae, coccolithophores and dinoflagellates. In many oil fields, hydrocarbons have marine organic matter source. In the formation of this organic matter, phytoplankton plays a huge role. Previous studies have shown that in extracts of phytoplankton and phytobenthos predominance n-C<sub>15</sub>, n-C<sub>17</sub> and n-C<sub>19</sub> alkanes (Tissot and Welte, 1984). A high concentration of regular steranes C<sub>27</sub> and relatively low C<sub>28</sub> and C<sub>29</sub> in extracts suggest the marine source of organic matter (Peters et al., 2005).

*Zooplankton* can be a significant source of organic matter for sediments (Killops and Killops, 2005). Zooplankton are heterotrophic organisms including zooflagellates, radiolarians and foraminifera. Zooplankton feeds primarily on phytoplankton and sometimes on other zooplankton. Therefore, zooplankton are mainly found in surface waters where the phytoplankton are abundant. Distribution of zooplankton are controlled by nutrient availability, salinity and temperature of the water. Zooplankton are capable of lipid storage (Lee et al., 2006; Najdek et al., 1994). The main stages of zooplankton production are associated with the appearance of graptolites during the Ordovician and Silurian periods, radiolarian in the Carboniferous and foraminifera in the Late Jurassic. Since zooplankton feeds on phytoplankton, there is some similarity in the molecular composition of their lipid fraction.

*Bacteria*. Most of the bacteria are heterotrophs. In relation to oxygen content, bacteria are divided into aerobic, which exists in the presence of oxygen, and anaerobic, which exists in the absence of free oxygen. The decomposition of organic remains in marine environments is primarily carried out by bacteria. Bacteria comprise <60 wt.% of proteins, 20 wt.% of lipids and 20 wt.% of carbohydrates (Table 2.1.1). The contribution of bacteria to the initial organic matter is undeniable. For bacterial organic matter typical n-alkane distribution from n-C<sub>15</sub> to n-C<sub>28</sub> with a maximum between n-C<sub>20</sub> and n-C<sub>25</sub> and with no marked odd/even preference (Gonzales-Vila, 1995). Hopanoids are ubiquitous in sediments and petroleum and are commonly used as indicators of depositional environment, thermal maturity and degree of biodegradation. Hopanes are derived from bacterial membrane lipids. Abundant gammacerane suggests a stratified water column, which generally arises in hypersaline conditions. The ratio of Ts (C<sub>27</sub> 18 $\alpha$ (H), 22,29,30-trisnorneohopane) and Tm (17 $\alpha$ (H), 22,29,30-trisnorneohopane) have been widely used as indicators of thermal maturity.

*Higher plants* are an important contributor to sedimentary organic matter. They are rich in carbohydrates and lignin, but depleted in lipids and proteins (Table 2.1.1). However, a high amount of lipids accumulate in such components of higher plants as leaves, pollen, spores, seeds and others. The growth and development of higher plants primarily depend on light, temperature, water, humidity and nutrition. Hydrocarbon biomarkers, derived from higher plants, are characterized by high concentrations of long-chain n-alkanes n-C<sub>25</sub>, n-C<sub>27</sub>, n-C<sub>29</sub> and n-C<sub>31</sub> with

the odd over even preference. The relative abundances of C<sub>29</sub> regular steranes over C<sub>27</sub> and C<sub>28</sub> homologues indicate a significant contribution of higher plants to the initial organic matter. At the same time, the predominance of C<sub>29</sub> regular steranes in oils and source rocks of the Pre-Devonian period will suggest an algal source, because higher plants did not yet exist. The presence of 18 $\alpha$ (H)-oleanane indicates a terrigenous input of organic matter.

## 2.2 General classification of kerogen types

Kerogen is organic matter, that insoluble in organic solvents. Kerogen represents a geopolymer derived from biomass remains. The type of kerogen is depending on organic materials from initial organic precursor. The major chemical elements that constitute the structure of kerogen are carbon, hydrogen, oxygen, nitrogen and sulfur. Therefore, the common classification of kerogen types is based on its elemental composition and its evolution pathways. The H/C ratio versus O/C ratio (van Krevelen diagram) provides useful approach to the classification of kerogen types (Figure 2.2.1). This diagram was first used by van Krevelen to characterize coals and their coalification paths.

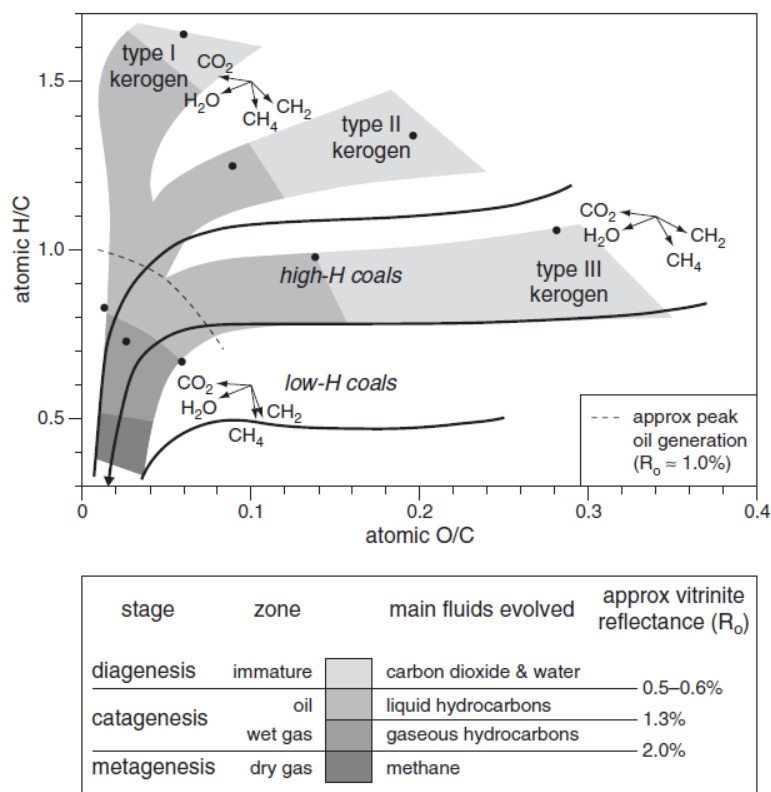


Figure 2.2.1. A van Krevelen diagram showing main types of kerogen and their evolution pathways (Killops and Killops, 2005)

With the improvement of methods for organic matter evaluation, in particular Rock-Eval pyrolysis, other approaches for the classification of kerogens have appeared. The plot of HI vs.  $T_{max}$  or HI vs. OI (modified van Krevelen diagrams) is used to characterize the type of kerogen and its thermal maturity (Figure 2.2.2).

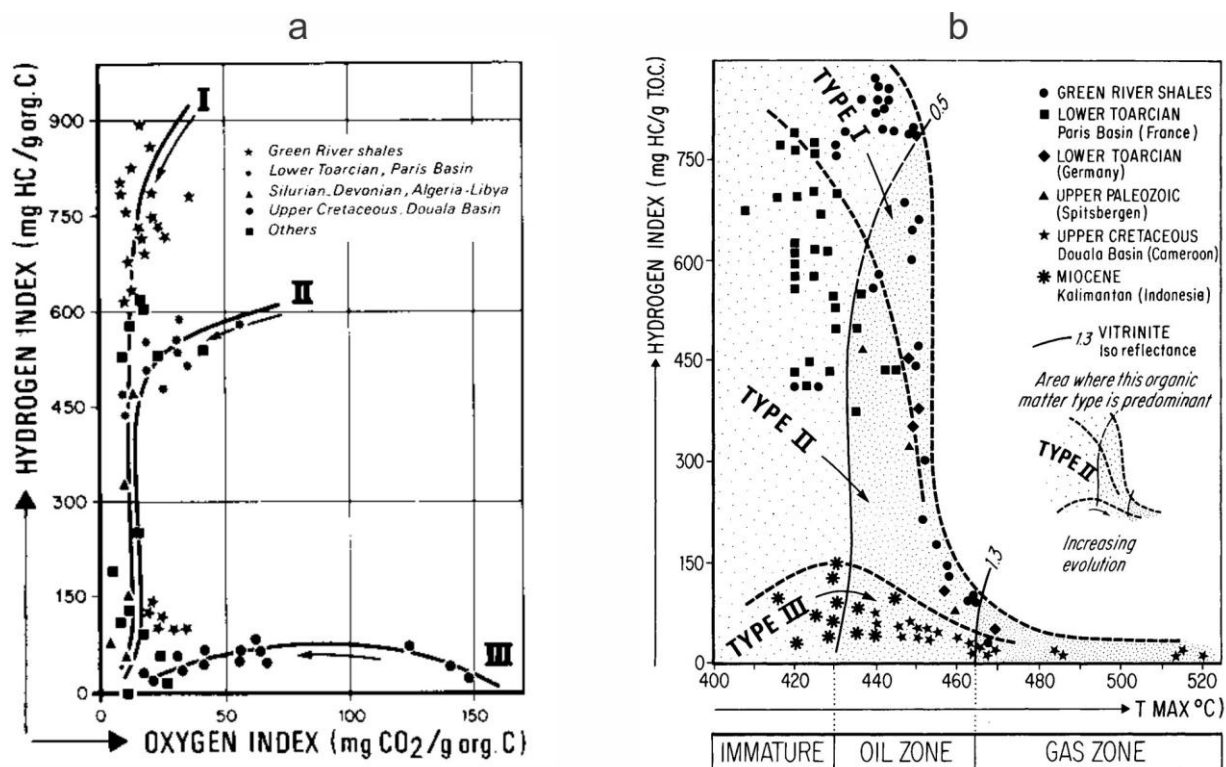


Figure 2.2.2. Kerogen classification based on hydrogen and oxygen indices (a) and hydrogen index and  $T_{max}$  (b) (Espitalié et al., 1977; Espitalié et al., 1984)

*Type I* is characterized by a high initial atomic H/C ratio ( $\geq 1.5$ ) and low O/C ( $< 0.1$ ). It is derived from the degraded remains of algae and bacteria. Type I kerogen comprises liptinite macerals, including alginite (telalginite or lamalginite). The structure of type I kerogen consists mostly of aliphatic structures. Type I kerogen is characterized by the highest hydrocarbon generation potential than other types. Straight and branched acyclic alkanes dominate the pyrolysis products. There is also type I-s, characterized by a high sulfur content in its structure (Sinninghe Damste et al., 1993). These types of kerogen are relatively rare and deposited predominantly in a lacustrine environment. Examples include the Green River Formation oil shales from Utah, Colorado and Wyoming Basins (USA), oil shales from East China and others.

*Type II* has a high atomic H/C (1-1.5) and low O/C (0.3-0.15) ratios initially. It originates from a mixture of autochthonous organic matter (phyto-, zooplankton and bacteria) and the allochthonous contribution of higher plant material. In the structure of type II kerogen, polyaromatic nuclei, the heteroatomic ketone and carboxylic acid groups are more major than in

type I. Initial hydrocarbon generation potential is higher than in type III but less so than in type I. The pyrolysis products are combined aliphatic and aromatic hydrocarbons. Sulfur-rich type II-s kerogen is characterized by a high concentration of sulfur compounds in the structure (8-14 wt.% of organic sulfur and atomic ratio of S/C>0.04) (Orr, 1986). Type II kerogen is more common for most petroleum source rocks and oil shales, including the Bazhenov Formation rocks of the West Siberian Basin (Russia), the Toarcian shales of the Paris Basin (France) or the Monterey Formation shales of California (USA).

*Type III* has a low initial atomic H/C ratio (<1.0) and a high O/C ratio (up to 0.3). It contains a significant contribution from higher plants. Type III kerogen is dominated by vitrinite macerals. The content of polyaromatic nuclei, the heteroatomic ketone and carboxylic acid groups is high, compared to the other types of kerogen. This type of kerogen is characterized by relatively low hydrocarbon generation potential and is mostly gas prone (primarily methane) if it reaches the temperature of the gas window. The pyrolysis products are phenols, simple aromatic hydrocarbons and n-alkanes from n-C<sub>23</sub> to n-C<sub>35</sub> predominance. The Triassic Tyrolean shale (Austria) contains type III kerogen. Most of the humic coals are characterized as type III kerogen.

Some publications consider *type IV kerogen* (residual type). It has no hydrocarbon generation potential. This type consists mainly of fragments of inertinite with a minor amount of vitrinite. Type IV kerogen was formed from higher plants highly oxidized on land.

### 2.3 Deposits containing type I kerogen

As mentioned above, deposits containing type I kerogen are relatively rare and represent specific depositional conditions leading to the selective accumulation of lipid-rich organic remains. The geochemical characterization of the deposits containing type I kerogen is given both according to the published data and according to the data of our own laboratory studies.



#### 2.3.1 Green River Formation

The Eocene Green River Formation extends over 410 000 km<sup>2</sup> in Colorado, Utah, and Wyoming (USA) and consists of lacustrine rocks with extensive oil shale beds. Its thickness ranges from about 360 m to a maximum of about 1500 m (averages about 600 m). The Green River Formation was deposited in two large paleo lakes during significant warming and cooling cycle in the early Eocene. The lithology of the Green River Formation includes mudstones, sandstones, oil shales, coal seams, stromatolitic limestones, halite beds and volcanic tuffs [Bradley W.H., 1931]. The rocks often include bivalves and gastropods.

The TOC values vary over a wide range from 1 to 40 wt.%, and the values of the residual petroleum potential (S<sub>2</sub>) reach 300 mg HC/g rock. The HI values reach 800-1000 mg HC/g TOC (French et al., 2020). The H/C atomic ratio of kerogen ranges from 1.28 to 1.98 for oil shales. The high values of hydrogen index and H/C ratio show that the Green River oil shales contain type I kerogen and could generate oil (Figure 2.3.1). Bulk kinetic parameters also suggest type I kerogen in the organic matter composition of oil shales (Figure 2.3.2). Most of the organic matter in these rocks is immature ( $T_{max}=420-435^{\circ}C$ ;  $PI=0.01-0.06$ ), and only deep buried horizons (from 2000 m) are characterized by a higher thermal maturity.

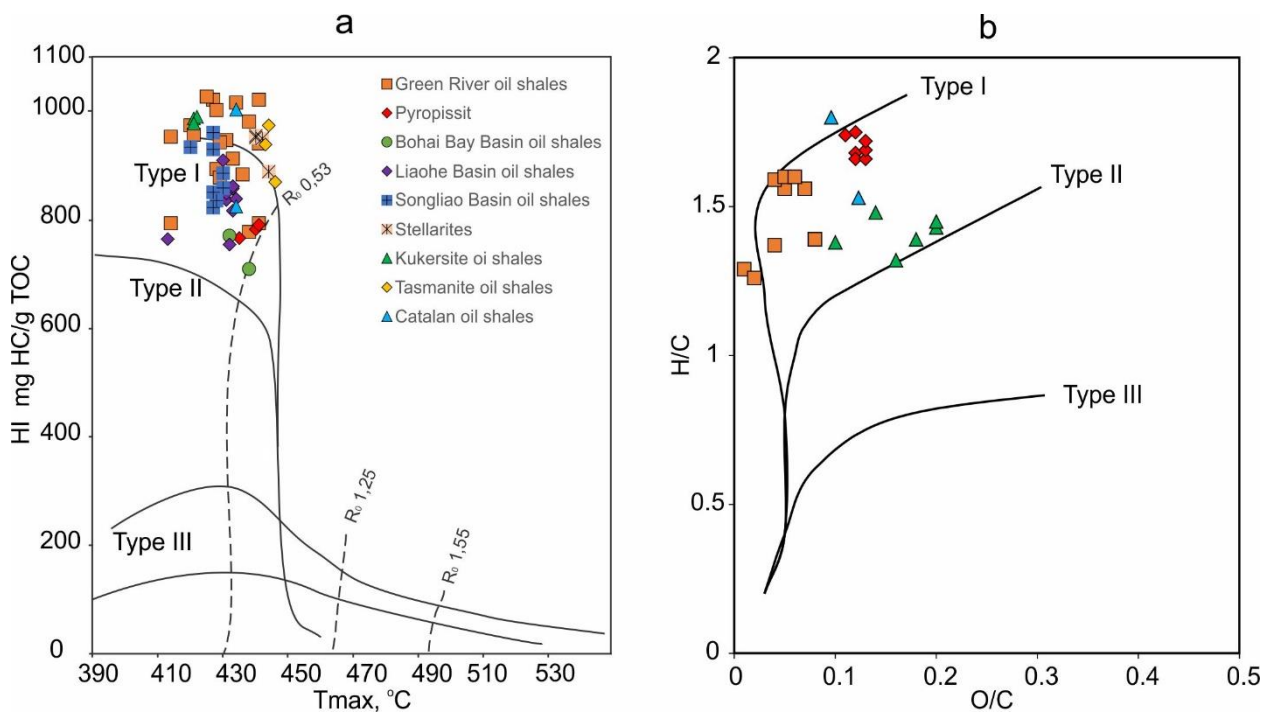


Figure 2.3.1. The cross plot of HI vs.  $T_{max}$  (a) and H/C vs. O/C (b) for deposits containing type I kerogen (Espitalié et al., 1984) (based on own and published data)



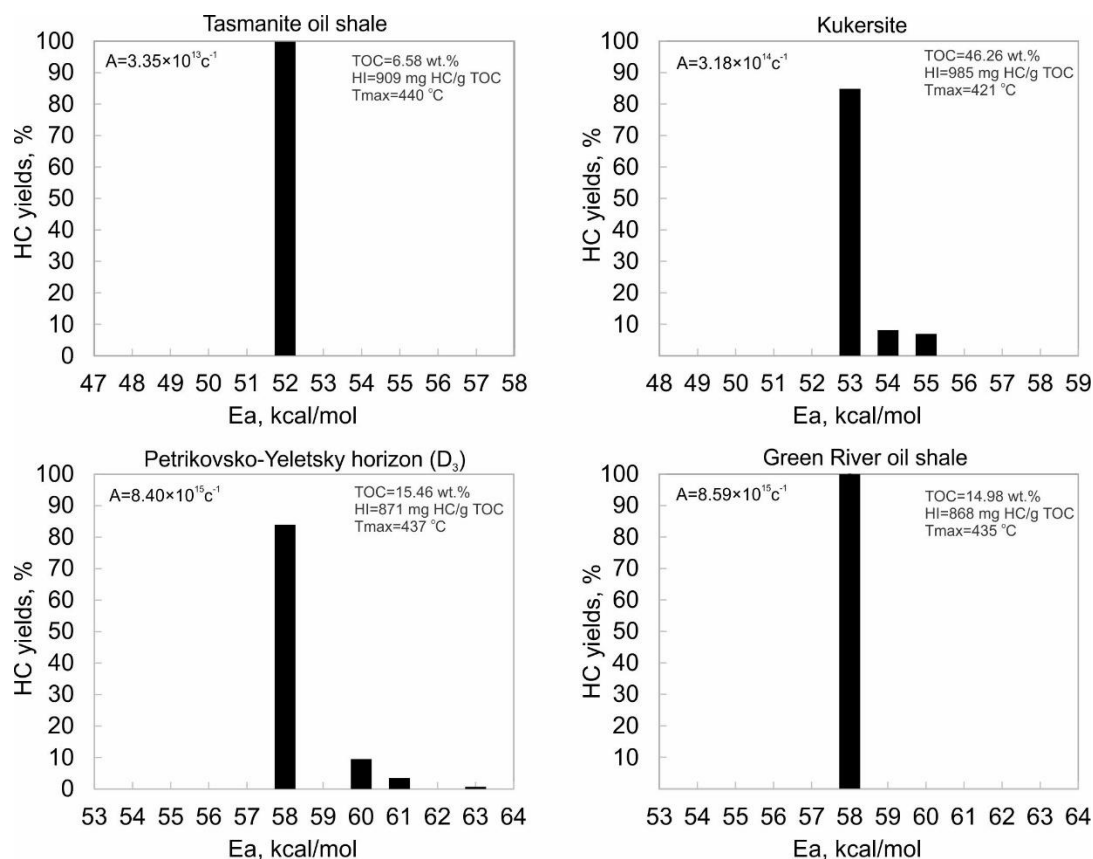


Figure 2.3.2. The Ea distribution for type I kerogen from different deposits (based on own data)

The maceral composition of the Green River oil shale is dominated by alginite, and the coal seams are dominated by vitrinite, which is convenient to use to determine the thermal maturity degree.

According to the data of GS-MS analysis, extracts contain a number of n-alkanes from C<sub>16</sub> to C<sub>36</sub> with the dominance of short-chain n-alkanes n-C<sub>17</sub> and from n-C<sub>20</sub> to n-C<sub>24</sub>, which is consistent with the main input characteristics of the algae and bacteria (Birdwell et al., 2016; Collister et al., 1994). The abundance of n-C<sub>29</sub> in some extracts indicates an admixture of higher plant input. The distributions of the Pr/Ph ratio in the extracts ranged from 0.07 to 0.99, indicating anoxic depositional conditions. Gammacerane,  $\beta$ -carotane (perhydro- $\beta$ -carotene), and tetracyclic polyprenoids (TPP) are common for extracts and linked to hypersaline depositional environment (Holba et al., 2003). The presence of 4-methylsterane is associated with dinoflagellates (Horsfield et al., 1994).

The bulk carbon isotopic composition of kerogen from the Green River Formation is from -41.4 ‰ to -28.8 ‰ (PDB), which shows depletion of <sup>13</sup>C (Tuttle, 1973). Isotopic composition of individual n-alkanes of samples from the Parachute Creek Member of Green River Formation shows the contribution of distinct sources (Collister et al., 1994). These appear to be cyanobacterial (C<sub>16</sub>-C<sub>18</sub>,  $\delta^{13}\text{C} = -37\text{‰}$  PDB), phytoplanktonic (C<sub>16</sub>-C<sub>23</sub>,  $\delta^{13}\text{C} = -32\text{‰}$ ),

chemoautotrophic bacterial (C<sub>20</sub>-C<sub>29</sub>,  $\delta^{13}\text{C} = -38\text{‰}$ ), phytoplanktonic or heterotrophic bacterial (C<sub>20</sub>-C<sub>29</sub>,  $\delta^{13}\text{C} = -30\text{‰}$ ), and vascular plants (C<sub>23</sub>-C<sub>29</sub>,  $\delta^{13}\text{C} = -29\text{‰}$ ). Nitrogen isotopic composition showed that kerogen isolates are extremely enriched in <sup>15</sup>N. The  $\delta^{15}\text{N}$  values are from 10.8 to 20.7‰ (AIR). The C/N ratio varies from 26 to 91 (Korte, 1973).

### 2.3.2 Kukersite

Kukersite is organic-rich Middle Ordovician oil shale found in the Baltic Shale basin. Stratigraphically, the kukersite occurs within the Viivikonna and the Kõrgekallas Formations (the Uhaku and Kukruse stages, respectively). Kukersite forms horizontal beds of different thicknesses between grey limestones, and marls. The kukersite layers contain predominantly brachiopods, trilobites, and fragments of bryozoans (Foster et al., 1990). The richness of fossils suggests oxygen-rich normal marine waters during sedimentation.

The TOC values reach 30-50 wt.%, the S<sub>2</sub> value up to 300-450 mg HC/g rock, and the HI range from 600 to 980 mg HC/g TOC. Elemental analysis of kerogen from the kukersite shows a high H/C atomic ratio (1.35-1.48) and relatively high O/C atomic ratio (0.15-0.25) (Mastalerz et al., 2003). The listed geochemical parameters of kukersite oil shale indicate type I kerogen, which is also confirmed by kinetics (Figure 2.3.1, Figure 2.3.2). The T<sub>max</sub> values range from 420 to 430 °C indicating thermally immature organic matter of kukersites.

Organic petrography revealed abundant telalginite, representing remains of ancient algae *Gloeocapsomorpha prisca*. This type of algae was common in the marine environments during the Middle and Upper Ordovician and has wide geography. Besides Estonia and Russia, the *G. prisca* oil shales occur in Australia, Canada and USA (Kiipli and Kiipli, 2013).

The extracted saturate fraction of kukersite shows a high abundance of n-alkanes with predominance principally at n-C<sub>15</sub> and n-C<sub>17</sub> (Figure 2.3.3). Phytane is the most abundant component, the Pr/Ph ratio in the range of 0.7-0.8.

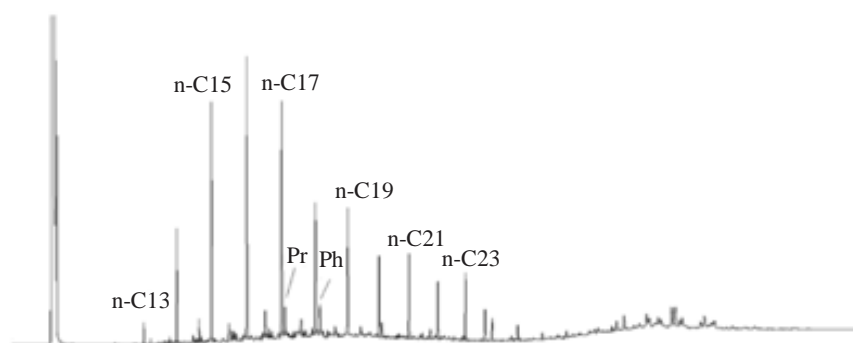


Figure 2.3.3. Gas chromatogram of kukersite extract from the Kohtla, Estonia (Burdelnaya et al., 2013)

Carbon isotope composition of kukersites organic matter show depletion of  $^{13}\text{C}$  (Mastalerz et al., 2003; Burdelnaya et al., 2013). The  $\delta^{13}\text{C}$  values is from -33.2 ‰ to -31.5 ‰ (PDB). The  $\delta^{15}\text{N}$  values range from 3.8 to 12 ‰ (AIR). Kukersite has a very low N content (0.02 до 0.12 %) compared to TOC (Kiipli and Kiipli, 2013). The C/N ration reach up to 476 (Mastalerz et al., 2003).

The listed above geochemical parameters and represented fossils point to the specific sedimentation conditions in the shallow marine basin. The increased content of oxygen-containing components, in this case, maybe a consequence of the peculiarities of diagenesis (Derenne et al., 1990). Probably, the accumulation of OM in the early diagenesis proceeded under oxidizing conditions, and only after burial, at the later stages of diagenesis, anoxic conditions were more prevalent.

### 2.3.3 Stellarites

The late Carboniferous Stellarton Formation of Stellarton Basin in Nova Scotia (Canada) is a sequence of interbedded coal and oil shale beds with a total thickness of about 2.6 km. Macroscopically and microscopically oil shales are subdivided into stellarites (boghead shales), alginite-bearing shales and cannel shales (Smith et al., 1991). Stellarites are characterized by the best generation characteristics, but their total thickness does not exceed 1.85 m. Gray to brownish-black stellarites contains numerous remains of fish remains and fecal pellets.

For stellarites TOC varies in the range of 12-30 wt.%, with an average of 19-21 wt.%. The sum of S1+S2 ranges from 80 to 280 mg HC/g rock. The HI values reach 700-900 mg HC/g TOC (Kalkreuth et al., 1990). Organic matter is immature. Based on Rock-Eval pyrolysis data, stellarites contain type I kerogen (Figure 2.3.1). In maceral composition predominate telalginite with bright yellow luminescence under UV light.

Gas chromatography data gave Pr/Ph ratio of 4.1 and Pr/n-C<sub>17</sub>=1.07, which suggests oxic depositional settings. Stellarites, probably, were deposited in stratified lakes with oxygenated surface waters and anoxic and reducing conditions within the bottom waters/sediment (Smith et al., 1991).

### 2.3.4 Lacustrine deposits of East China

Eocene and Cretaceous lacustrine deposits containing a type I kerogen are common in various basins of East China.

*Songliao Basin.* The Upper Cretaceous Qingshankou Formation consists of grey sandstones, siltstones and dark grey mudstones and oil shales with high hydrocarbon generation

potential. The TOC values for these organic-rich deposits vary from 2.5 to 12 wt.%; S<sub>2</sub> is 34.64-118.37 mg HC/g rock; HI ranges from 820 to 1080 mg HC/g TOC indicating type I kerogen (Figure 2.3.1). The low T<sub>max</sub> values (420-430 °C) suggest immature organic matter. The predominance of n-alkanes from n-C<sub>19</sub> to n-C<sub>23</sub> characterizes the main input of algae and bacteria (Figure 2.3.4). The distributions of the Pr/Ph ratio range from 0.52 to 0.82; Pr/n-C<sub>17</sub> in range of 0.76-1.36 and Ph/n-C<sub>18</sub> in range of 1.04-1.19; CPI=1.02-1.40; GI=0.18-0.31 (He et al., 2019; Zhang et al., 2020). Distribution of regular steranes show a higher proportion of C<sub>27</sub> (46-56 %) than C<sub>28</sub> (16-19 %) and C<sub>29</sub> (28-36 %). The geochemical parameters indicate an anoxic brackish water environment in the lake basin.

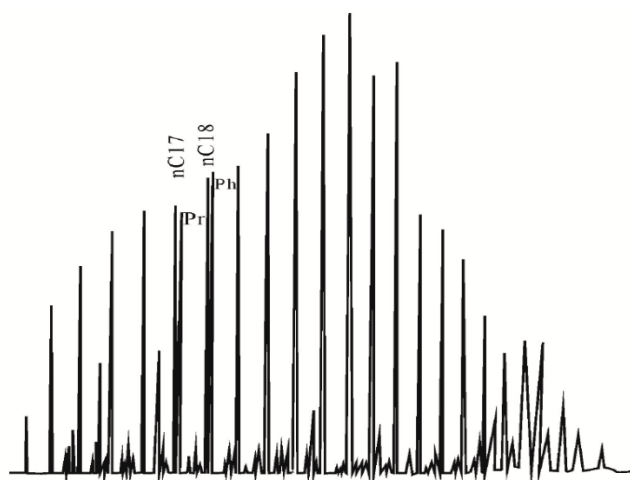


Figure 2.3.4. Gas chromatogram of the oil shale extracts from the Qingshankou Formation (He et al., 2019)

*Bohai Bay Basin.* The Eocene–Oligocene Shahejie Formation has excellent potential as petroleum source rocks. The lithology of the formation includes grey, dark grey mudstones, limestones and oil shales with gypsum and halite interbeds. The TOC content range from 5 to 12 wt.%; S<sub>2</sub> varies from 39.14 to 56.29 mg HC/g rock; HI reaches up to 770 mg HC/g TOC (Figure 2.3.1). The organic matter contained in these rocks consists primarily of type I kerogen, originating from algae. The well-preserved algae include dinoflagellates of the *Defladrea*, *Senegalinium*, *Subtilisphaera luxadinium*, *Bohaidina granulata*, green algae of the *Reticuloffenesira bohaiensis* species, blue algae of the *Pediastrum* and *Botryococcus* genera (Li et al., 2005). The saturated hydrocarbons of rock extracts are dominated by short-chain n-alkanes from n-C<sub>14</sub> to n-C<sub>18</sub> (Figure 2.3.5). The Pr/Ph ratio is between 0.55-0.99; Pr/n-C<sub>17</sub>=1.01-1.36; Ph/n-C<sub>18</sub>=1.06-3.66; CPI=1.40-1.43; OEP=1.29-1.37; GI=0.10-0.22. Among the regular steranes, C<sub>27</sub> predominates over. The organic-rich rocks of the Shahejie Formation were deposited under anoxic conditions in the brackish lake basin.

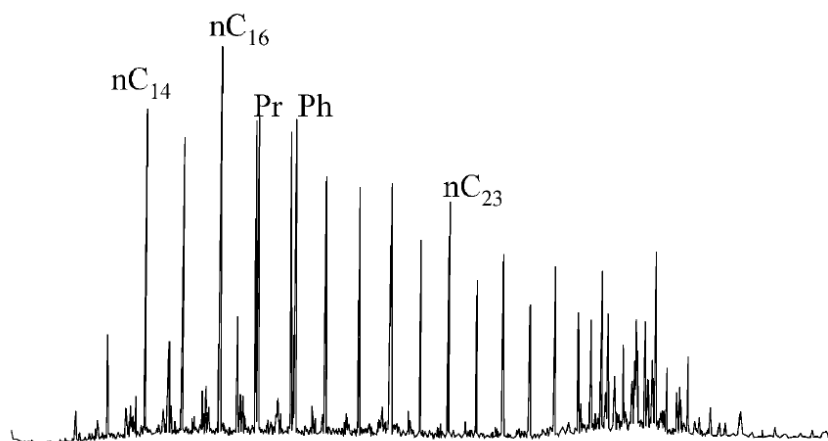


Figure 2.3.5. Saturate gas chromatogram of the Shahejie source rock (Li et al., 2005)

*Liaohé Basin.* In the Liaohé Basin, the offshore extension of the Shahejie Formation consists of dolomites, oil shales, dolomitic shales and evaporates. The TOC concentration in the rocks varies from 4 to 17.6 wt%, S<sub>2</sub> range from 32.38 to 151.36 mg HC/g rock and HI range between 700 and 900 mg HC/g TOC (Fuhrmann et al., 2004). These data indicate that the rocks contain type I kerogen (Figure 2.3.1). The low T<sub>max</sub> (430-435 °C) suggests immature organic matter. The most common macerals of the rocks are alginite, lamalginite and telalginite (*Botryococcus braunii*). The Pr/Ph < 0.4 indicates anoxic sedimentation conditions. The GI = 0.25-0.31 with the presence of β-carotane are indicate a saline depositional environment with a stratified water column.

### 2.3.5 Pyropissite

Pyropissite is brown to orange coal rich in paraffin and wax. Occurs in the Middle Eocene lignites of the Zeitz-Weißenfels coal mining area in central Germany and Konin and Turów cast mines in Poland.

The TOC content varies between 50 and 75 wt.%; HI values in studied samples reach up to 700-800 mg HC/g TOC. High atomic H/C ratio of 1.66-1.75 and atomic O/C ratio of 0.11-0.22 suggesting type I kerogen (Martínez-Tarazona et al., 1994) (Figure 2.3.1). In maceral composition predominate xanthinite – liptinitic to huminitic groundmass and considered it as a product of aerobic conversion and liptinisation of cell walls lignin and lumen fillings (Gerschel et al., 2018). Gas chromatograms have a pronounced odd/even preference of the higher molecular weight n-alkanes and a maximum at n-C<sub>29</sub> (Maxwell, 1967). The pyropissite was deposited in the Upper Eocene on a swamp plain at the southern shoreline of the Tertiary Northwest European Sea.

### 2.3.6 Australian tasmanites

Permian tasmanite oil shales of Tasmania in Australia contain abundant marine algal remains. The TOC of tasmanite deposits varies in the range of 6.6-31.3 wt.%; HI=868-972 mg HC/g TOC; S<sub>2</sub>=60.2-304.2 mg HC/g rock (Revill et al., 1994). These and kinetic data for tasmanite oil shales indicate type I kerogen (Figure 2.3.1). The saturated hydrocarbons from the tasmanite extracts show n-alkane distributions with a maximum between n-C<sub>11</sub> and n-C<sub>13</sub>, with little odd or even predominance (Figure 2.3.6). Values of 0.45 to 1.6 for the Pr/Ph ratio are consistent to predominantly anoxic sedimentation conditions. The Pr/n-C<sub>17</sub> and Ph/n-C<sub>18</sub> values are up to 0.89 and 1.05, respectively (Xie et al., 2021). The CPI values vary from 0.92 to 0.98. Tasmanite kerogen has δ<sup>13</sup>C values of -11 to -16.6 ‰. The <sup>13</sup>C enrichment of tasmanite kerogen likely corresponds to global glaciation in the Early Permian combined with a drawdown of partial pressure of CO<sub>2</sub> during algal blooms (Revill et al., 1994; Simonei et al., 1993).

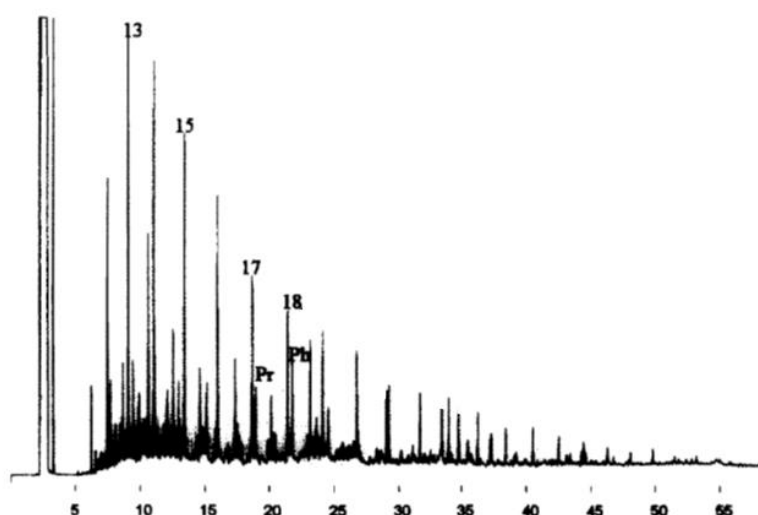


Figure 2.3.6. Gas chromatogram of the aliphatic fractions of tasmanite extracts from sample taken from Douglas River (Revill et al., 1994)

### 2.3.7 Catalan oil shales

Tertiary lacustrine oil shales of Catalonia in Spain have been deposited from the late Eocene to the late Miocene. Lithology includes laminated dolostones and mudstones. According to Rock-Eval pyrolysis, TOC is 6-10.3 wt%; S<sub>2</sub> is 49.38-103.10 mg HC/g rock; HI is 823-1001 mg HC/g TOC; OI is 26-35 mg CO<sub>2</sub>/g TOC (Sinninghe et al., 1993). The low T<sub>max</sub> values (434 °C) are in the range of immature organic matter. Elemental analysis of isolated kerogen revealed high H/C (1.53-1.80) and low O/C (0.096-0.123) suggesting highly aliphatic type I kerogen,

simultaneously high S/C (0.051-0.056) indicating sulfur-rich type I-s kerogen (Figure 2.3.1). Flash pyrolysis products (e.g., alkan-9- and -10-ones, alkadienes) of the kerogen revealed that it is predominantly composed of fossilized organic matter of the freshwater alga *Botryococcus braunii* (Figure 2.3.7).

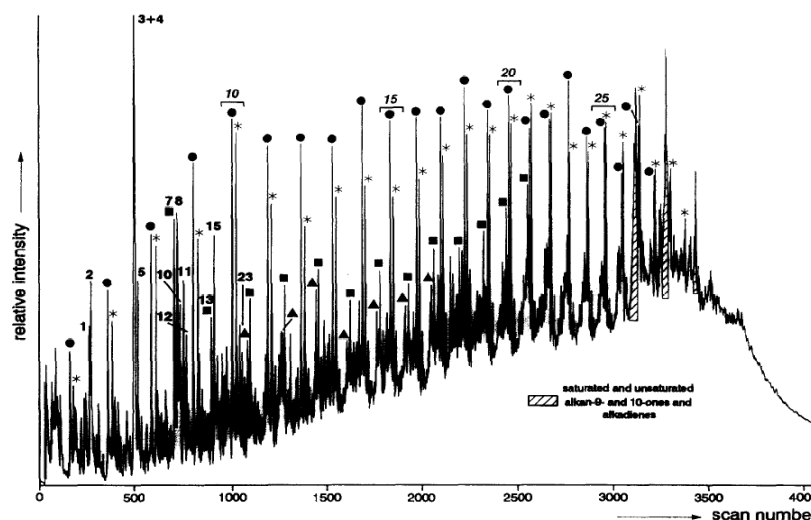


Figure 2.3.7. Total ion current trace of the flash pyrolysate (Curie temperature 610 °C) of the kerogen of the oil shale (Sinninghe et al., 1993)

## 2.4 Summary

Type I kerogen is present in deposits of various ages from the Paleozoic to the Cenozoic. The accumulation and preservation of organic matter in different facial settings predestinate its various geochemical characteristics. The considered deposits are united by their anomalously high hydrocarbon generation potential. The TOC content can be different. For the studied rocks TOC varies from 4 to 70 wt.%. The HI values are high and exceed 1000 mg HC/g TOC for the initial organic matter (Table 2.4.1).

The main factors in the formation of so unique organic-rich deposits are: *precursor biota* – lipid-rich green algae, diatoms, yellow-green algae, dinoflagellates, microorganisms, as well as lipid-rich components of higher plants (spores, pollen, leaves, etc.); *nutrients* are necessary to increase the productivity of phytoplankton from various sources; *redox conditions* affect the preservation of organic matter during sedimentation, specifically, anoxic and sulfidic conditions. Additional factors are climate, sedimentation rate, size of the sedimenting mineral grains and others.

Table 2.4.1. Comparison of geochemical characteristics of deposits containing type I kerogen

| Parameter                                  | Type of oil shale     |                   |                    |                                     |               |                       |                            |
|--|-----------------------|-------------------|--------------------|-------------------------------------|---------------|-----------------------|----------------------------|
|  | Green River oil shale | Kukersite         | Stellarites        | East China oil shales               | Pyropissite   | Australian tasmanites | Catalan oil shale          |
| Age  | Eocene                | Middle Ordovician | Late Carboniferous | Late Cretaceous/ Eocene – Oligocene | Middle Eocene | Permian               | Late Eocene – Late Miocene |
| Depositional setting                       | Lacustrine            | Marine            | Lacustrine         | Lacustrine                          | Terrestrial   | Marine                | Lacustrine                 |
| <i>Rock-Eval pyrolysis</i>                 |                       |                   |                    |                                     |               |                       |                            |
| TOC, wt. %                                 | up to 40              | 30-50             | 12-30              | 2.5-17.6                            | 50-75         | 6.6-31.3              | 6-10.3                     |
| S <sub>2</sub> , mg HC/g rock              | up to 300             | 300-450           | 80-280             | 24.02-151.36                        | 300-400       | 65-304                | 50-100                     |
| HI, mg HC/g TOC                            | 800-1000              | 600-980           | 700-900            | 700-1080                            | 700-800       | 868-972               | 823-1001                   |
| <i>Elemental analysis</i>                  |                       |                   |                    |                                     |               |                       |                            |
| H/C  | 1.28-1.57             | 1.35-1.48         | –                  | –                                   | 1.66-1.75     | –                     | 1.53-1.80                  |
| O/C  | <0.1                  | 0.15-0.25         | –                  | –                                   | 0.11-0.22     | –                     | 0.096-0.123                |
| <i>Gas chromatography</i>                  |                       |                   |                    |                                     |               |                       |                            |
| Pr/Ph                                      | 0.07-0.99             | 0.70-0.80         | 4.10               | <1.00                               | –             | 0.45-1.60             | –                          |
| Pr/n-C <sub>17</sub>                       | 0.15-2.00             | –                 | 1.07               | 0.76-1.36                           | –             | 0.45-0.69             | –                          |
| Ph/n-C <sub>18</sub>                       | 0.10-4.00             | –                 | –                  | 1.04-3.66                           | –             | –                     | –                          |
| <i>Isotope composition</i>                 |                       |                   |                    |                                     |               |                       |                            |
| δ <sup>13</sup> C <sub>org</sub> , ‰ (PDB) | -41.4...-28.8         | -33.2...-31.5     | –                  | –                                   | -28.2         | -16.6...-11.0         | –                          |

## CHAPTER 3. MATERIALS AND METHODS

### 3.1 Samples

During the study, more than 60 Bazhenov cross-sections on the territory of central part of the West Siberian Petroleum Basin were analyzed (including the Bazhenov Formation and stratigraphic analogues of Tithonian – early Valanginian). A total of 28 samples of the alginite-rich layers were sampled based on lithological description, luminescent analysis and Rock-Eval pyrolysis data (Figure 3.1.1). In addition, 34 samples of the surrounding host rocks were also sampled. The sampling distance between the alginite-rich layers and the host rocks usually did not exceed 5 cm.

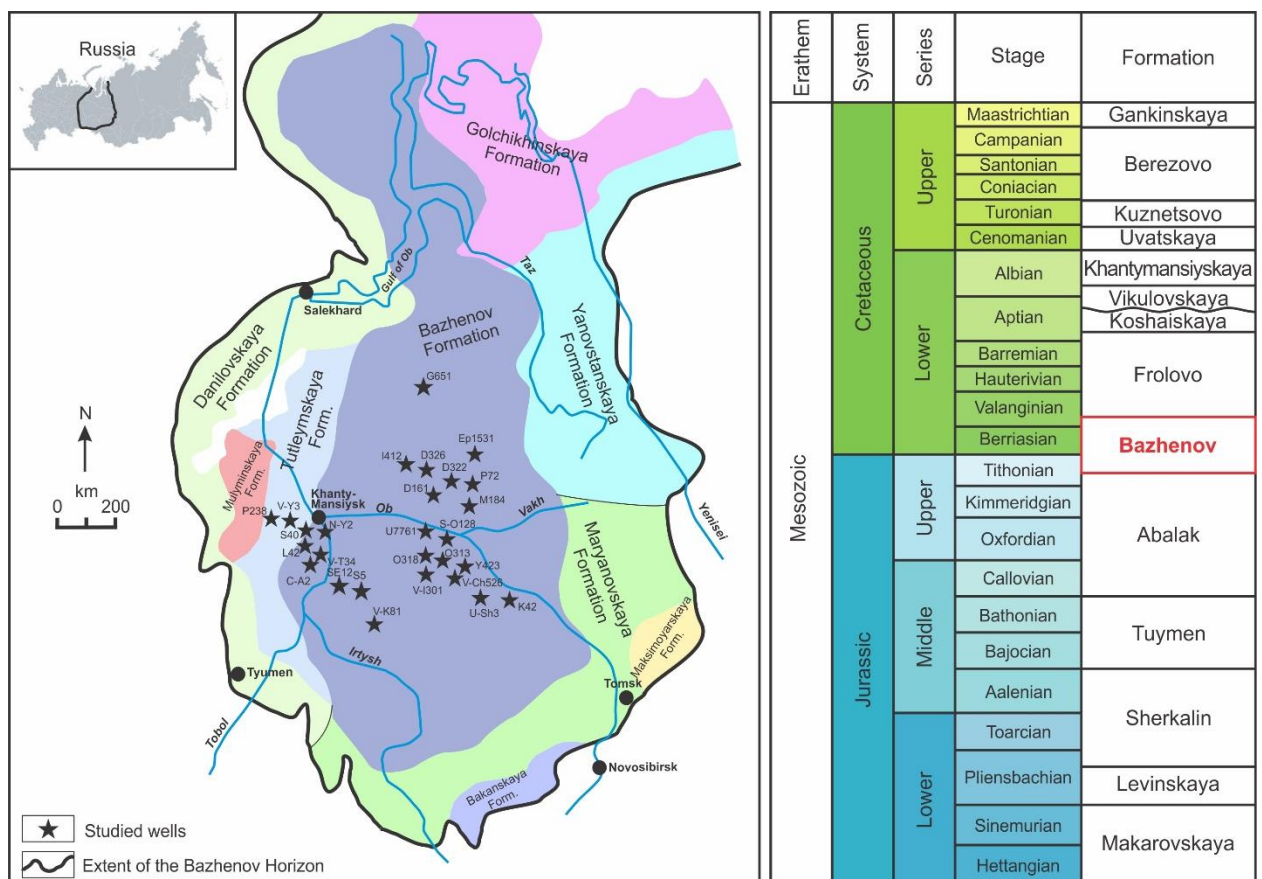


Figure 3.1.1. Map of the Bazhenov Horizon showing the location of studied wells contained luminescent alginite layers (left) and stratigraphy of Mesozoic deposits of Western Siberia (right), modified from [Amon et al., 2010]

Sample preparation techniques were directed towards obtaining clean rock samples, free of drilling mud. Core samples were wire-brushed, washed with organic-free water and then dried. Samples of the core were finely milled to powder (~200 mesh) for forward geochemical analyses.

## 3.2 Analysis

### 3.2.1 Thin section petrography

The samples for thin section petrographic examination were cut perpendicular to the bedding planes, oriented down-up, 0.03 mm thick, polished, and covered slipped. The thin sections were examined using Axioscop 5 polarizing microscope (Zeiss) equipped with an Axiocam 506 color digital camera (Zeiss).

### 3.2.2 Organic petrography

Polished whole-rock samples were prepared and examined. The maceral analysis was performed using a QDI-300 Craic micro-spectrophotometer (CRAIC Technologies) with a DM 2500 P base microscope (Leica) under reflected white light and UV light illumination in the air. A quartz halogen lamp (12 V, 100 W) was used for white light. A high-pressure mercury lamp (100 W HBO®, OSRAM) was used for the UV light. The maceral nomenclature used in this study follows the International Committee for Coal and Organic Petrology (Pickel et al., 2017; Sýkorová et al., 2005).

### 3.2.3 Scanning electron microscopy

Scanning electron microscopy (SEM) was performed using a Quattro S (Thermo Fisher) microscope coupled to an energy dispersive X-ray analyzer Quantax (Bruker). For the SEM analysis, thin-sectioned samples were polished by an Argon ion mill with two ion sources. Samples were then coated with carbon to render them conductive for both mineral and texture characterization. SEM images that were obtained by detecting the backscattered and secondary electrons.

### 3.2.4 X-Ray diffraction

The X-ray diffraction (XRD) analysis was performed on selected samples for bulk mineral composition analyses. The XRD analyses were carried out with ARL X'TRA X-ray diffractometer (Thermo) using CuK $\alpha$  radiation, operated at 40 kV and 40 mA and analyzed over the 2–60° 2 $\theta$  angular range. For indexing of diffraction peaks and identification of mineral phases, the Siroquant software package (Siroquant) was used. We used the Rietveld refinement procedure and obtained data through a concerted theory-experiment comparison.

### 3.2.5 X-Ray fluorescence

The X-ray fluorescence (XRF) analysis was performed using ARL Perform'X spectrometer (Thermo), applying the fundamental parameters method. The samples were prepared as pressed powder pellets on a boric acid ( $\text{BO}_3\text{H}_3$ ) substrate. Quantitative analysis of major elements was obtained using “GeolQuant” calibration.

### 3.2.6 Inductively coupled plasma mass spectrometry

Quadrupole inductively coupled plasma mass spectrometry (ICP-MS) has been used to determine concentrations of trace and rare elements (Li, Be, Sc, V, Cr, Co, Ni, Cu, Zn, Ga, Ge, As, Se, Rb, Sr, Y, Zr, Nd, Mo, Cd, Sb, Cs, Ba, La, Ce, Pr, Nd, Sm, Eu, Gd, Tb, Dy, Ho, Er, Tm, Yb, Lu, Hf, Ta, Re, Tl, Pb, Th and U) in rock samples. The analysis was performed by using a Neptune Plus (Thermo Fisher Scientific) instrument.

### 3.2.7 Bitumen extraction

For bitumen extraction, chloroform ( $\text{CHCl}_3$ ) was used to extract the bitumen from powdered rock and carried out using Soxhlet apparatus and Dionex ASE350 (Thermo Fisher Scientific), where 5–10 g of samples (depending on TOC) were extracted in triplicate by the injection of 100 ml of  $\text{CHCl}_3$  divided equally into three static cycles (20 min each), at 100 °C and 100 atm (1470 psi). A rinse cycle was performed after each extraction.

### 3.2.8 Kerogen isolation

Kerogen isolation was performed on milled to powder rock samples using a technique involving sequential acid treatments with hydrochloric acid (HCl), followed by hydrofluoric acid (HF) to dissolve the mineral components. The quality of mineral dissolution was checked by XRD.

### 3.2.9 CHNS/O elemental analysis

The CHN628 elemental analyzer (LECO) was used to determine the carbon, hydrogen, and nitrogen content via combustion (at 950 °C) into  $\text{CO}_2$ ,  $\text{H}_2\text{O}$ , and  $\text{NO}_2$  contents, respectively. A helium carrier gas swept the combustion gas to separate infrared cells utilized for the detection of  $\text{H}_2\text{O}$  and  $\text{CO}_2$ , while a thermal conductivity cell was used for the detection of nitrogen. The 628 S module (LECO) was used to determine the sulfur content. Sulfur evolved (at 1350 °C) from the sample and formed  $\text{SO}_2$ . From the combustion system, the gases flowed through the sulfur infrared

detection cell. Combustion occurred in the pure oxygen for CHN and S analyses. Oxygen content in the ultimate analysis was determined indirectly by subtracting C, H, N, and S from 100%.

### 3.2.10 Rock-Eval pyrolysis

Rock-Eval pyrolysis was performed using HAWK Resource Workstation (Wildcat Technologies) to obtain source rock characteristics of the samples. The Classical Pyrolysis-TOC method (Bulk Rock) was developed for all studied samples (Espitalié et al., 1985; Behar et al., 2001; Maende and Weldon, 2013; Kozlova et al., 2015). The S0, S1 and S2 peaks successively determined with flame ionization detector (FID), correspond first to the amount of free hydrocarbons (S0+S1) volatilized at 300 °C, the peak S2 representing the hydrocarbons generated from kerogen and heavy hydrocarbons cracking between 300 and 650 °C, with a heating rate of 25 °C/min in an inert atmosphere (helium) (Figure 3.2.1). The amounts of CO<sub>2</sub> and CO generated from organic matter during pyrolysis stage detected with an IR cell and represent the S3 and S3CO peaks, respectively. The residual organic and inorganic carbon content of the sample is obtained by combustion in air from 300 to 850 °C. The CO<sub>2</sub> and CO resulting from this combustion of organic matter are also detected with an IR cell and correspond to peaks S4CO<sub>2</sub> and S4CO for CO<sub>2</sub> and CO, respectively. The S3'CO and S5 peak represent amount of CO<sub>2</sub> from the mineral source. Parameter T<sub>max</sub> indicates the temperature of the maximum generation of hydrocarbons during the cracking of kerogen and heavy hydrocarbons including resins and asphaltenes, which release together in the S2 peak.

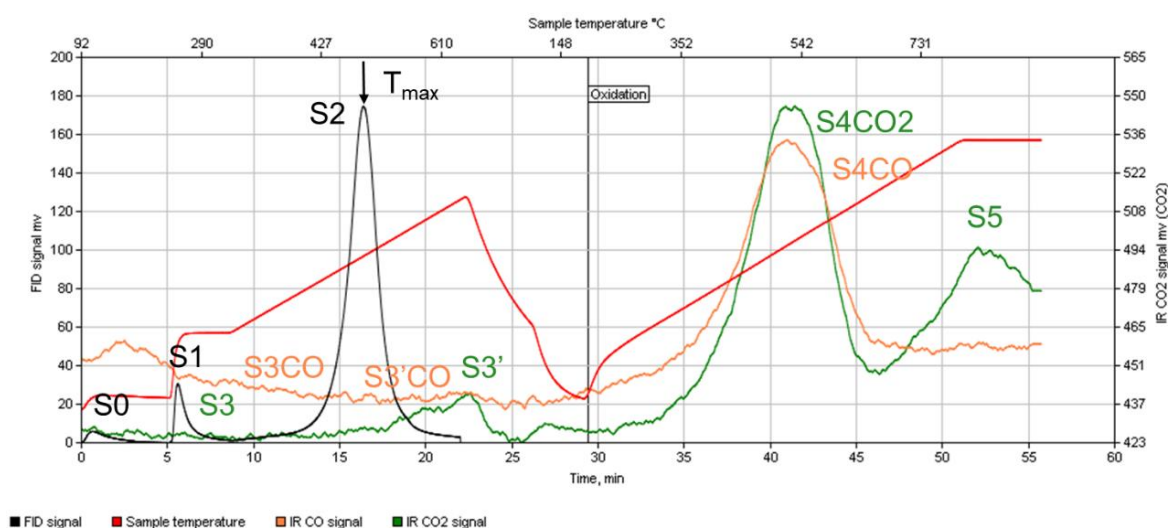


Figure 3.2.1. Example of HAWK pyrogram

Total organic carbon (TOC) is calculated as the sum of generated organic carbon (GOC) and non-generated organic carbon (NGOC). The GOC (or pyrolyzable carbon, PC) is calculated as:

$$GOC = \frac{(S0 + S1 + S2) \times 0.83 + \left(S3 \times \frac{12}{44}\right) + (S3CO + \frac{S3'CO}{2}) \times \frac{12}{28}}{10}$$

The NGOC (or residual carbon, RC) is calculated as:

$$NGOC = \frac{S4CO \times \frac{12}{28} + S4CO2 \times \frac{12}{44}}{10}$$

Carbonate carbon content (CC) or mineral carbon (MinC) is determined by following equation:

$$CC = \frac{S3' \times \frac{12}{44} + \frac{S3'CO}{2} \times \frac{12}{28} + S5 \times \frac{12}{44}}{10}$$

Production index  $PI = S1/(S1+S2)$  represents the amount of generated hydrocarbons to the total amount of hydrocarbon which the sample can produce. Hydrogen index  $HI = S2/TOC \times 100$  has been used as a predictor of the quality and type of OM. The HI represents the hydrogen richness of the organic matter. Oxygen index  $OI = S3/TOC \times 100$  indicates the oxidation of the organic matter of the sample. Oil saturation index  $OSI = S1/TOC \times 100$  depicts producible hydrocarbons in unconventional reservoirs. The proportion of pyrolyzable organic carbon  $K_{goc} = GOC/TOC \times 100$  has been used as an indicator of thermal maturation (Spasennykh et al., 2021).

The reliability of the analysis results on the HAWK RW instrument is ensured by checking the WT standard. Running samples, every 20th analysis is performed for the WT standard. The results of rock analysis are considered reliable if the deviation of the values of the pyrolysis parameters for the standard does not exceed the values established by Wildcat Technologies (Table 3.2.1).

Table 3.2.1. Values of pyrolysis parameters for the WT standard

| Parameter                                      | Values | Deviation |
|--|--------|-----------|
| S1, mg HC/g rock                               | 0.23   | +/-0.07   |
| S2, mg HC/g rock                               | 9.02   | +/-0.50   |
| S3, mg CO <sub>2</sub> /g rock                 | 0.4    | +/-0.20   |
| T <sub>max</sub> , °C                          | 418    | +/-2      |
| TOC, wt.%                                      | 3.01   | +/-0.14   |
| S3CO, mg CO/g rock                             | 0.368  | +/-0.2    |
| S4CO <sub>2</sub> , mg CO <sub>2</sub> /g rock | 60.63  | +/-6      |
| S4CO, mg CO/g rock                             | 12.747 | +/-1.35   |
| CC, wt.%                                       | 0.35   | +/-0.2    |

To study the organic matter of the Bazhenov Formation, we use Rock-Eval pyrolysis before and after bitumen extraction to exclude the influence of heavy hydrocarbons (including asphaltenes and resins) on the results (Kozlova et al., 2015; Vtorushina et al., 2018).

### 3.2.11 Kinetic analysis

Open system kinetics were carried out for samples after extraction using HAWK Resource Workstation device (Wildcat Technologies). The extracted rock samples were subjected to non-isothermal pyrolysis at a temperature from 300 to 650 °C, at three different heating rates of 3, 10, and 30 °C/min (Figure 3.2.2). The Kinetics 2015 software (CoeIsoChem Corporation) was used to obtain the kinetic parameters ( $E_a$ , kcal/mol and  $A$ ,  $s^{-1}$ ). Discrete distribution of activation energies we used to calculate hydrocarbon generation (Braun and Burnham, 1987; Burnham et al., 1988; Leushina et al., 2021).

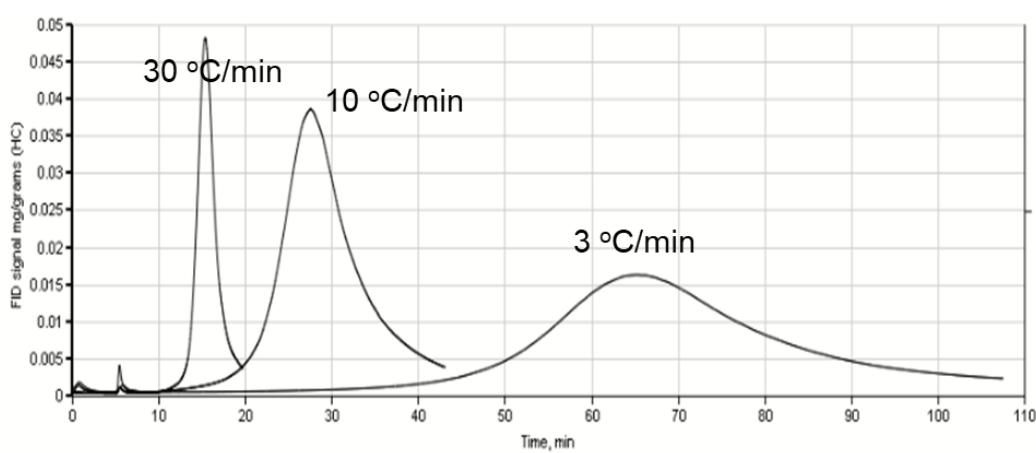


Figure 3.2.2. S2 peaks at different heating rates

The method is based on a kinetic model, according to which the thermal destruction of OM is described by a series of parallel first-order reactions according to the Arrhenius equation:

$$k = Ae^{-\frac{E_a}{RT}}, \text{ where}$$

$A$  is the frequency (pre-exponential) factor and  $\exp(-E_a/RT)$  represents the fraction of collisions that have enough energy to overcome the activation barrier at temperature  $T$ .

### 3.2.12 Fourier transform infrared spectroscopy

Fourier transform infrared (FTIR) spectroscopy was applied to identify the functional groups. For this study, samples were analyzed at room temperature using a Spectrum 100 (Perkin Elmer). Fine powder samples were mixed with KBr and then pressed to form pellets. The spectra were recorded with a step of  $1 \text{ cm}^{-1}$  in the range of wave numbers  $4000\text{-}700 \text{ cm}^{-1}$ .

### 3.2.13 GC×GC-TOFMS and Py-GC×GC-TOFMS

The organic geochemical analyses were carried out on the GC×GC-TOFMS Pegasus 4D system (LECO). The Pegasus 4D is equipped with a dual-stage modulator with chilled air (-80°C), a time-of-flight mass spectrometric detector (MS) and a flame ionization detector (FID). Helium is used as the carrier gas. The capillary columns were placed in an Agilent 7890B gas chromatograph. Capillary columns were used for 2D experiments: the first polar column (Rxi-17Sil MS, Restek, 30 m × 0.25 mm, 0.25 μm) and the second column of medium polarity (Rxi-5HT, Restek, 1.6 m × 0.25 mm, 0.10 μm).

Pyrolysis-two-dimensional gas chromatography coupled with time-of-flight mass spectrometry (Py-GC×GC-TOFMS) were performed using the Pegasus 4D (LECO) equipped with a cryo-modulator and injection modules for thermal desorption and pyrolysis (Gerstel). Chromatographic separation of the products was carried out using a reverse-order column set. Samples were heated to a final temperature of 500 °C. Pyrolysis products were detected simultaneously using FID and time-of-flight mass spectrometer detectors.

### 3.2.14 Stable isotope composition

The whole rock samples were analyzed for their stable isotope composition of carbon, nitrogen and sulfur. Isotope and elemental analyses were performed on a DELTA V Plus mass spectrometer (Thermo) equipped with a Flash HT elemental analyzer (Thermo). The validation of analytical procedures was established using the following international standards: oil NBS 22, ammonium sulfate IAEA-N-2, and barium sulfate NBS 127 for carbon, nitrogen and sulfur, respectively, as well as the laboratory standards, whose elemental and isotope composition was determined during interlaboratory comparison measurements. In accordance with the generally accepted rules, all the measured isotopic ratios were recalculated and are given in δ values characterizing the deviation of the isotopic ratio of the sample from the isotopic ratio of the standard (in ‰), i.e., PDB, AIR and CDT for carbon, nitrogen and sulfur, respectively. The absolute error of measurement for δ values is ±0.3‰ for carbon, ±0.5‰ for sulfur and nitrogen. The relative error of element content measurements is ±10%.

### 3.2.15 Compound-specific isotope analysis

#### *Sample preparation*

Total extractable material was obtained by Dionex ASE350 extraction with chloroform. Extracts were separated into four major classes of compounds – saturates, aromatics, resins and asphaltenes (SARA) – using a chromatographic column. Extracts were mixed with n-hexane to

separate asphaltenes. Oil samples were directly diluted with n-hexane mixture. The maltene fractions were freed from the solvent to the greatest possible extent, then weighed, and added to the chromatographic column with activated silica saturated with n-heptane and eluted sequentially with n-hexane (elution of saturates); toluene (elution of aromatics); and toluene-methanol solution (50:50) (elution of resins).

The isolation of n-alkanes from saturated HC fractions was carried out by their precipitation with carbamide ((NH<sub>2</sub>)<sub>2</sub>CO) from methanol. The saturated fraction (10-15 mg) was dissolved in 0.5 cm<sup>3</sup> of dichloromethane. To the resulting solution was added 5 ml of methanol solution saturated with carbamide (≈ 1 g of carbamide per 5 ml of methanol) and mixed. The resulting mixture was frozen in a thermostat at -20°C for 2 hours. Then, the methanol layer was removed by decantation and the carbamide crystals were washed three times with 10 cm<sup>3</sup> of cold n-hexane, discarding the washing solution. Carbamide crystals with precipitated n-alkanes were dissolved in deionized water at a volume of 20 ml, and n-alkanes were extracted from water with n-hexane three times, 10 cm<sup>3</sup> each, in a separatory funnel. To increase the efficiency of the extraction of n-alkanes, sodium chloride (NaCl) was added to the aqueous solution until the transparency of the aqueous layer (extract) appeared. The top n-hexane layer was collected in a separate vial. Residual water from the extract was removed with anhydrous sodium sulfate. The dehydrated extract was evaporated to a volume of 0.5 ml on a rotary evaporator. The quality of isolation of n-alkanes from saturated fraction was controlled by GC-MS data by the absence of unresolved peaks in the chromatograms of isoprenoids and the naphthenic hump.

#### *Gas chromatography-Isotope mass spectrometry*

Gas chromatography coupled with mass spectrometry and isotope ratio mass spectrometry (GC-MS-IRMS) was carried out on a Delta V Advantage isotope mass spectrometer (Thermo Fisher Scientific, Germany) connected to a Trace 1310 gas chromatograph with an ISQ7000 mass spectrometric detector through an oxidizing reactor and a GC Isolink II flow switching system. A simplified schematic of a GC-IRMS system equipped with a combustion reactor for δ<sup>13</sup>C measurements shown on Figure 3.2.3. Calculation of δ<sup>13</sup>C in samples was carried out relative to the value of δ<sup>13</sup>C of the reference gas CO<sub>2</sub>, which was preliminarily injected into the mass spectrometer by a series of pulses before the sample was injected. The laboratory reference CO<sub>2</sub> gas was calibrated against a standard solution of n-alkanes (n-C<sub>11</sub>, n-C<sub>15</sub> and n-C<sub>20</sub>) Chiron No. 0451.3-150-CY with a known δ<sup>13</sup>C value (relative to the primary VPDB standard). The result of measuring δ<sup>13</sup>C of n-alkanes in the sample was taken as the average of two measurements.

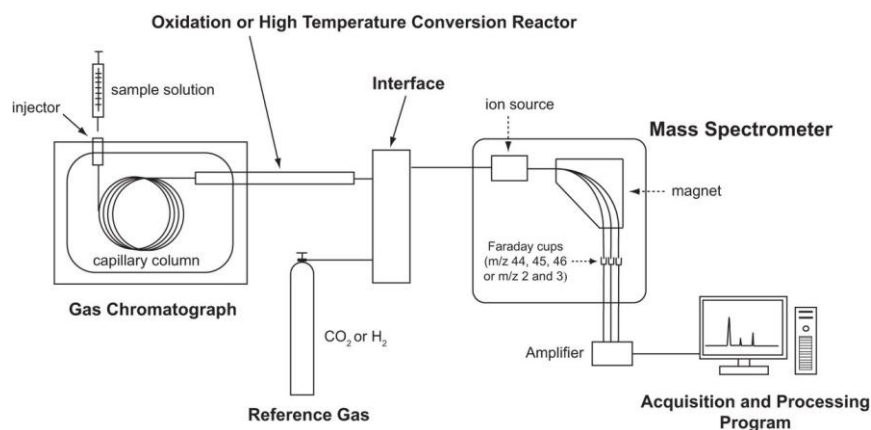


Figure 3.2.3. A simplified schematic of a GC-IRMS system for  $\delta^{13}\text{C}$  measurements (Pedentchouk and Turich, 2018)

For gas chromatographic separation of n-alkanes, a TR-5MS capillary column (30 m x 0.25 mm x 0.25  $\mu\text{m}$ ; 100% dimethylpolysiloxane) was used. The analysis was performed in the programmed thermostat heating mode – from 60°C (1 min) to 300°C, at a rate of 4°C/min, injector temperature 310°C, the temperature of the chromatograph-mass spectrometer transfer line 300°C, source switching delay for passage of the solvent front 6 min, the constant flow rate of the helium carrier gas 1 ml/min, automatic injection of 2  $\mu\text{l}$  into the chromatograph evaporator (in splitless mode).

After gas chromatographic separation of n-alkanes in a capillary column, the stream of analyzed components was divided in a microchannel divider (Microchannel Devices (MCDs) into two analytical units: one part of the stream was sent to the GC Isolink, where the separated n-alkanes were burned in an oxidizing magnetic mass spectrometric detector Delta V Advantage and recorded there as  $\text{CO}_2$  with the mass of the corresponding carbon isotope (m/z 44, 45 and 46) (Figure 3.2.4). The other part of the stream was sent in parallel to the quadrupole mass spectrometric detector ISQ for the possibility of their identification.

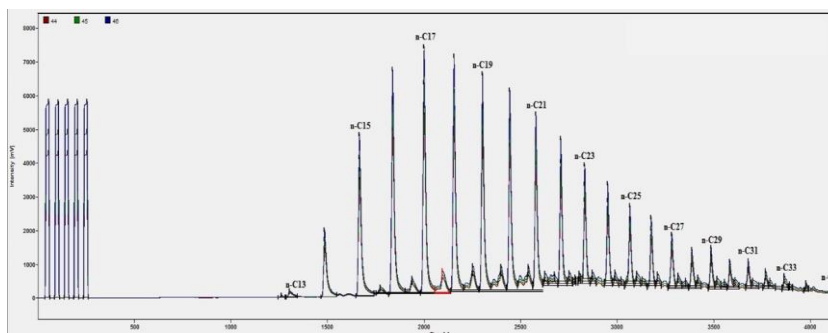


Figure 3.2.4. A chromatogram showing an m/z 44, 45 and 46 trace corresponding to  $\text{CO}_2$  produced from the combustion of individual n-alkanes

Collection and processing of isotope analysis data were carried out using the Isodat 3.0 program, analysis and processing of GC-MS data (identification of separated n-alkanes) using the

Xcalibur 4.0 program for characteristic fragment ions ( $m/z$  57, 71 and 85) and molecular ions of the corresponding n-alkanes.

### 3.3 Accepted classifications

#### 3.3.1 Tectonic units

The tectonic zoning of the territory of Western Siberia was adopted according to V.I. Shpilman (Shpilman et al., 1998). First-order tectonic elements (Megadepressions, Arches, Megaswells, etc.) are subdivided into local tectonic elements (Swells, Peaks, Terraces, etc.). The study wells are located within the Frolovskaya Megadepression, the Krasnoleninsky Arch, the Surgutsky Arch, the Nizhnevartovsky Arch, the Yuganskaya Megadepression, etc.

#### 3.3.2 Thermal maturity of organic matter

In this work, gradations of catagenesis are adopted according to N.B. Vassoevich, who distinguishes three stages: protocatagenesis (abbreviations PC1, PC2, PC3), mesocatagenesis (MC1, MC2, MC3, MC4, MC5) and apocatagenesis (AC1, AC2, AC3, AC4), which correspond to the stages of coalification and thermal maturity of disperse organic material (Vassoevich, 1986). Also in this study, intermediate stages of catagenesis (MC1-2; MC2-3, etc.) are used, identified by the average values of the intervals with the same set of the Rock-Eval pyrolysis characteristics (Table 3.3.1). In the geochemistry laboratory of the Center for Hydrocarbon Recovery was developed classification of thermal maturity for the Bazhenov organic matter based on Rock-Eval pyrolysis (Spasennykh et al., 2021).

Table 3.3.1. Thermal maturity assessment based on Rock-Eval pyrolysis data

| Stages of thermal maturity | Catagenesis stages | $T_{max}$ , °C        | HI, mg HC/g TOC       | $K_{goc}$ , % |
|----------------------------|--------------------|-----------------------|-----------------------|---------------|
| Immature                   | PC3                | $\frac{418-434}{436}$ | $\frac{510-730}{650}$ | 50-70         |
| Early mature               | Oil window         | $\frac{429-442}{436}$ | $\frac{455-670}{570}$ | 40-60         |
| Early to middle mature     |                    | $\frac{435-443}{439}$ | $\frac{390-630}{480}$ | 35-55         |
| Middle mature              |                    | $\frac{436-445}{442}$ | $\frac{220-480}{290}$ | 25-45         |
| Middle to late mature      |                    | $\frac{435-448}{444}$ | $\frac{120-350}{240}$ | 20-35         |
| Late mature                |                    | $\frac{443-453}{449}$ | $\frac{150-260}{180}$ | 15-30         |
| Over mature                | MC3-4              | $\frac{449-462}{456}$ | $\frac{70-90}{80}$    | <20           |

### 3.3.3 Stratification of the Bazhenov sequence



The stratigraphic units of the Bazhenov Formation are not unified, and different studies have subdivided them according to different criteria. Nonetheless, most studies accept the division of the Bazhenov Formation into an upper part and a lower part due to lithological characteristics and concentration of OM, which is higher in the Upper Bazhenov. In this study, we adopt the stratigraphic units reported in (Panchenko et al., 2016). According to I.V. Panchenko, the Bazhenov Formation is divided into two parts, each consisting of three distinct units. Thus, the Bazhenov section is comprised of six units, possessing certain paleontological, lithological, and geochemical characteristics, which have been identified based on well logging data (Figure 3.3.1). Such an integrated approach allows one to establish units that reflect event-driven changes in the sedimentation conditions during the Tithonian-early Valanginian age.

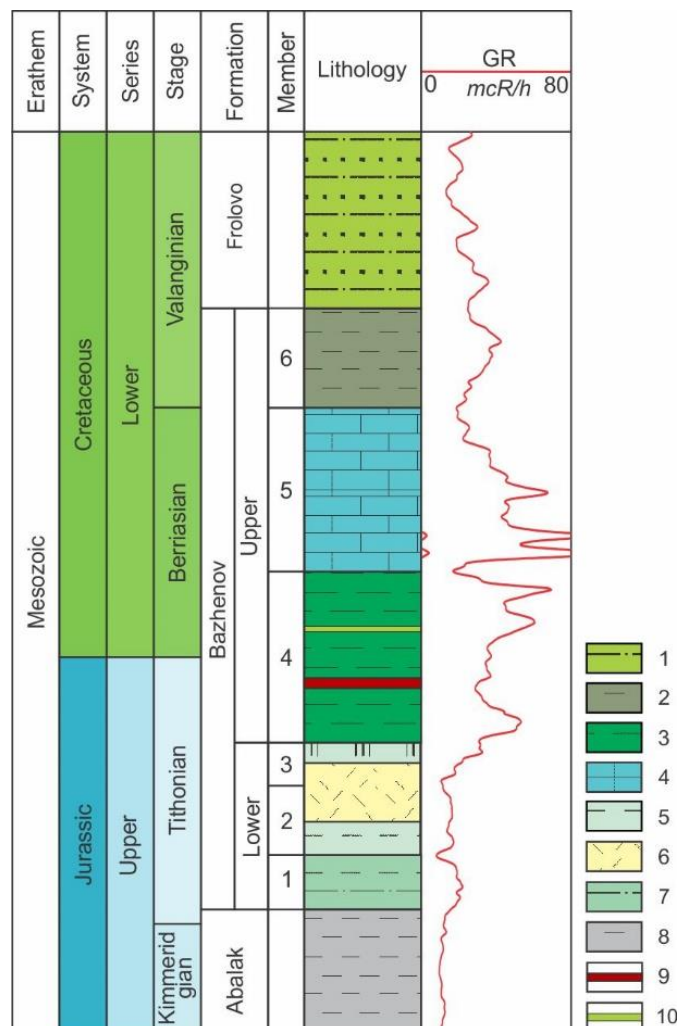


Figure 3.3.1. Example of the Bazhenov Formation succession.

Lithology: 1 – alternation of siltstones, claystone, and sandstones; 2 – siliceous claystone with high pyritization; 3 – organic-rich siliceous rocks; 4 – organic-rich calcareous rocks; 5 – siliceous rocks with low clay content; 6 – radiolarite; 7 – organic-rich claystone; 8 – claystone; 9 – alginite-rich layers; 10 – tuff interlayer. Well-log: GR, gamma-ray log

## CHAPTER 4. LITHOLOGICAL CHARACTERIZATION OF THE ALGINITE-RICH LAYERS

### 4.1 Visual description

Generally, the Bazhenov Formation is visually homogeneous black colored source rocks. The Bazhenov cross-section is mainly composed of organic-rich siliceous rocks with varying admixtures of clay and carbonate minerals. During a detailed study of the core of some wells drilled in the central part of the West Siberian basin in the interval of the Bazhenov Formation was founded thin layers and series of interlayers with a characteristic bright yellow and orange luminescence under UV light. We suggest calling these layers the “alginite-rich layers”. The luminescence was not associated with oil saturation (no oil smell), high carbonate material (no reaction with HCl acid) or luminescent tuff interlayers, as described in many works (Bulatov et al., 2017; Karnyshina, 2003; Panchenko et al., 2021).

The thicknesses of the individual alginite-rich layers vary from 1 to 50 mm, and the total thickness is up to 1 m in the cross-section. The studied cross-sections of the Bazhenov Formation have a thickness of about 20–50 m. The alginite-rich layers usually constitute about 1–5% of the entire cross-section. They can be macroscopically distinguished by their bright yellow or orange luminescence under UV light and less often by lighter coloring as compared with the darker host rocks (organic-rich siliceous rocks) under white light (Figure 4.1.1).

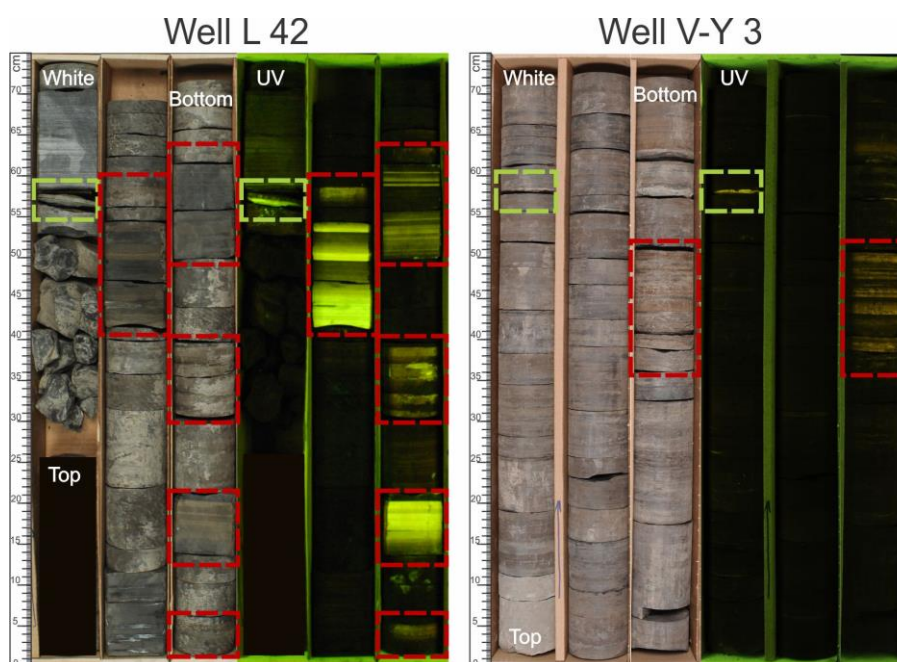


Figure 4.1.1. Core layout showing typical appearance of the Bazhenov Formation organic-rich siliceous rocks with presence of the luminescent alginite-rich layers (marked in red) and luminescent tuffs (marked in light green)  
Core photographs under white and UV light

Luminescent alginite-rich layers are located in the lower part of the Upper Bazhenov, in Member 4. There are other luminescent layers present in Member 4, i.e., tuffs (Figure 3.3.1). Tuffs appear as highly fractured greenish-gray or brown rocks with a relict volcanoclastic microstructure. They are mostly composed of devitrified volcanic glass, which has been subjected to hydration activity. The alginite-rich layers and tuffs have a different nature of luminescence. Various studies have associated the luminescence of tuffs with the mineralogy of clay minerals (Shaldybin et al., 2019), whereas the alginite-rich layers have an organic nature of luminescence.

Usually, the alginite-rich layers pass gradually to the organic-rich siliceous rocks. This gradation gives the rocks a banded appearance under UV light (Figure 4.1.2). Another interesting feature of the alginite-rich layers is their plasticity and flexibility, as well as their low density.

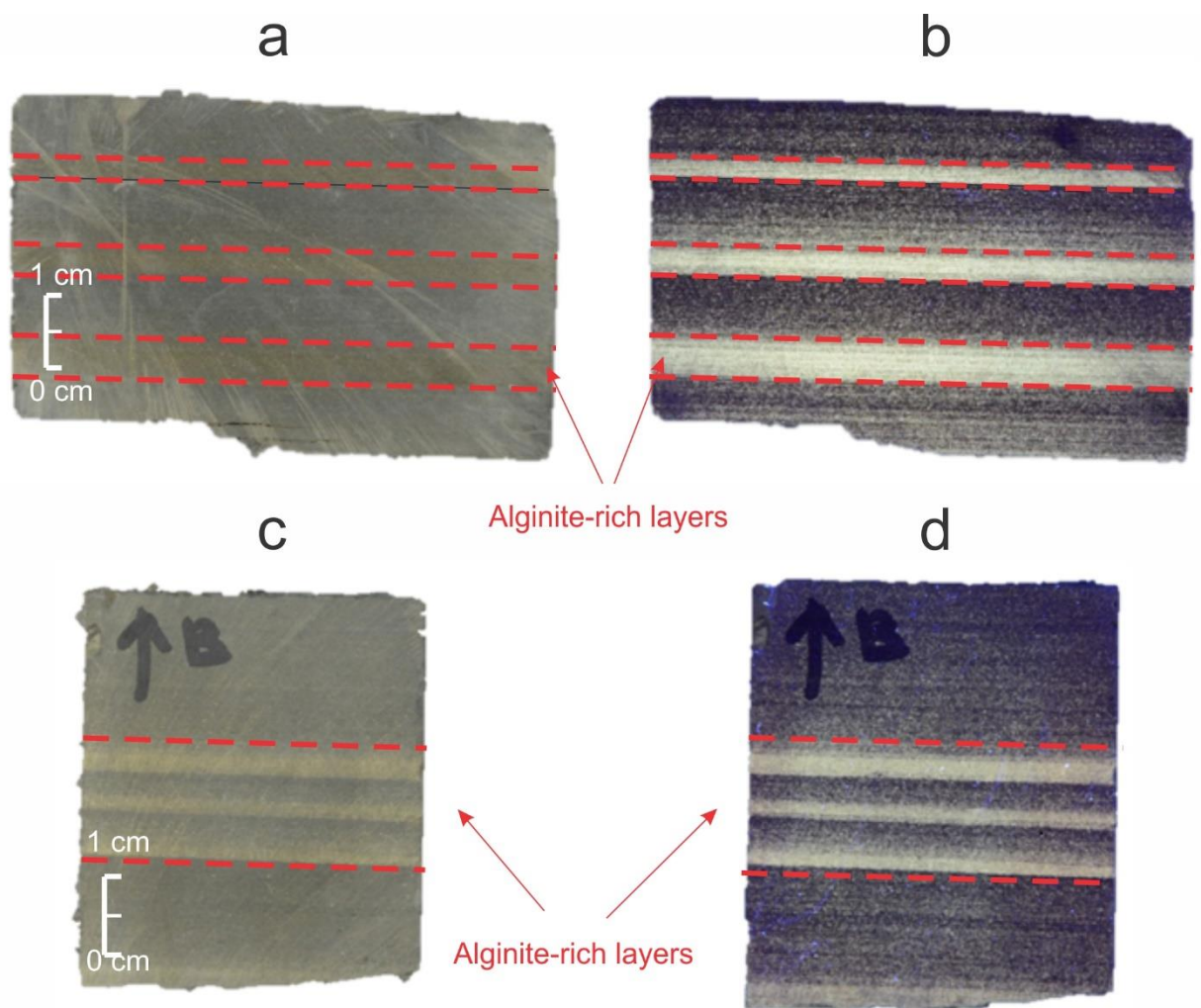


Figure 4.1.2. Photographs of the alginite-rich layers under white (a, c) and UV light (b, d) showing normal grading

## 4.2 Thin section petrography

According to the petrographic description, the alginite-rich layers are mainly composed of yellow and yellow-brown organic matter and quartz grains of  $0.02 \times 0.05$  to  $0.1 \times 0.3$  mm (Figure 4.2.1). The alginite-rich layers are alternated with the host rocks. The boundaries between the alginite-rich layers and the underlying rocks are sharp, while the upper contacts are gradually replaced by the overlying rocks. Pyrite is represented by framboids, which are distributed in the rock uniformly. Remains of fish bones, calcispheres, and radiolarians are rare.

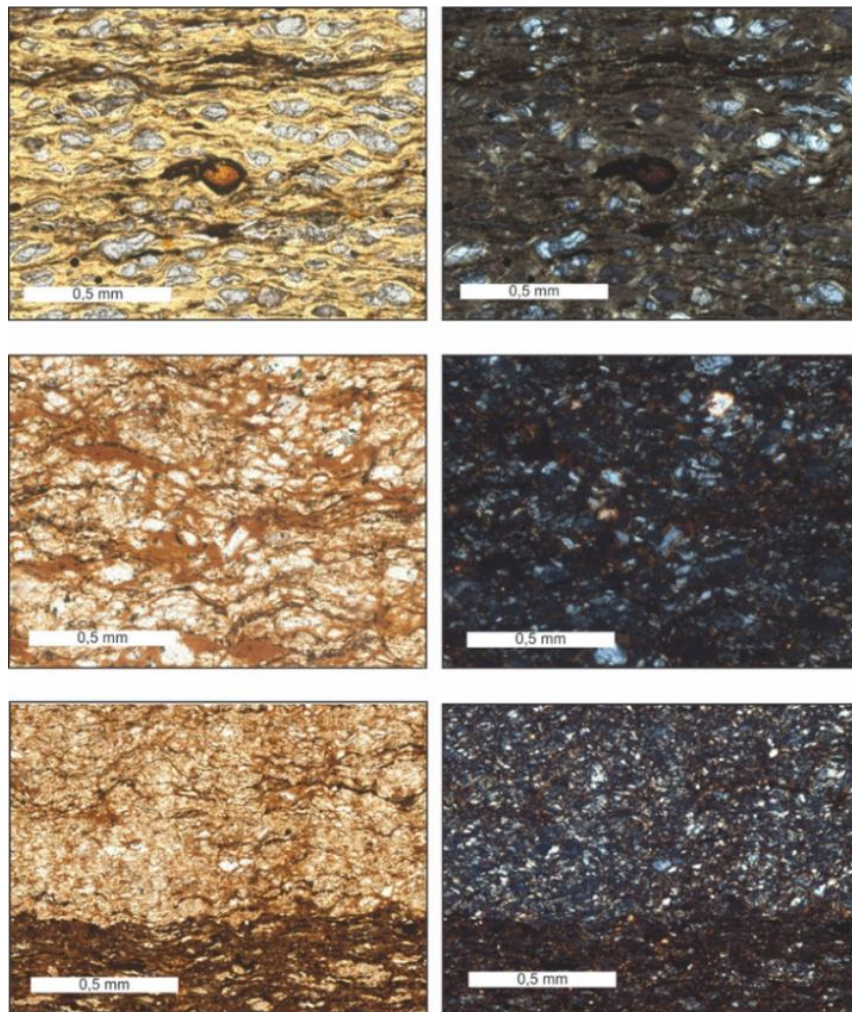


Figure 4.2.1. Typical thin section photomicrographs of the alginite-rich layers with and without analyzer

The host rocks are organic-rich silicites (Figure 4.2.2). These rocks have a wavy-layered microtexture and a pelitic structure. The bulk of the rock is predominantly composed of amorphous silica, clayey material and organic matter. The uneven distribution of organic matter causes a wavy microtexture of the rock and colors it brown. Organic matter is concentrated mainly in thin, wavy,

sometimes filamentous layers. Pyrite is finely dispersed, framboidal and replaces fragments of fish bones or radiolaria.

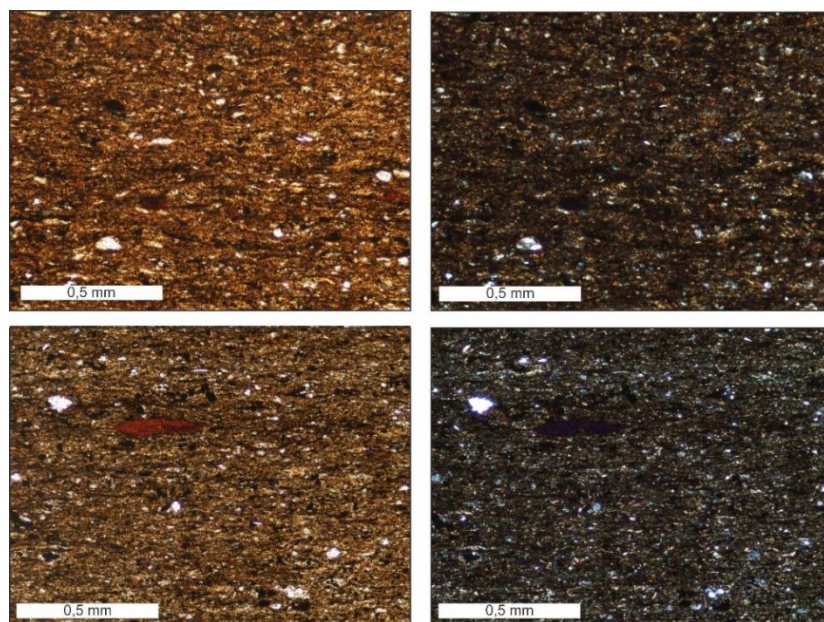


Figure 4.2.2. Typical thin section photomicrographs of the host rocks with and without analyzer

### 4.3 Mineralogy

The alginite-rich layers are dominated by quartz (67-89 wt.%), with a lesser amount of clays (9-19 wt.%), feldspars (up to 8 wt.%) and pyrite (0.9-4.2 wt.%), according to XRD (Table 4.3.1). Dolomite and calcite are minor. Clay minerals are represented by mixed-layer clay minerals, kaolinite and illite. The host rocks are characterized by relatively lower quartz content (56-71 wt.%), higher clay content (14-24 wt.%), feldspars (9.5-15 wt.%) and pyrite (2.30-8.10 wt.%). The general presence of pyrite indicates, probably, anoxic environment and sulfate reduction processes.

Table 4.3.1. Mineralogical composition of the alginite-rich layers and host rocks

| Sample |                      | Mineral content (wt. %) |             |        |           |           |        |          |         |
|--------|----------------------|-------------------------|-------------|--------|-----------|-----------|--------|----------|---------|
|        |                      | Quartz                  | Mixed-layer | Illite | Kaolinite | Feldspars | Pyrite | Dolomite | Calcite |
| 9      | Alginite-rich layers | 77.20                   | 16.70       | 0.00   | 1.90      | 2.40      | 1.70   | 0.00     | 0.00    |
| 10     |                      | 78.50                   | 13.30       | 0.00   | 3.60      | 0.90      | 1.80   | 0.00     | 1.90    |
| 11     |                      | 80.70                   | 13.80       | 0.00   | 3.40      | 0.80      | 1.20   | 0.00     | 0.00    |
| 12     |                      | 81.90                   | 13.70       | 0.00   | 2.40      | 0.70      | 1.30   | 0.00     | 0.00    |
| 13     |                      | 73.30                   | 0.00        | 6.20   | 8.50      | 7.90      | 4.10   | 0.00     | 0.00    |
| 17     |                      | 77.50                   | 0.00        | 3.10   | 7.60      | 5.60      | 4.00   | 2.20     | 0.00    |
| 18     |                      | 67.50                   | 13.20       | 0.90   | 4.80      | 3.60      | 4.20   | 5.70     | 0.00    |
| 19     |                      | 88.80                   | 7.10        | 0.90   | 1.40      | 0.00      | 0.90   | 0.90     | 0.00    |

Table 4.3.1 continued

| Sample |            | Mineral content (wt. %) |             |        |           |           |        |          |         |
|--------|------------|-------------------------|-------------|--------|-----------|-----------|--------|----------|---------|
|        |            | Quartz                  | Mixed-layer | Illite | Kaolinite | Feldspars | Pyrite | Dolomite | Calcite |
| 29     | Host rocks | 63.1                    | 20.10       | 0.00   | 0.00      | 12.40     | 3.90   | 0.00     | 0.50    |
| 30     |            | 61.8                    | 18.13       | 0.00   | 1.47      | 9.80      | 8.10   | 0.00     | 0.70    |
| 31     |            | 66.00                   | 15.57       | 0.00   | 1.33      | 10.70     | 6.30   | 0.00     | 0.00    |
| 32     |            | 68.00                   | 16.39       | 0.00   | 1.11      | 10.40     | 4.10   | 0.00     | 0.00    |
| 33     |            | 61.30                   | 22.56       | 0.00   | 1.44      | 10.80     | 3.10   | 0.80     | 0.00    |
| 34     |            | 67.80                   | 17.00       | 0.00   | 0.00      | 10.40     | 3.50   | 1.20     | 0.00    |
| 35     |            | 56.10                   | 15.57       | 0.00   | 1.13      | 15.00     | 6.90   | 1.80     | 3.50    |
| 36     |            | 70.60                   | 14.60       | 0.00   | 0.00      | 9.50      | 2.30   | 3.00     | 0.00    |

#### 4.4 Chemical composition

The results of the XRF confirm the mineral composition data and indicate a predominance of the siliceous component in an inorganic part of the alginite-rich layers (Table 4.4.1). The most abundant oxides are SiO<sub>2</sub>, Al<sub>2</sub>O<sub>3</sub> and Fe<sub>2</sub>O<sub>3</sub>, whereas CaO, MgO, TiO<sub>2</sub>, MnO, K<sub>2</sub>O, P<sub>2</sub>O<sub>5</sub>, and Na<sub>2</sub>O are present in minor quantities. The host rocks have SiO<sub>2</sub> percentage varying from 59 to 71 wt.%, Al<sub>2</sub>O<sub>3</sub> is from 6-9 wt.% and Fe<sub>2</sub>O<sub>3</sub> is from 2.5-12 wt.%, while other oxides are minor. Minor differences in MgO, CaO and P<sub>2</sub>O<sub>5</sub> concentrations are associated, probably, with secondary carbonatization and the predominant influence of organic sedimentation, respectively.

Table 4.4.1. Major oxides composition of the alginite-rich layers and host rocks

| Sample |                      | Oxides concentration (wt.%) |                                |      |                                |                  |      |                  |                               |      | LOI* |                  |
|--------|----------------------|-----------------------------|--------------------------------|------|--------------------------------|------------------|------|------------------|-------------------------------|------|------|------------------|
|        |                      | SiO <sub>2</sub>            | Al <sub>2</sub> O <sub>3</sub> | MgO  | Fe <sub>2</sub> O <sub>3</sub> | TiO <sub>2</sub> | CaO  | K <sub>2</sub> O | P <sub>2</sub> O <sub>5</sub> | MnO  |      | N <sub>2</sub> O |
| 9      | Alginite-rich layers | 71.04                       | 5.89                           | 0.93 | 3.73                           | 0.29             | 2.34 | 1.07             | 0.09                          | 0.01 | 0.24 | 14.36            |
| 10     |                      | 73.91                       | 4.66                           | 0.73 | 4.72                           | 0.37             | 0.99 | 1.37             | 0.07                          | 0.02 | 0.23 | 12.93            |
| 11     |                      | 71.22                       | 4.79                           | 0.79 | 5.96                           | 0.39             | 0.83 | 1.41             | 0.07                          | 0.02 | 0.24 | 14.27            |
| 12     |                      | 76.43                       | 5.74                           | 0.52 | 3.57                           | 0.28             | 0.37 | 0.94             | 0.25                          | 0.01 | 0.22 | 11.68            |
| 13     |                      | 84.40                       | 1.08                           | 0.40 | 4.68                           | 0.07             | 1.18 | 0.23             | 0.07                          | 0.02 | 0.18 | 7.71             |
| 17     |                      | 74.64                       | 8.73                           | 1.69 | 3.38                           | 0.82             | 0.51 | 1.26             | 0.16                          | 0.04 | 0.37 | 10.40            |
| 18     |                      | 66.26                       | 7.13                           | 2.42 | 4.40                           | 0.44             | 1.72 | 1.44             | 0.13                          | 0.02 | 0.28 | 15.75            |
| 19     |                      | 70.88                       | 6.54                           | 1.92 | 2.75                           | 0.50             | 1.04 | 1.25             | 0.17                          | 0.02 | 0.31 | 14.63            |
| 29     | Host rocks           | 63.10                       | 7.58                           | 0.64 | 4.09                           | 0.45             | 0.22 | 1.53             | 0.09                          | 0.00 | 1.24 | 16.99            |
| 30     |                      | 63.40                       | 7.74                           | 0.63 | 6.65                           | 0.46             | 0.22 | 1.50             | 0.11                          | 0.01 | 1.16 | 18.12            |
| 31     |                      | 67.56                       | 6.83                           | 0.62 | 5.83                           | 0.41             | 0.38 | 1.35             | 0.15                          | 0.01 | 1.11 | 15.75            |
| 32     |                      | 70.82                       | 6.40                           | 0.52 | 4.69                           | 0.39             | 0.16 | 1.21             | 0.06                          | 0.00 | 1.04 | 14.73            |
| 33     |                      | 68.96                       | 8.56                           | 0.75 | 4.08                           | 0.52             | 0.26 | 1.74             | 0.09                          | 0.01 | 1.18 | 13.84            |
| 34     |                      | 70.86                       | 7.10                           | 0.65 | 4.09                           | 0.42             | 0.33 | 1.38             | 0.10                          | 0.00 | 1.08 | 14.00            |
| 35     |                      | 59.22                       | 7.20                           | 0.67 | 12.19                          | 0.42             | 0.48 | 1.36             | 0.12                          | 0.01 | 1.62 | 16.72            |
| 36     |                      | 69.44                       | 6.14                           | 0.67 | 2.54                           | 0.37             | 0.57 | 1.23             | 0.14                          | 0.01 | 1.06 | 17.83            |

\*LOI – loss on ignition content (wt.%)

Table 4.4.2 is compilation data of REE and trace elements composition data for the alginite-rich layers and host rocks.

Table 4.4.2. Trace elements and REE concentration of the alginite-rich layers and host rocks

| Trace and REE (ppm) | Sample               |      |       |      |      |       |       |       |            |        |       |       |        |        | North American Shale Composite (NASC)* |
|---------------------|----------------------|------|-------|------|------|-------|-------|-------|------------|--------|-------|-------|--------|--------|--|
|                     | Alginite-rich layers |      |       |      |      |       |       |       | Host rocks |        |       |       |        |        |  |
|                     | 4                    | 9    | 13    | 13-1 | 17   | 22    | 26    | 27    | 36         | 49     | 52    | 52-1  | 55     | 56     |  |
| Li                  | 22.9                 | 8.9  | 19.1  | 12.9 | 14.7 | 12.6  | 28.9  | 19.3  | 33.0       | 40.8   | 40.9  | 27.9  | 39.5   | 36.4   | –                                      |
| Be                  | 0.4                  | –    | 0.0   | –    | –    | 0.9   | 1.3   | 1.0   | 1.1        | 0.9    | 1.2   | –     | 3.2    | 2.4    | –                                      |
| Sc                  | 6.7                  | –    | 1.0   | –    | –    | 7.4   | 8.3   | 11.4  | 12.8       | 15.2   | 11.3  | –     | 21.8   | 16.5   | –                                      |
| V                   | 258                  | –    | 23    | –    | –    | 390   | 400   | 343   | 479        | 879    | 344   | –     | 777    | 724    | –                                      |
| Cr                  | 50.4                 | –    | 4.4   | –    | –    | 42.5  | 45.6  | 54.3  | 98.4       | 88.3   | 62.6  | –     | 109.1  | 79.8   | –                                      |
| Co                  | 13.5                 | –    | 2.3   | –    | –    | 17.3  | 15.2  | 12.4  | 27.8       | 24.5   | 19.6  | –     | 22.3   | 28.1   | –                                      |
| Ni                  | 124.5                | –    | 19.5  | –    | –    | 184.1 | 187.4 | 105.2 | 287.9      | 290.1  | 210.9 | –     | 169.0  | 324.9  | –                                      |
| Cu                  | 69.1                 | –    | 9.5   | –    | –    | 84.2  | 88.6  | 46.4  | 116.1      | 137.9  | 96.6  | –     | 101.8  | 155.9  | –                                      |
| Zn                  | 439.9                | –    | 23.5  | –    | –    | 669.2 | 547.8 | 343.2 | 620.1      | 2561.3 | 609.6 | –     | 1171.8 | 1212.8 | –                                      |
| Ga                  | 5.3                  | –    | 1.1   | –    | –    | 11.0  | 7.9   | 12.2  | 11.0       | 18.5   | 11.6  | –     | 27.1   | 18.0   | –                                      |
| Ge                  | 3.5                  | –    | 1.6   | –    | –    | 5.4   | 4.3   | 6.7   | 6.7        | 8.5    | 6.0   | –     | 12.0   | 8.6    | –                                      |
| As                  | 28.5                 | –    | 16.5  | –    | –    | 45.5  | 42.1  | 33.2  | 46.9       | 54.6   | 28.0  | –     | 37.3   | 90.9   | –                                      |
| Se                  | 2.2                  | –    | 0.8   | –    | –    | 3.2   | 2.3   | 4.0   | 3.8        | 7.2    | 4.3   | –     | 7.6    | 6.2    | –                                      |
| Rb                  | 19.4                 | –    | 2.5   | –    | –    | 33.8  | 30.5  | 50.2  | 38.6       | 67.2   | 40.1  | –     | 112.7  | 61.2   | 112.0                                  |
| Sr                  | 189                  | 77   | 62    | 48   | 51   | 82    | 134   | 459   | 128        | 182    | 141   | 129   | 417    | 205    | 350.0                                  |
| Y                   | 15.9                 | 6.8  | 3.2   | 2.6  | 9.0  | 23.0  | 13.3  | 15.2  | 14.7       | 21.0   | 24.3  | 16.9  | 28.0   | 37.3   | 22.0                                   |
| Zr                  | 44.8                 | –    | 13.0  | –    | –    | 51.2  | 60.0  | 71.9  | 84.4       | 108.2  | 84.7  | –     | 166.5  | 117.7  | 190.0                                  |
| Nb                  | 2.9                  | –    | 0.5   | –    | –    | 3.4   | 3.6   | 5.6   | 5.7        | 6.7    | 5.6   | –     | 13.6   | 7.2    | 12.0                                   |
| Mo                  | 249.6                | 75.2 | 175.8 | 16.9 | 52.6 | 294.9 | 322.0 | 222.9 | 363.2      | 357.8  | 369.6 | 216.6 | 265.0  | 437.4  | –                                      |
| Cd                  | 8.3                  | –    | 0.3   | –    | –    | 11.0  | 9.8   | 5.6   | 10.2       | 37.7   | 10.9  | –     | 18.8   | 19.8   | –                                      |
| Sb                  | 3.4                  | –    | 1.3   | –    | –    | 8.9   | 8.3   | 6.1   | 8.3        | 15.1   | 5.9   | –     | 11.3   | 15.7   | –                                      |
| Cs                  | 1.7                  | –    | 0.2   | –    | –    | 4.4   | 2.7   | 4.0   | 3.4        | 6.8    | 3.4   | –     | 8.4    | 4.9    | 4.6                                    |
| Ba                  | 1098                 | 279  | 545   | 442  | 478  | 633   | 786   | 966   | 1726       | 1540   | 956   | 871   | 2107   | 1249   | 550.0                                  |
| La                  | 8.1                  | 7.5  | 2.1   | 1.8  | 7.4  | 17.9  | 10.5  | 18.0  | 12.3       | 22.8   | 17.3  | 15.6  | 38.4   | 24.2   | 30.0                                   |
| Ce                  | 15.6                 | 14.2 | 4.0   | 3.6  | 14.3 | 30.8  | 21.8  | 36.4  | 28.8       | 47.4   | 34.9  | 30.7  | 74.9   | 50.2   | 64.0                                   |

Table 4.4.2 continued

| Trace and REE (ppm) | Sample               |      |      |      |      |      |      |      |            |       |      |      |       |       | North American Shale Composite (NASC)* |
|---------------------|----------------------|------|------|------|------|------|------|------|------------|-------|------|------|-------|-------|--|
|                     | Alginite-rich layers |      |      |      |      |      |      |      | Host rocks |       |      |      |       |       |  |
|                     | 4                    | 9    | 13   | 13-1 | 17   | 22   | 26   | 27   | 36         | 49    | 52   | 52-1 | 55    | 56    |  |
| Pr                  | 1.9                  | 1.9  | 0.5  | 0.5  | 1.8  | 4.0  | 2.7  | 4.7  | 3.5        | 5.9   | 4.3  | 3.7  | 9.3   | 6.3   | 7.1                                    |
| Nd                  | 8.4                  | 7.6  | 1.9  | 1.7  | 7.0  | 17.2 | 11.4 | 18.6 | 15.0       | 24.4  | 17.4 | 14.1 | 36.4  | 27.9  | 26.0                                   |
| Sm                  | 1.8                  | 1.7  | 0.4  | 0.4  | 1.7  | 3.7  | 2.3  | 3.9  | 3.2        | 4.7   | 3.7  | 3.1  | 7.0   | 6.0   | 4.5                                    |
| Eu                  | 0.5                  | 0.4  | 0.1  | 0.0  | 0.3  | 0.9  | 0.5  | 0.9  | 0.8        | 1.1   | 0.9  | 0.6  | 1.5   | 1.4   | 0.9                                    |
| Gd                  | 2.2                  | 1.6  | 0.5  | 0.5  | 1.6  | 4.0  | 2.4  | 3.5  | 3.2        | 4.7   | 4.0  | 3.1  | 6.0   | 6.6   | 3.8                                    |
| Tb                  | 0.3                  | 0.2  | 0.1  | 0.1  | 0.2  | 0.6  | 0.4  | 0.5  | 0.5        | 0.7   | 0.6  | 0.5  | 0.8   | 1.0   | 0.6                                    |
| Dy                  | 2.1                  | 1.3  | 0.5  | 0.4  | 1.6  | 3.4  | 2.1  | 2.8  | 2.7        | 3.9   | 3.6  | 2.8  | 5.0   | 6.0   | 3.5                                    |
| Ho                  | 0.5                  | 0.3  | 0.1  | 0.1  | 0.3  | 0.7  | 0.4  | 0.6  | 0.6        | 0.8   | 0.8  | 0.6  | 1.0   | 1.3   | 0.8                                    |
| Er                  | 1.5                  | 0.8  | 0.3  | 0.2  | 0.9  | 2.3  | 1.4  | 1.6  | 1.6        | 2.3   | 2.4  | 1.9  | 2.9   | 3.9   | 2.3                                    |
| Tm                  | 0.2                  | 0.1  | 0.0  | 0.0  | 0.1  | 0.3  | 0.2  | 0.2  | 0.2        | 0.3   | 0.4  | 0.3  | 0.4   | 0.5   | 0.3                                    |
| Yb                  | 1.7                  | 0.7  | 0.3  | 0.3  | 0.9  | 2.2  | 1.4  | 1.5  | 1.6        | 2.1   | 2.4  | 1.9  | 2.8   | 3.8   | 2.2                                    |
| Lu                  | 0.2                  | 0.1  | 0.0  | 0.0  | 0.1  | 0.3  | 0.2  | 0.2  | 0.2        | 0.3   | 0.3  | 0.3  | 0.4   | 0.5   | 0.3                                    |
| Hf                  | 0.9                  | –    | 0.2  | –    | –    | 1.0  | 1.0  | 1.7  | 1.6        | 2.1   | 1.5  | –    | 3.9   | 2.1   | 5.8                                    |
| Ta                  | 0.2                  | –    | 0.0  | –    | –    | 0.2  | 0.2  | 0.3  | 0.3        | 0.4   | 0.3  | –    | 0.8   | 0.4   | 1.0                                    |
| Re                  | 0.1                  | 0.2  | 0.0  | 0.0  | 0.1  | 0.1  | 0.1  | 0.0  | 0.2        | 0.1   | 0.1  | 0.1  | 0.1   | 0.2   | –                                      |
| Tl                  | 1.4                  | –    | 0.3  | –    | –    | 1.9  | 1.3  | 1.3  | 2.1        | 3.1   | 1.3  | –    | 2.9   | 2.3   | –                                      |
| Pb                  | 4.6                  | –    | 11.6 | –    | –    | 4.8  | 5.0  | 8.2  | 7.6        | 12.1  | 6.7  | –    | 18.2  | 12.2  | 17.0                                   |
| Th                  | 1.7                  | 1.9  | 0.4  | 0.4  | 1.7  | 3.0  | 3.0  | 5.2  | 3.2        | 5.8   | 3.6  | 4.0  | 12.7  | 7.2   | 10.7                                   |
| U                   | 25.8                 | 14.3 | 5.1  | 5.4  | 11.8 | 31.8 | 25.4 | 12.6 | 39.3       | 39.6  | 38.6 | 29.1 | 19.0  | 63.4  | 2.8                                    |
| ΣLREE*              | 25.6                 | 23.6 | 6.6  | 5.9  | 23.6 | 52.7 | 34.9 | 59.1 | 44.6       | 76.1  | 56.5 | 50.0 | 122.6 | 80.8  | 101.1                                  |
| ΣMREE*              | 15.3                 | 12.8 | 3.4  | 3.1  | 12.5 | 29.7 | 19.2 | 30.3 | 25.4       | 39.5  | 30.1 | 24.3 | 56.6  | 48.9  | 39.3                                   |
| ΣHREE*              | 4.1                  | 2.0  | 0.8  | 0.7  | 2.4  | 5.9  | 3.7  | 4.0  | 4.3        | 5.8   | 6.3  | 5.0  | 7.6   | 10.0  | 6.0                                    |
| ΣREE*               | 45.1                 | 38.4 | 10.8 | 9.6  | 38.5 | 88.3 | 57.8 | 93.4 | 74.3       | 121.5 | 92.9 | 79.3 | 186.8 | 139.7 | 146.4                                  |

LREE, light rare earth elements (La-Pr); MREE, middle rare earth elements (Nd-Dy); HREE, heavy rare earth elements (Ho-Lu); NASC values according to Taylor and McLennan, 1985.

The alginite-rich layers are characterized by relatively low total REE (9.6-93.4 ppm) compared to the total REE abundance of the host rocks (74.3-186.8 ppm). The NASC-normalized REE of the alginite-rich layers is plotted together with the NASC-normalized REE concentrations of the host rocks, showing relatively lower abundances and similar patterns (Figure 4.4.1a). The NASC-normalized REE abundances for all studied samples show a relatively sloping LREE trend and a relatively flat HREE trend. Sample 13-1 show negative Eu anomaly.

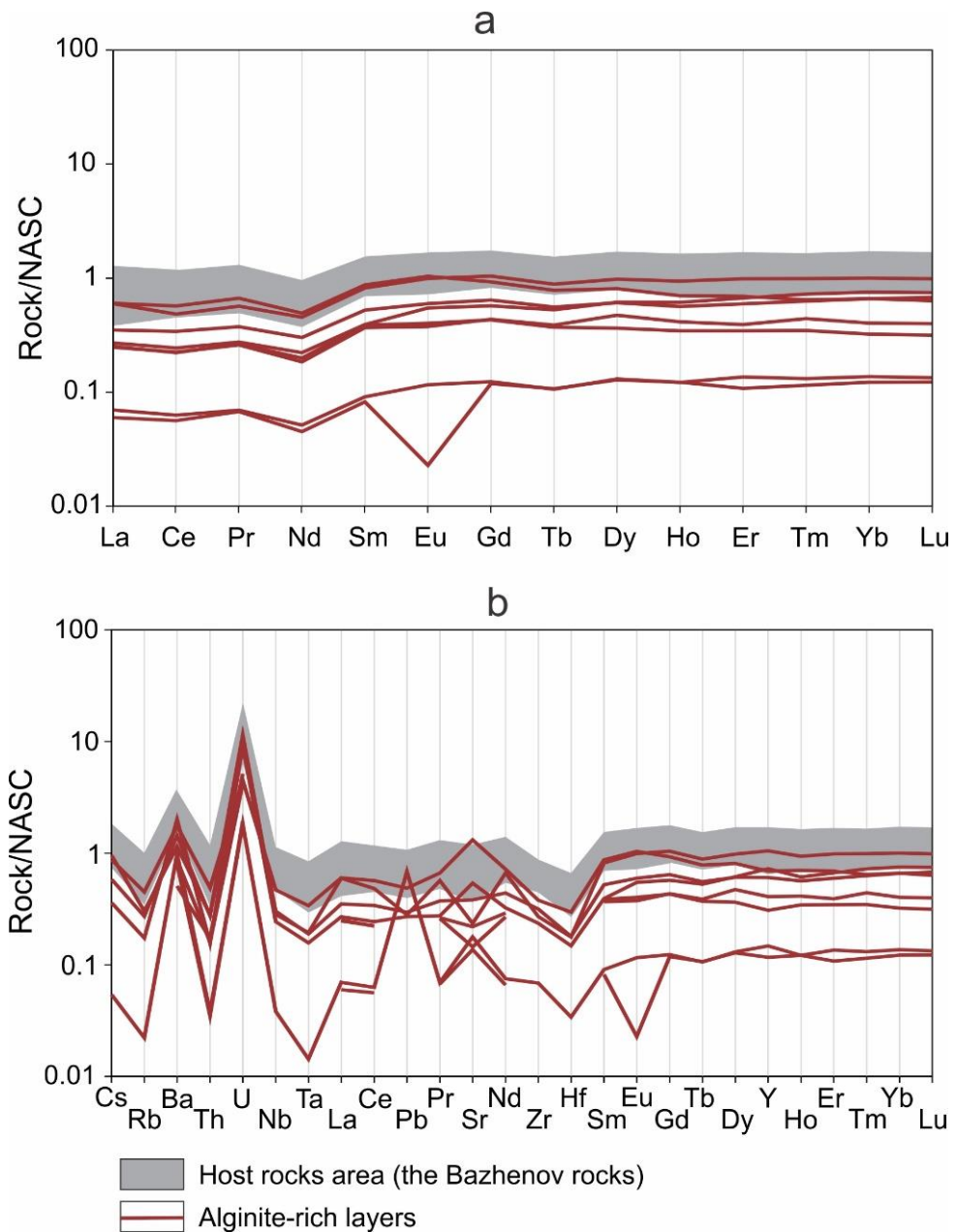


Figure 4.4.1. NASC-normalized REE (Taylor and McLennan, 1985) distribution pattern (a) and NASC-normalized trace element diagram (b) for the alginite-rich layers and host rocks

On the NASC-normalized trace elements diagram (Figure 4.4.1b), the alginite-rich layers and host rocks show marked negative anomalies of Th, Nb and Ta, slightly negative anomalies of Rb, and Hf, enrichment in Ba and U, variable concentrations of Pb, Pr, Sr and Eu.

Maximum REE concentrations are observed in the host rocks. In the alginite-rich layers, there is a positive correlation between the total amount of REE and TOC contents (Figure 4.4.2). In the host rocks,  $\Sigma$ REE has a negative relative correlation with TOC suggesting that REE are not associated with the organic matter but, probably, with the mineral matrix. Meanwhile, the positive correlation of  $\Sigma$ REE and TOC in the alginite-rich layers suggest that the bulk of REE are incorporated in organic matter. To refute or confirm this statement, analysis of more samples is required.

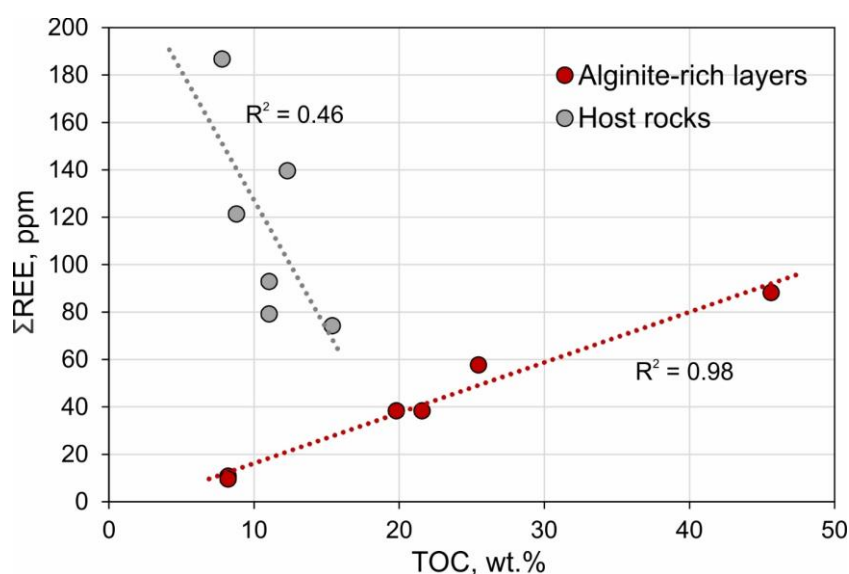


Figure 4.4.2. Correlations between  $\Sigma$ REE and TOC of the alginite-rich layers and host rocks

#### 4.5 Morphological characteristic

The study of samples by SEM allows for clarification of the morphological characteristics of the rocks at high magnifications. The brighter gray level reflects higher density. The organic matter in SEM images has a dark grey color and the brightest gray level represents pyrite. The photomicrographs show that the alginite-rich layers are composed of dark organic matter laminae, quartz grains and platy clay minerals (Figure 4.5.1). The framboidal pyrite is associated with organic matter. The smooth and non-porous surface of the organic matter indicates that kerogen is in the early stages of the oil window or has not yet reached it (Karamov et al. 2021).

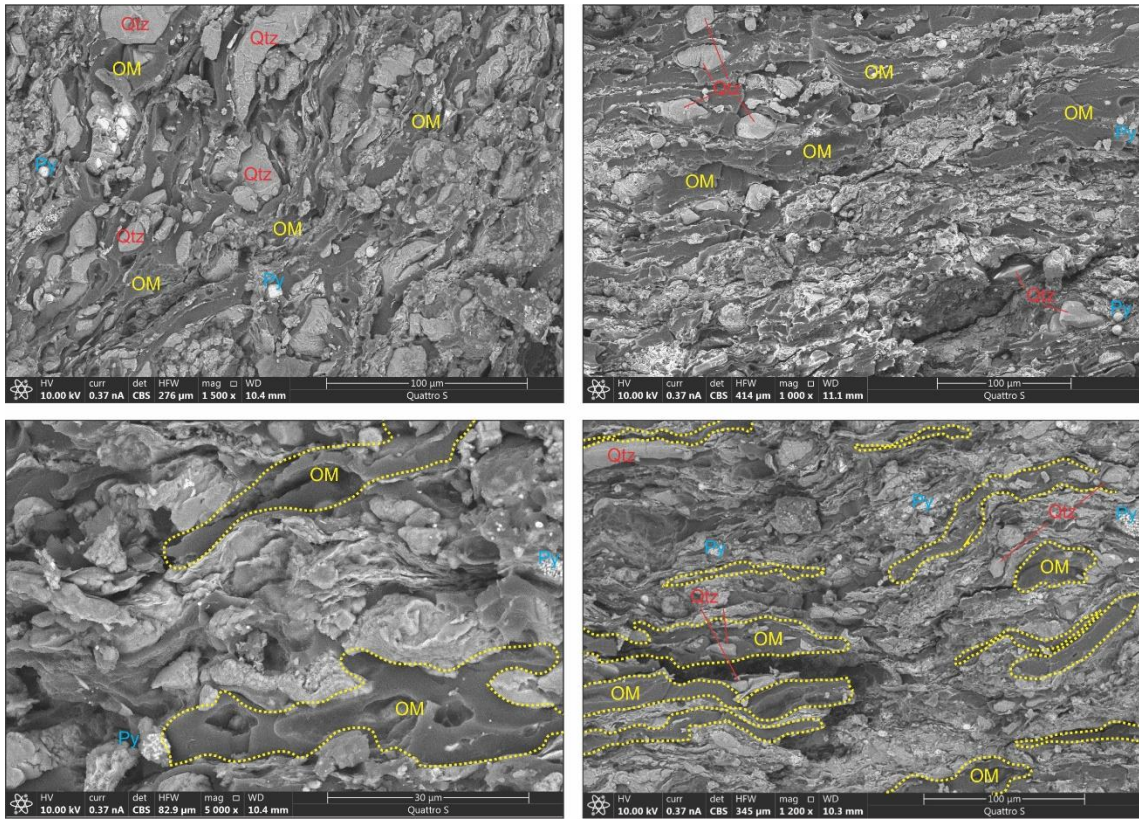


Figure 4.5.1. Back-scattered scanning electron micrographs showing organic and mineral grain morphology of the alginite-rich layers  
Qtz – quartz, OM – organic matter, Py – pyrite

#### 4.6 Stratigraphic occurrence

The alginite-rich layers are discovered and studied in the Bazhenov Formation of the central part of Western Siberia over an area of more than 0.5 million km<sup>2</sup> (Figure 3.1.1). Wells with the founded alginite-rich layers are located in different regions of Western Siberia and are associated with various tectonic units (the Frolovskaya Megadepression, the Krasnoleninsky Arch, the Surgutsky Arch, the Nizhnevartovsky Arch, the Yuganskaya Megadepression, etc.).

In the studied cross-sections of the Bazhenov Formation, luminescent alginite layers are located in organic-rich Member 4 and lie below the luminescent tuff interlayers (Figure 4.6.1). The wide distribution on the territory of the central part of Western Siberia allows using alginite-rich layers and tuff interlayers as marker horizons for stratification of the Bazhenov deposits.

Problems with the Jurassic-Cretaceous boundary are largely the result of stratigraphic difficulties caused by a lack of a faunas. The choice of boundary depends primarily on its correlation potential. Since the alginite-rich layers and tuff interlayers are isochronous and have good correlation through the Bazhenov sequence within the central part of Western Siberia, they can be chosen as the possible Jurassic-Cretaceous boundary.

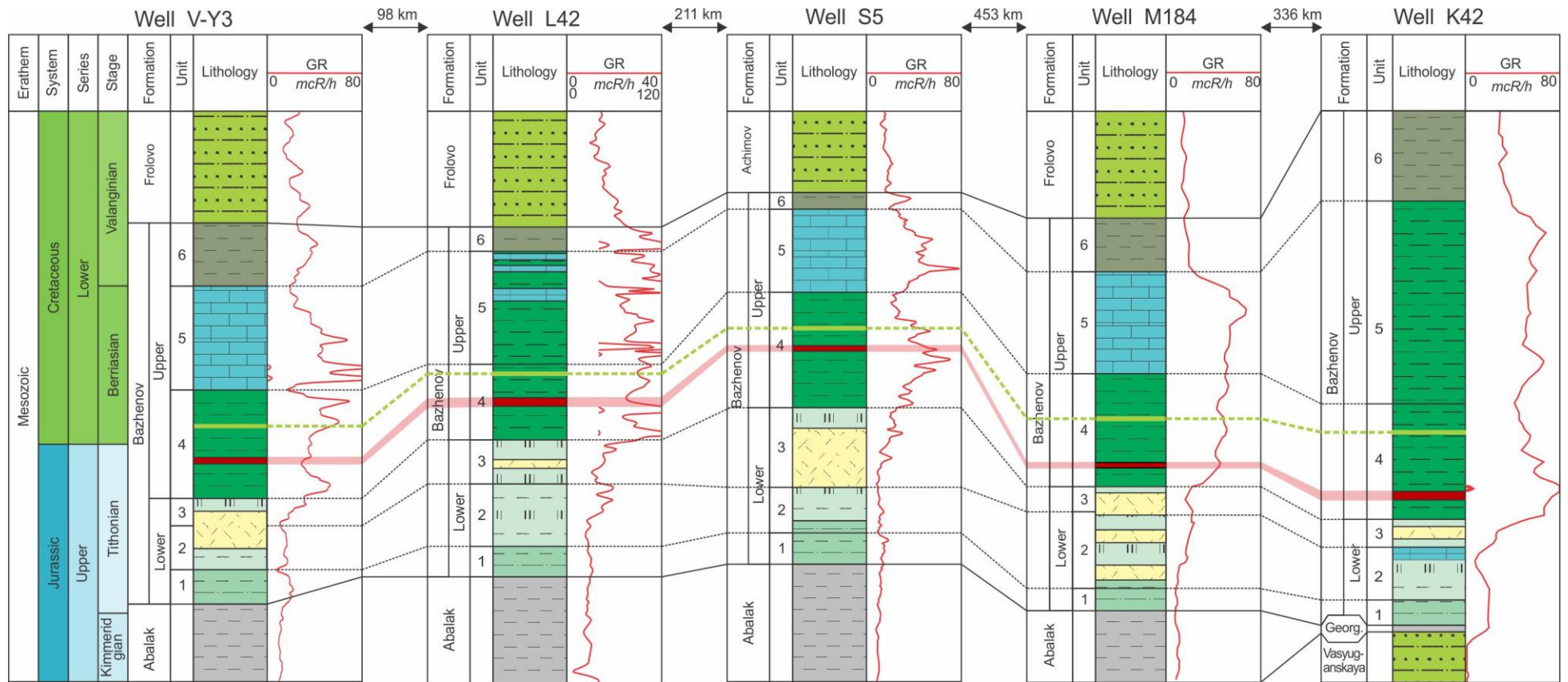


Figure 4.6.1. Correlation of the Bazhenov sequence with the luminescent alginite-rich layers.  
The legends of lithology are the same as those in Figure 3.3.1

#### 4.7 Summary

Alginite-rich layers were discovered by luminescence under UV light. The thickness of the individual layers is up to 50 mm, but the total thickness is up to 1 m in the cross-section (1–5% of the cross-section). Microscopic studies show predominance of organic matter in the constitution of the layers. The mineralogical composition of the alginite-rich layers is dominated by quartz, which is in good agreement with XRF data. The positive correlation between  $\Sigma$ REE and TOC in the alginite-rich layers suggest that the bulk of REE are incorporated in organic matter. Alginite-rich layers are situated in the Member 4 of the Bazhenov Formation and has wide distribution on the territory of the central part of Western Siberia.

## CHAPTER 5. ORGANIC GEOCHEMISTRY, PETROGRAPHY, ISOTOPE CHARACTERIZATION AND DEPOSITION ENVIRONMENT OF THE ALGINITE-RICH LAYERS

### 5.1 Source rock richness

Alginite-rich layers were identified in the Bazhenov Formation based on Rock-Eval pyrolysis for about 5000 samples from different wells drilled in Western Siberia. The alginite-rich layers, examined in 19 wells, have excellent organic richness (TOC=8.19-55.74 wt.%) and excellent hydrocarbon generation potential ( $S_0+S_1+S_2=66.36-524.59$  mg HC/g rock) (Figure 5.1.1a). The host rocks also have high TOC values (6.24-15.76 wt.%) and  $S_2$  (48.49-105.47 mg HC/g rock). However, the TOC vs.  $S_2$  plot shows that the alginite-rich layers have much better hydrocarbon generation potential than host rocks (Figure 5.1.1b).

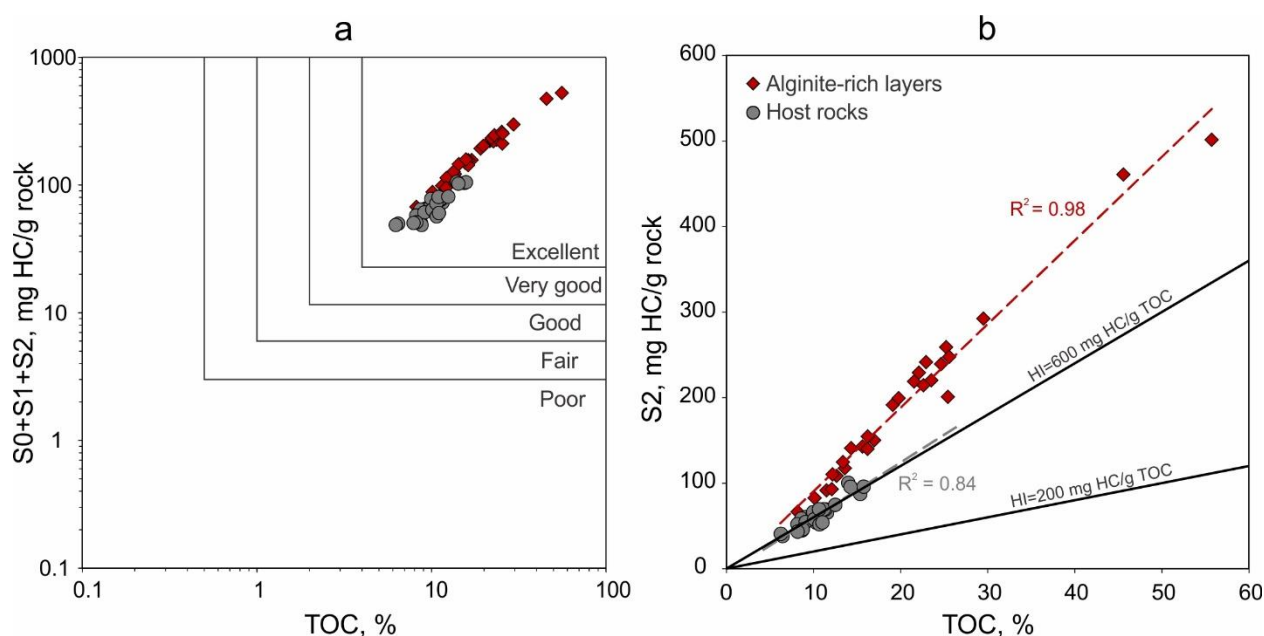


Figure 5.1.1. The  $S_0+S_1+S_2$  vs TOC plot (a) and TOC vs  $S_2$  plot (b) for the alginite-rich layers and host rocks

The geochemical log in Figure 5.1.2 show the Rock-Eval parameters obtained directly on rocks of the Bazhenov Formation. As can be seen from the geochemical logs, the alginite layers occur in organic-rich Member 4 with a high TOC  $\sim 11.8$  wt.%, high HI=480-570 mg HC/g TOC and low OI between 3 and 11 mg  $\text{CO}_2$ /g TOC (Table 5.1.1). The high OI value of 52 mg  $\text{CO}_2$ /g TOC is corresponding to the tuff interlayer (TOC=1.4 wt.%;  $S_2=2.45$  mg HC/g rock). Member 4 of the Bazhenov Formation corresponds to the time of maximum flooding surface, which led to the good preservation of organic matter.

Table 5.1.1. Rock-Eval pyrolysis data for the alginite-rich layers and host rocks

| Sample               |    | S0+S1            | S2               | PI   | TOC   | T <sub>max</sub> | HI              | OI                            | K <sub>goc</sub> | CC    |
|----------------------|----|------------------|------------------|------|-------|------------------|-----------------|-------------------------------|------------------|-------|
|                      |    | mg HC/<br>g rock | mg HC/<br>g rock |      | wt. % | °C               | mg HC/<br>g TOC | mg CO <sub>2</sub> /<br>g TOC | %                | wt. % |
| Alginite-rich layers | 1  | 4.07             | 117.58           | 0.02 | 13.60 | 447              | 864             | 3                             | 76               | 1.18  |
|                      | 2  | 3.76             | 108.73           | 0.02 | 12.66 | 444              | 858             | 5                             | 76               | 0.53  |
|                      | 3  | 5.08             | 82.86            | 0.05 | 10.13 | 438              | 818             | 5                             | 64               | 0.63  |
|                      | 4  | 6.78             | 91.83            | 0.06 | 11.51 | 454              | 798             | 11                            | 73               | 0.54  |
|                      | 5  | 5.59             | 142.99           | 0.04 | 15.62 | 447              | 915             | 1                             | 81               | 0.32  |
|                      | 6  | 6.33             | 150.34           | 0.04 | 16.97 | 449              | 886             | 1                             | 79               | 0.26  |
|                      | 7  | 4.64             | 292.64           | 0.02 | 29.52 | 454              | 991             | 3                             | 86               | 0.64  |
|                      | 8  | 4.81             | 220.43           | 0.02 | 23.55 | 445              | 936             | 3                             | 82               | 0.17  |
|                      | 9  | 1.43             | 154.73           | 0.01 | 16.24 | 441              | 952             | 2                             | 83               | 0.27  |
|                      | 10 | 1.25             | 191.68           | 0.01 | 19.11 | 446              | 1003            | 1                             | 86               | 0.18  |
|                      | 11 | 1.15             | 219.02           | 0.01 | 21.56 | 443              | 1015            | 1                             | 87               | 0.16  |
|                      | 12 | 2.45             | 140.25           | 0.01 | 16.21 | 440              | 865             | 2                             | 76               | 0.14  |
|                      | 13 | 0.58             | 66.78            | 0.01 | 8.19  | 439              | 815             | 4                             | 72               | 0.22  |
|                      | 14 | 3.03             | 110.48           | 0.02 | 12.2  | 450              | 905             | 6                             | 79               | 0.42  |
|                      | 15 | 1.76             | 93.05            | 0.01 | 12.1  | 447              | 769             | 5                             | 69               | 0.37  |
|                      | 16 | 2.30             | 124.83           | 0.01 | 13.39 | 442              | 932             | 5                             | 81               | 0.53  |
|                      | 17 | 4.73             | 239.49           | 0.02 | 24.68 | 440              | 970             | 1                             | 85               | 0.14  |
|                      | 18 | 2.53             | 199.53           | 0.01 | 19.79 | 445              | 1008            | 1                             | 87               | 0.16  |
|                      | 19 | 4.82             | 214.66           | 0.02 | 22.63 | 442              | 948             | 1                             | 83               | 0.16  |
|                      | 20 | 2.71             | 229.29           | 0.01 | 22.12 | 449              | 1036            | 2                             | 89               | 0.73  |
|                      | 21 | 3.24             | 241.65           | 0.01 | 22.94 | 445              | 1053            | 1                             | 91               | 0.48  |
|                      | 22 | 11.15            | 461.11           | 0.02 | 45.61 | 447              | 1011            | 2                             | 88               | 0.21  |
|                      | 23 | 0.81             | 259.24           | 0.00 | 25.25 | 451              | 1026            | 3                             | 88               | 0.64  |
|                      | 24 | 4.20             | 141.13           | 0.02 | 14.33 | 443              | 985             | 5                             | 87               | 0.26  |
|                      | 25 | 3.45             | 154.60           | 0.02 | 15.76 | 443              | 981             | 3                             | 87               | 0.17  |
|                      | 26 | 9.70             | 201.11           | 0.02 | 25.45 | 428              | 790             | 2                             | 71               | 0.24  |
|                      | 27 | 4.61             | 247.86           | 0.01 | 25.59 | 445              | 968             | 3                             | 84               | 0.25  |
|                      | 28 | 23.00            | 501.59           | 0.04 | 55.74 | 439              | 899             | 1                             | 80               | 0.03  |

Table 5.1.1 continued

| Sample     |      | S0+S1            | S2               | PI    | TOC   | T <sub>max</sub> | HI              | OI                            | K <sub>goc</sub> | CC    |
|------------|------|------------------|------------------|-------|-------|------------------|-----------------|-------------------------------|------------------|-------|
|            |      | mg HC/<br>g rock | mg HC/<br>g rock |       | wt. % | °C               | mg HC/<br>g TOC | mg CO <sub>2</sub> /<br>g TOC | %                | wt. % |
| Host rocks | 29   | 6.59             | 59.7             | 0.07  | 10.55 | 438              | 566             | 6                             | 54               | 0.33  |
|            | 30   | 7.08             | 65.68            | 0.06  | 11.57 | 435              | 567             | 4                             | 54               | 0.46  |
|            | 31   | 7.43             | 69.42            | 0.06  | 11.36 | 437              | 611             | 4                             | 58               | 0.31  |
|            | 32   | 5.40             | 45.03            | 0.08  | 8.71  | 437              | 517             | 8                             | 50               | 0.3   |
|            | 33   | 4.28             | 60.58            | 0.05  | 9.16  | 433              | 661             | 8                             | 61               | 0.26  |
|            | 34   | 5.50             | 58.6             | 0.06  | 8.63  | 436              | 679             | 9                             | 64               | 1.07  |
|            | 35   | 5.43             | 52.21            | 0.07  | 8.17  | 433              | 639             | 6                             | 60               | 0.41  |
|            | 36   | 16.12            | 87.44            | 0.10  | 15.38 | 440              | 568             | 4                             | 57               | 0.41  |
|            | 37   | 13.63            | 57.51            | 0.14  | 10.54 | 440              | 545             | 11                            | 58               | 0.28  |
|            | 38   | 12.84            | 54.07            | 0.15  | 10.3  | 440              | 524             | 7                             | 56               | 0.34  |
|            | 39   | 7.25             | 61.02            | 0.11  | 9.89  | 437              | 616             | 2                             | 59               | 0.24  |
|            | 40   | 6.06             | 54.78            | 0.10  | 9.11  | 439              | 601             | 1                             | 57               | 0.29  |
|            | 41   | 7.27             | 69.66            | 0.09  | 11.19 | 440              | 622             | 2                             | 59               | 0.28  |
|            | 42   | 11.51            | 38.25            | 0.23  | 6.45  | 431              | 592             | 5                             | 66               | 0.21  |
|            | 43   | 11.44            | 66.27            | 0.15  | 9.97  | 432              | 664             | 3                             | 67               | 0.22  |
|            | 44   | 7.81             | 40.80            | 0.16  | 6.24  | 432              | 654             | 3                             | 67               | 0.20  |
|            | 45   | 8.79             | 96.02            | 0.06  | 15.76 | 437              | 609             | 2                             | 57               | 0.20  |
|            | 46   | 6.14             | 57.87            | 0.08  | 10.09 | 440              | 573             | 2                             | 54               | 0.13  |
|            | 47   | 4.97             | 100.50           | 0.04  | 13.99 | 438              | 718             | 2                             | 64               | 0.28  |
|            | 48   | 6.52             | 95.82            | 0.04  | 14.25 | 435              | 672             | 2                             | 61               | 0.27  |
|            | 49   | 2.28             | 46.21            | 0.03  | 8.77  | 438              | 527             | 11                            | 48               | 0.11  |
|            | 50   | 2.04             | 69.59            | 0.01  | 10.65 | 444              | 653             | 7                             | 58               | 0.24  |
|            | 51   | 4.72             | 51.93            | 0.05  | 10.69 | 430              | 485             | 3                             | 46               | 0.19  |
|            | 52   | 5.97             | 54.25            | 0.06  | 11.03 | 431              | 491             | 5                             | 48               | 0.18  |
|            | 53   | 7.43             | 43.50            | 0.10  | 8.18  | 434              | 532             | 6                             | 50               | 4.62  |
|            | 54   | 6.67             | 73.77            | 0.09  | 10.98 | 432              | 671             | 2                             | 63               | 0.39  |
|            | 55   | 3.25             | 47.07            | 0.06  | 7.90  | 446              | 596             | 9                             | 56               | 0.33  |
| 56         | 5.67 | 75.17            | 0.07             | 12.49 | 436   | 602              | 3               | 57                            | 0.12             |       |
| 57         | 7.14 | 40.43            | 0.12             | 9.01  | 432   | 448              | 7               | 46                            | 0.18             |       |

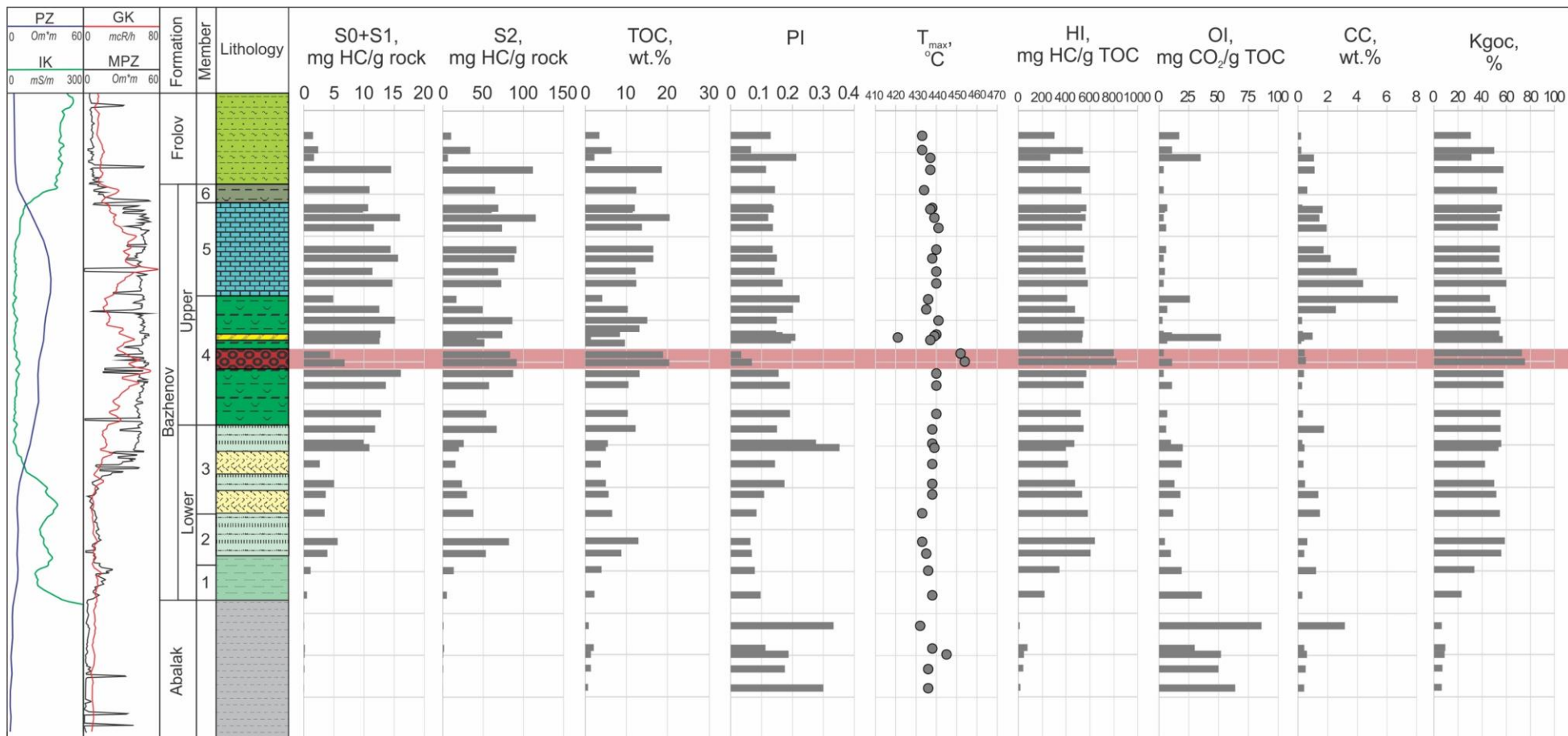


Figure 5.1.2. Geochemical log of well S5.  
 The legends of lithology are the same as those in Figure 3.3.1

## 5.2 Type of kerogen and thermal maturity

The alginite-rich layers are characterized by very high HI (769-1053 mg HC/g TOC), compared to the host rocks. The host rock has different HI depending on the maturity of organic matter. For studied samples of the host rocks HI between 485 and 718 mg HC/g TOC. Therefore, the difference in HI between the alginite-rich layers and host rocks is about 250-500 mg HC/g TOC.

In the modified van Krevelen diagram (HI- $T_{max}$ ), the alginite-rich layers are located in the area that is typical for type I kerogens, while the organic matter of the host rocks is characterized as type II kerogen (Figure 5.2.1a). The type I kerogen of the alginite-rich layers has a high atomic H/C up to 1.88 and a low atomic O/C (0.05–0.07). The kerogen of host rocks is characterized by a high atomic H/C (1.09–1.19) and a low atomic O/C (0.06–0.09) (Figure 5.2.1b).

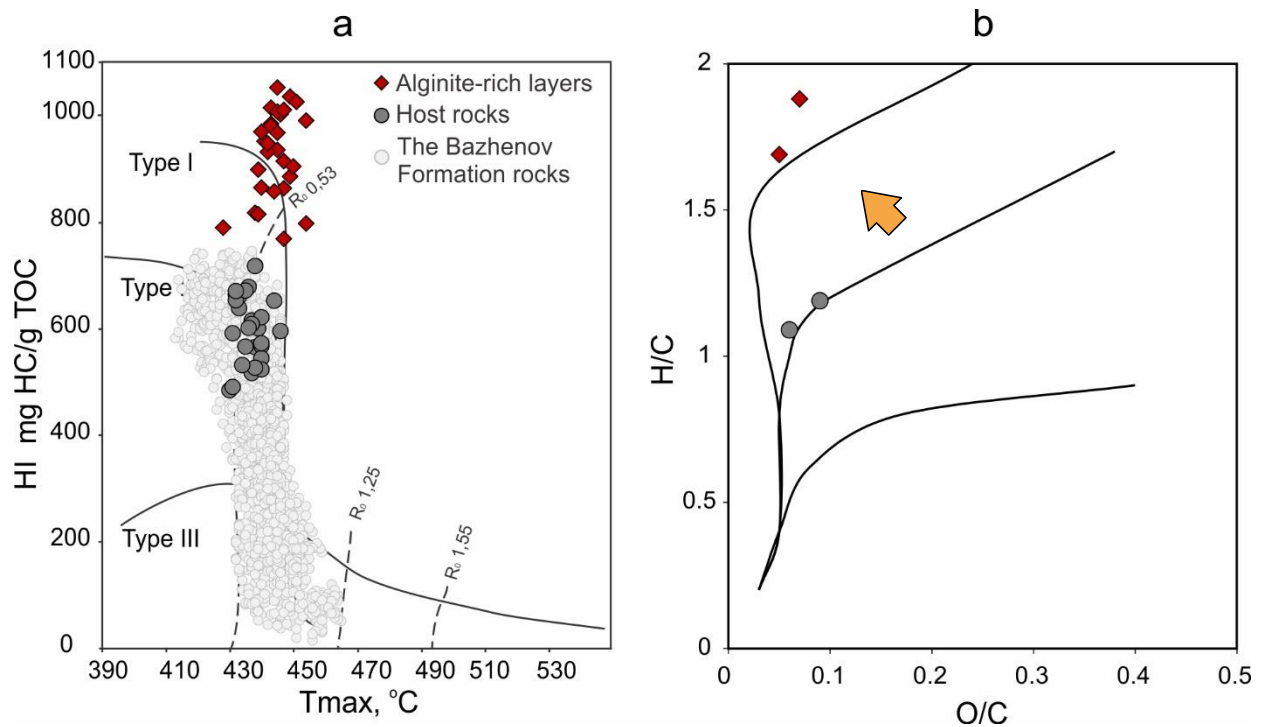


Figure 5.2.1. The HI to  $T_{max}$  plot (a) and H/C to O/C plot (b) showing different type of kerogen for the alginite-rich layers and host rocks

Figure 5.2.2 illustrates a section of a core sample (7 cm thick) with alternating layers of bright and dull luminescent intensities, related to alginite contents. The samples were analyzed by Rock-Eval pyrolysis, and we observed significant variations of the parameters even in such a small interval.

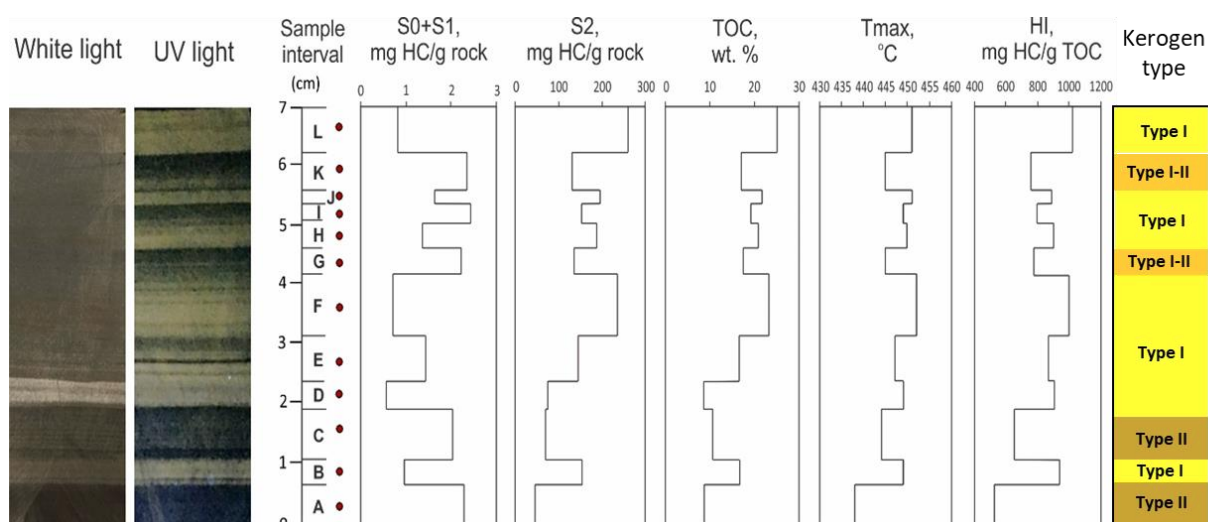


Figure 5.2.2. Detailed (layer-by-layer) Rock-Eval pyrolysis for core sample with interbedding of the alginite-rich layer and hosting organic-rich siliceous rock from well V-K 81. A–L, sampling points

Rock-Eval pyrolysis parameters obtained for the first background Point A (Figure 5.2.2) are common for the Bazhenov Formation rocks; for darker non-luminescent layers, the TOC is 8-11 wt.%; and for the luminescent alginite-rich layers, the TOC is 13-25 wt.%. For the luminescent layers, we observe a significant increase in  $T_{max}$  by 5-11 °C more than the darker ones. The difference in HI for the nearby layers reaches 450 mg HC/g TOC. The amount of free hydrocarbons (S0+S1) changes inversely to S2 and TOC, i.e., for luminescent rocks S2 is high and S0+S1 is low, and *vice versa* for the darker layers. Thus, the layer-by-layer Rock-Eval pyrolysis emphasizes the heterogeneous saturation of the Bazhenov Formation rocks with type I kerogen, which interbeds and mixes with different types of organic matter (type I and type II of kerogen).

The maturity parameters of the alginite-rich layers are inconsistent with each other. At very low PI we observe very high  $T_{max}$  values (Table 5.1.1). These values exceed the corresponding values in the host rocks by 6-14 °C, which reflects the differences in the OM maturation pathways for different kerogen types, provided the OM type remains comparable (Tissot et al., 1987). The organic matter of studied samples from the different wells is characterized from immature (PC3) to early to middle mature (MC1-2).

The alginite-rich layers capable of luminescence are not found in wells with organic matter maturity after the middle mature stage (MC2) (Figure 5.2.3; Figure 5.2.4). Apparently, the alginite-rich layers lose their luminescence after a certain thermal maturity stage. Speight and Huc described samples of type I kerogen that contained algal-bacterial material that was luminescent under UV light at low thermal maturity stages, and the intensity of luminescence gradually decreased and disappeared with maturation (Huc, 2013; Speight, 2020). Therefore, since organic matter reached the middle of the oil window, the luminescence of the alginite-rich layers was

extinguished. The decreasing alginite luminescence at the high maturity level is due to a decrease in the ratios of both hydrogen and oxygen to carbon and increased molecular aromatization (Bertrand et al., 1986; Hackley and Cardott, 2016)

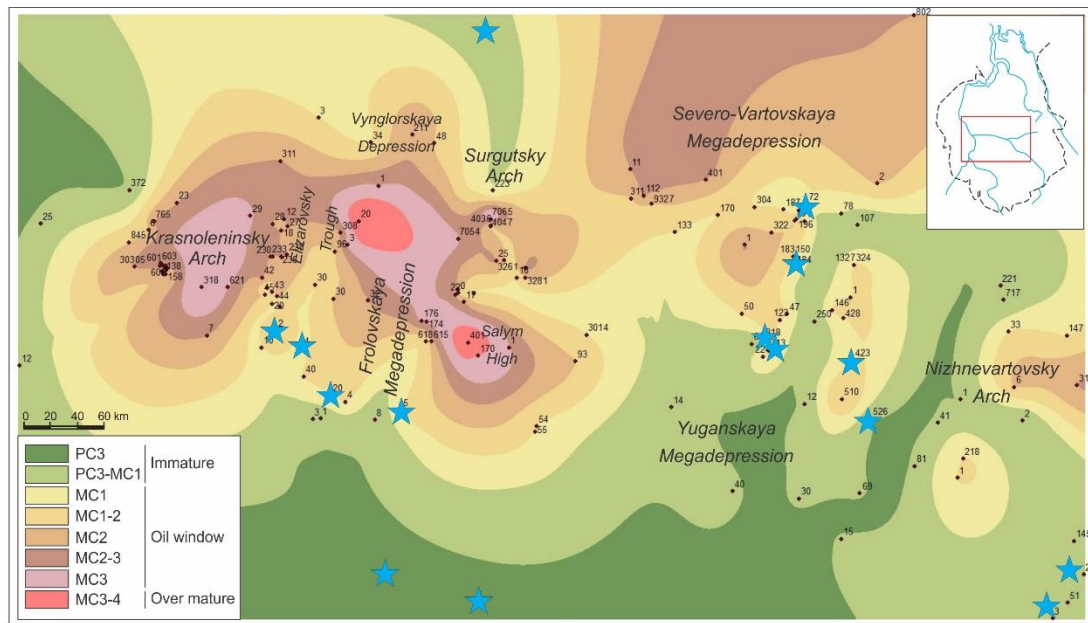


Figure 5.2.3. The location of wells with alginite-rich layers finds (blue stars), mapped on the map of the thermal maturity of the Bazhenov Formation (based on Rock-Eval pyrolysis data Table 3.3.1)

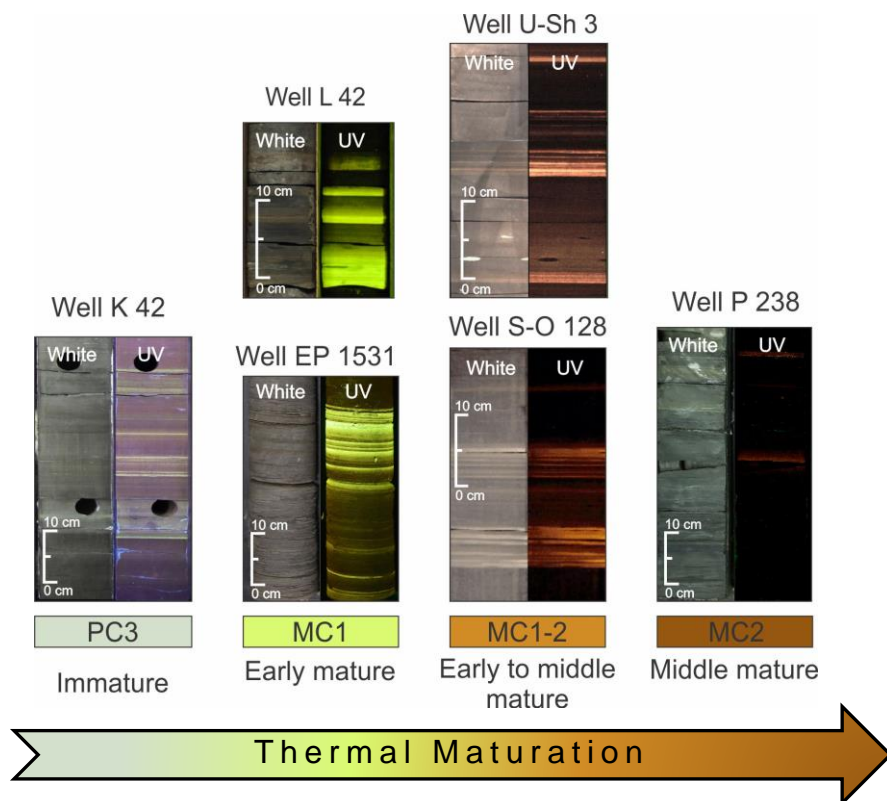


Figure 5.2.4. Color of the luminescent alginite-rich layers in the Bazhenov deposits of different thermal maturity (based on Rock-Eval pyrolysis data Table 3.3.1)

Generally, the luminescent colors of the alginite-rich layers change from a greenish-yellow color to a bright yellow and orange under UV light before luminescence is mostly extinguished at the middle oil window (Figure 5.2.4).

### 5.3 Maceral composition

The organic petrography shows that alginite is a major organic component (40-50 vol.%). The shape of the organic matter has a fan, lumps, and clots morphology. Alginite (telalginite) has a distinctive external form and, in most cases, an internal structure of specific recognizable algal remains. Under reflected white light, alginite is brownish (Figure 5.3.1). During the analysis in the incident fluorescent mode (under UV light), alginite is a greenish-yellow color to bright yellow color (Figure 5.3.1). Therefore, alginite is separated from the amorphous material, i.e., bituminite, which lacks distinctive morphology and originates from the various precursors.

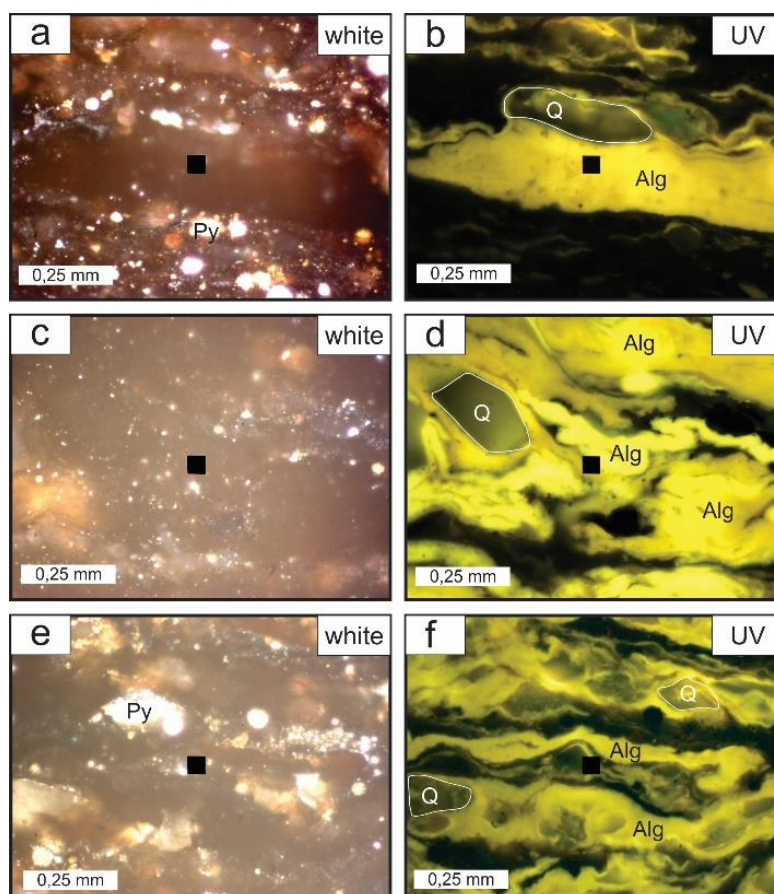


Figure 5.3.1. Photomicrographs illustrating a typical maceral composition of the alginite-rich layers

(a,c,e) Samples under reflected white light shows enrichment of organic matter in mineral matrix. Many colonies contain pyrite; (b,d,f) same samples under UV light shows high intensity yellow luminescence of alginite. Air, magnification of 50× for all photomicrographs. Alg, alginite; Q, quartz; Py, pyrite

Host rocks are characterized by the predominance of bituminite (Figure 5.3.2). The luminescence of bituminite is very weak. Bituminite occurs in the form of lumps, lenses and puffs of various sizes and shapes. In reflected light, it has gray tones.

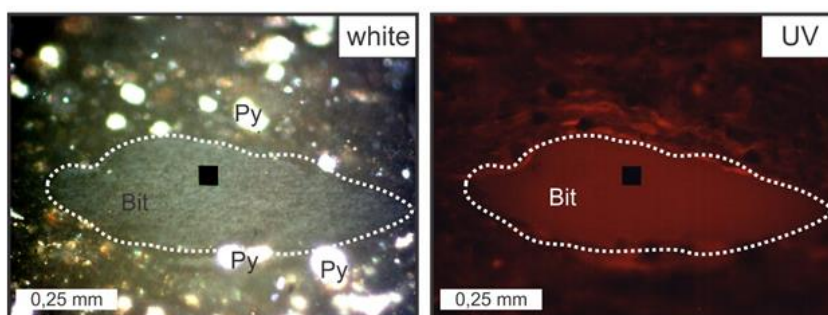


Figure 5.3.2. Photomicrographs illustrating a maceral composition of the host rock. Bit, bituminite; Py, pyrite

#### 5.4 Structural characteristics of kerogen

FTIR spectroscopy was applied to investigate structure of kerogen by analyzing the data for different functional groups. As it was shown above, the alginite-rich layers contain type I kerogen with high HI values and H/C ratio. The host rocks contain type II kerogen also high HI and H/C, but lower than in type I. Identifying types of bonding include the various aliphatic and aromatic carbon-carbon and carbon-hydrogen bonds and oxygen-containing functional groups. In this study, peaks measured from 2990 to 2800  $\text{cm}^{-1}$  and 1470-1450  $\text{cm}^{-1}$  correspond to aliphatic C-H bonds and from 1690 to 1620  $\text{cm}^{-1}$  for aromatic groups. Absorption band frequencies of minerals are characterized by peaks from 1090 to 1040  $\text{cm}^{-1}$  and from 790 to 780  $\text{cm}^{-1}$ .

All spectra of the alginite-rich layers display high aliphatic C-H stretching band peaks (Figure 5.4.1). The samples of the host rocks possess relatively high aromatic ring stretching bands peaks C=C than the samples obtained from the alginite-rich layers.

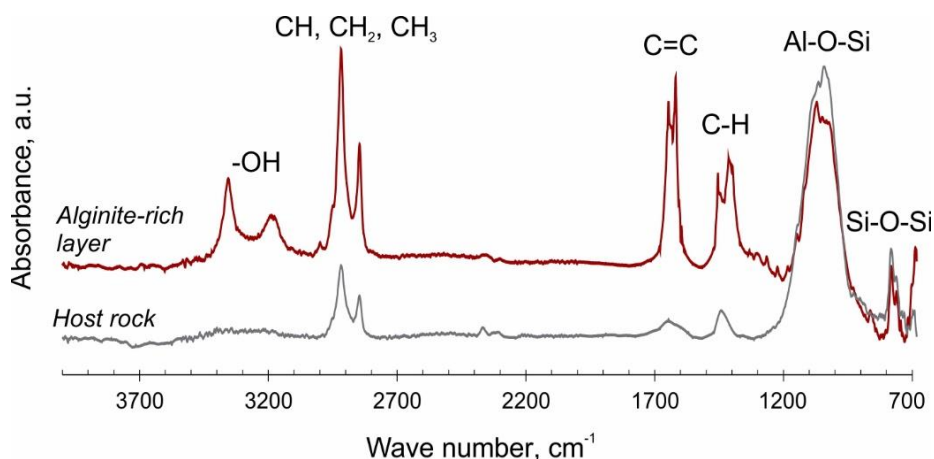


Figure 5.4.1. FTIR spectra of the alginite-rich layers and host rocks

The relatively broad band around  $3350\text{ cm}^{-1}$  is associated with the appearance of hydrogen bonds and -OH groups included in strong hydrogen bonds. However, the existence of hydrate ( $\text{H}_2\text{O}$ ) makes a certain contribution to the intensity of this band. Therefore, FTIR analysis of the layers showed the predominance of aliphatic chain bonds in the structure of organic matter over aromatic structures, which correspond to a high H/C ratio.

## 5.5 Bulk kinetics

The presence of type I kerogen in the alginite-rich layers is confirmed by the bulk kinetic characteristics of the organic matter thermal decomposition. Figure 5.5.1 presents the activation energy distribution for the sample pairs (from the alginite-rich layers and their host rocks).

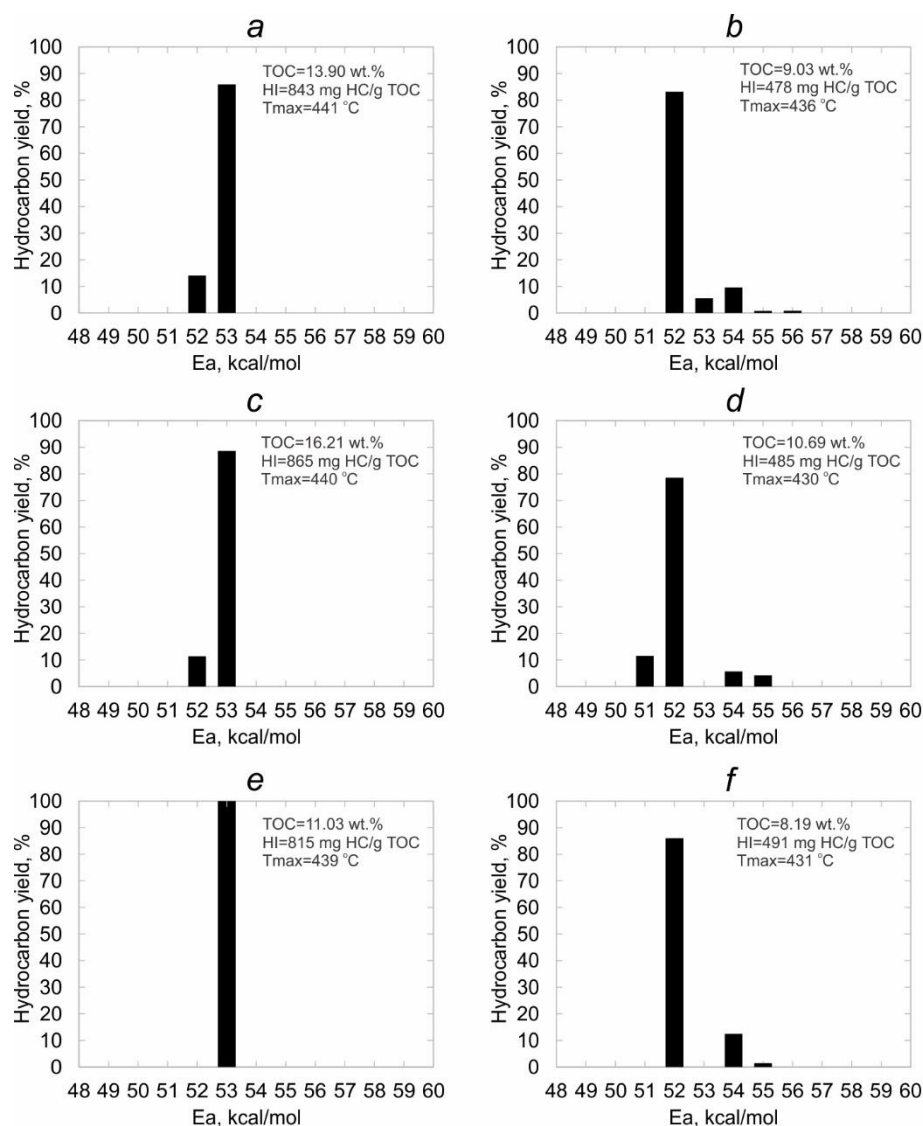


Figure 5.5.1. The distribution of Ea for kerogen of (a, c, e) the alginite-rich layers and (b, d, f) the host rocks.

For all spectra, the frequency factor  $A=1 \times 10^{14}\text{ s}^{-1}$

The spectrum of activation energies is very narrow for the alginite-rich layers and consists mainly of single energy  $E_a = 53$  kcal/mol, which is typical of type I kerogen (Tissot et al., 1987). The form and distribution of  $E_a$  (with a maximum of 52 kcal/mol) are typical of the Bazhenov Formation OM and characterize OM from the host rocks as type II kerogen. Type I kerogen of the alginite-rich layers has a narrower energy range of HC generation in contrast to type II kerogen contained in the host rocks. Therefore, on the geological time scale, organic matter from the alginite-rich layers generates HCs instantly; however, the generation begins later than in the other rocks of the Bazhenov Formation, which is indicated by the shifted  $E_a$  maximum in the histograms of distributed activation energies. Thus, the alginite-rich layers have an improved quality of OM and its generation potential based on pyrolysis parameters, which is reflected in the instantaneous formation of HCs. In contrast, the Bazhenov Formation rocks containing type II kerogen are characterized by a wider interval of the distributed activation energies.

## 5.6 Biomarker analysis

The n-alkanes are specifically useful as tool for organic matter evaluation (Peters et al., 2005). The n-alkanes derive from lipids within living organisms, such as phytoplankton, bacteria or higher plants. Marine organisms are characterized by the lower content of long-chain n-alkanes ( $C_{27}$ - $C_{33}$ ) in comparison with terrestrial ones. Studied samples show a predominance of lower carbon number homologs between the n- $C_{11}$  and n- $C_{20}$ , which are typically attributed to algal and/or cyanobacteria origin (Figure 5.6.1). The  $n-C_{27}/n-C_{17} < 0.24$ , the carbon preference index (CPI) values are close to 1 (Table 5.6.1).

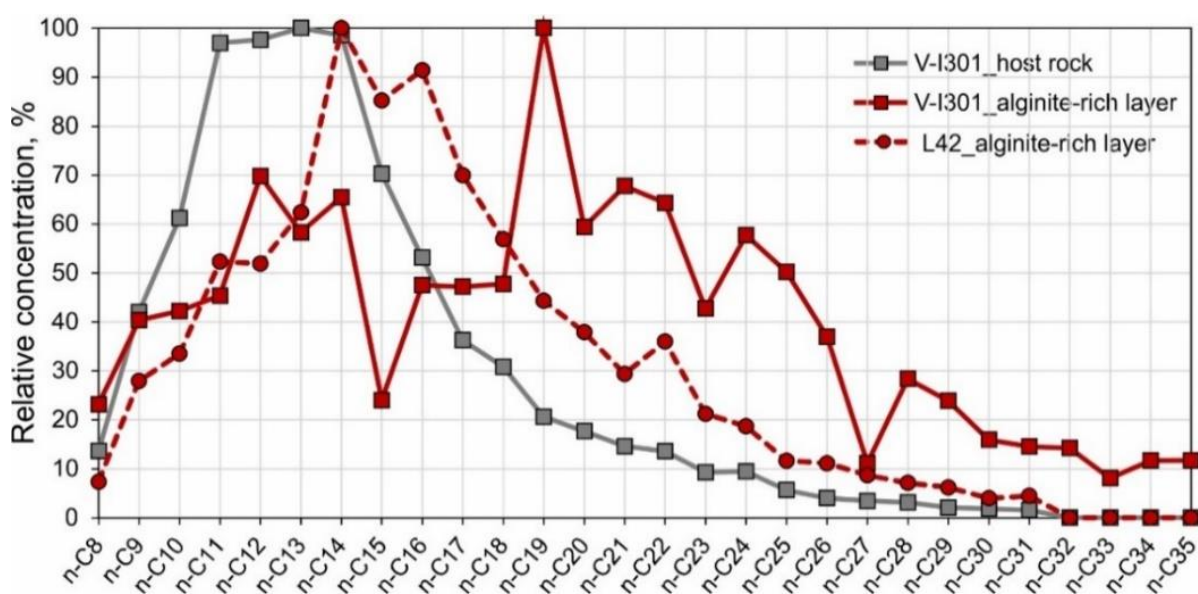


Figure 5.6.1. Distribution pattern of n-alkanes for the alginite-rich layers and host rock

The acyclic isoprenoid hydrocarbons pristane and phytane are widely applied as redox indicators. Differences in Pr/Ph ratio reflect the level of anoxia within the water column. Studied samples of the alginite-rich layers and the host rocks show strongly anoxic depositional conditions (Table 5.6.1). The ratios Pr/n-C<sub>17</sub> and Ph/n-C<sub>18</sub> were used to reflect the type of organic matter, depositional environmental conditions and thermal maturity. The analyzed samples show a high contribution of marine source that was deposited in a reducing environment as demonstrated by Pr/n-C<sub>17</sub><1.12 and Ph/n-C<sub>18</sub><1.43 (Figure 5.6.2a). According to these data and compared to the other Bazhenov host rocks, organic matter is characterized as immature, which is in good agreement with Rock-Eval pyrolysis data.

Table 5.6.1. Selected biomarker ratios and indices for extracts of the alginite-rich layers and

| Parameter   | V-I301<br>Host rock | V-I301<br>Alginite-rich layer | L42<br>Alginite-rich layer |
|---|---------------------|-------------------------------|----------------------------|
| Pr/Ph   | 0.86                | 0.59                          | 0.73                       |
| Pr/n-C <sub>17</sub>                              | 0.72                | 0.79                          | 1.12                       |
| Ph/n-C <sub>18</sub>                              | 1.12                | 1.18                          | 1.43                       |
| K <sub>i</sub>                                    | 0.89                | 1.00                          | 1.28                       |
| CPI   | 0.91                | 1.03                          | 0.90                       |
| n-C <sub>27</sub> /n-C <sub>17</sub>              | 0.09                | 0.24                          | 0.12                       |
| C <sub>27</sub> :C <sub>28</sub> :C <sub>29</sub> | 53:26:21            | 61:23:16                      | 47:39:14                   |
| DBT/Phen  | 0.93                | 0.91                          | 0.93                       |
| 4MDBT/1MDBT                                       | 1.05                | 0.94                          | 0.82                       |
| MPI 1   | 0.76                | 2.14                          | 1.01                       |
| Ts/(Ts+Tm)  | 0.46                | 0.38                          | 0.34                       |
| TA(I)/TA(I+II)                                    | 0.27                | 0.21                          | 0.15                       |

Pr, Pristane, m/z 57; Ph, Phytane, m/z 85; K<sub>i</sub> = (Pr + Ph)/(n-C<sub>17</sub> + n-C<sub>18</sub>), m/z 57; CPI = [(C<sub>17</sub> + C<sub>19</sub> + ... + C<sub>27</sub> + C<sub>29</sub>) + (C<sub>19</sub> + C<sub>21</sub> + ... + C<sub>29</sub> + C<sub>31</sub>)]/2(C<sub>18</sub> + C<sub>20</sub> + ... + C<sub>28</sub> + C<sub>30</sub>), m/z 57; C<sub>27</sub> = C<sub>27</sub>ααα20R sterane/(C<sub>27</sub> + C<sub>28</sub> + C<sub>29</sub>)ααα20R steranes, m/z 217, 218; C<sub>28</sub> = C<sub>28</sub>ααα20R sterane/(C<sub>27</sub> + C<sub>28</sub> + C<sub>29</sub>)ααα20R steranes, m/z 217, 218; C<sub>29</sub> = C<sub>29</sub>ααα20R sterane/(C<sub>27</sub> + C<sub>28</sub> + C<sub>29</sub>)ααα20R steranes, m/z 217, 218; DBT/Phen, dibenzothiophene/phenanthrene, m/z 178, 184; 4MDBT/1MDBT, 4 methylidibenzothiophene/1 methylidibenzothiophene, m/z 198; MPI 1 = 1.5(2-MP + 3-MP)/(P + 1-MP + 9-MP), MP, methylphenanthrene, m/z 192; Ts/(Ts+Tm) = C<sub>27</sub> 18α trisnorhopane / (C<sub>27</sub> 18α trisnorhopane + C<sub>27</sub> 17α trisnorhopane), m/z 191; TA(I)/TA(I+II) = (C<sub>20</sub> + C<sub>21</sub> TA)/(C<sub>20</sub> + C<sub>21</sub> TA + (C<sub>26</sub> + C<sub>27</sub> + C<sub>28</sub> TA)), TA, triaromatic steroids, m/z 231

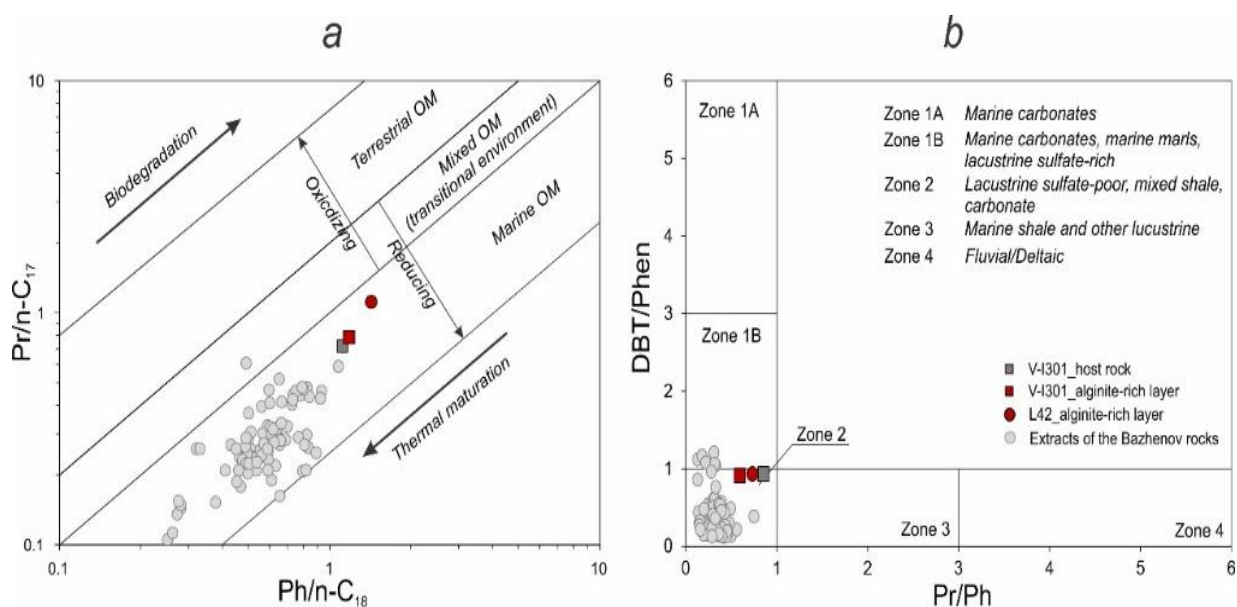


Figure 5.6.2. A cross-plot diagram of (a) Pr/n-C<sub>17</sub> vs. Ph/n-C<sub>18</sub>; (b) DBT/Phen vs. Pr/Ph for the studied samples and extracts of the Bazhenov rocks

The ratios of dibenzothiophene to phenanthrene (DBT/Phen) and Pr/Ph is widely used to interpreted depositional environments and lithology of source rocks (Hughes et al., 1995). The studied samples falls into the zone 2, confirming marine paleoenvironmental interpretations (Figure 5.6.2b). The low DBT/Phen (0.91–0.93) suggests that these values may be affected by iron enrichment in the water column.

The C<sub>27</sub>-C<sub>29</sub> regular steranes are also widely used to conclude the source of organic matter input. In this study, the analyzed samples show a higher proportion of C<sub>27</sub> (47–61 %) than C<sub>28</sub> (23–39 %) and C<sub>29</sub> (14–21 %) regular steranes suggest deposition in open marine environment with a major contribution from phytoplankton.

Thermal maturity indicators, such as K<sub>i</sub>, Ts/(Ts+Tm), 4MDBT/1MDBT and TA(I)/TA(I+II) are widely used for evaluation of maturity of the Bazhenov Formation organic matter (Goncharov et al., 2021). The high K<sub>i</sub> (0.89-1.28) and low Ts/(Ts+Tm) from 0.34 to 0.46 suggest low thermal maturity (Figure 5.6.3a). The plot of TA(I)/TA(I+II) vs. 4MDBT/1MDBT also indicate immature organic matter for studied samples (Figure 5.6.3b).

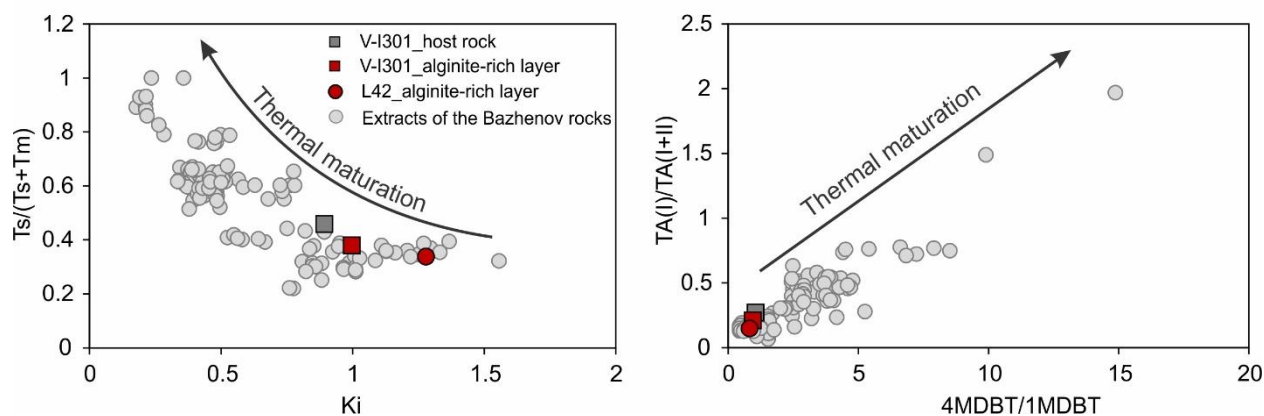


Figure 5.6.3. Relationships between different thermal maturity parameters in the studied samples and extracts of the Bazhenov Formation rocks

Therefore, composition of mobile extractable organic matter is close for the alginite-rich layers and host rocks, probably, due to the millimeter thickness. Thermally immature organic matter of the alginite-rich layers compared to host rocks organic matter has not generated enough hydrocarbons to be elated yet.



## 5.7 Pyrolysis products

The results of the pyrolysis-gas chromatography/mass spectrometry provide us with information about the quantitative and qualitative chemistry of the thermal decomposition products from the cracking of kerogen (Horsfield, 1989). This method provides a direct indicator for the geochemical typing of kerogens and types of hydrocarbons that can be generated during thermal maturation. A comparison of the aliphatic and aromatic nature of kerogens has been previously described in previous studies (Dembicki, 2009).

Numerous compound hydrocarbon classes have been found in pyrolysis products of kerogen, including light hydrocarbons C<sub>1</sub>-C<sub>7</sub>; n-alkanes C<sub>8</sub>-C<sub>40</sub>; unsaturated HC; naphthenes; and mono-, di-, tri- and poly-aromatic compounds (Table 5.7.1). Type I kerogen of the alginite-rich layers produces dominantly long-chain n-alkanes and n-alkenes, whereas type II kerogen of host rocks produces more unsaturated HC, naphthenes, and aromatic compounds (Figure 5.7.1). These differences are also reflected in the elemental composition.

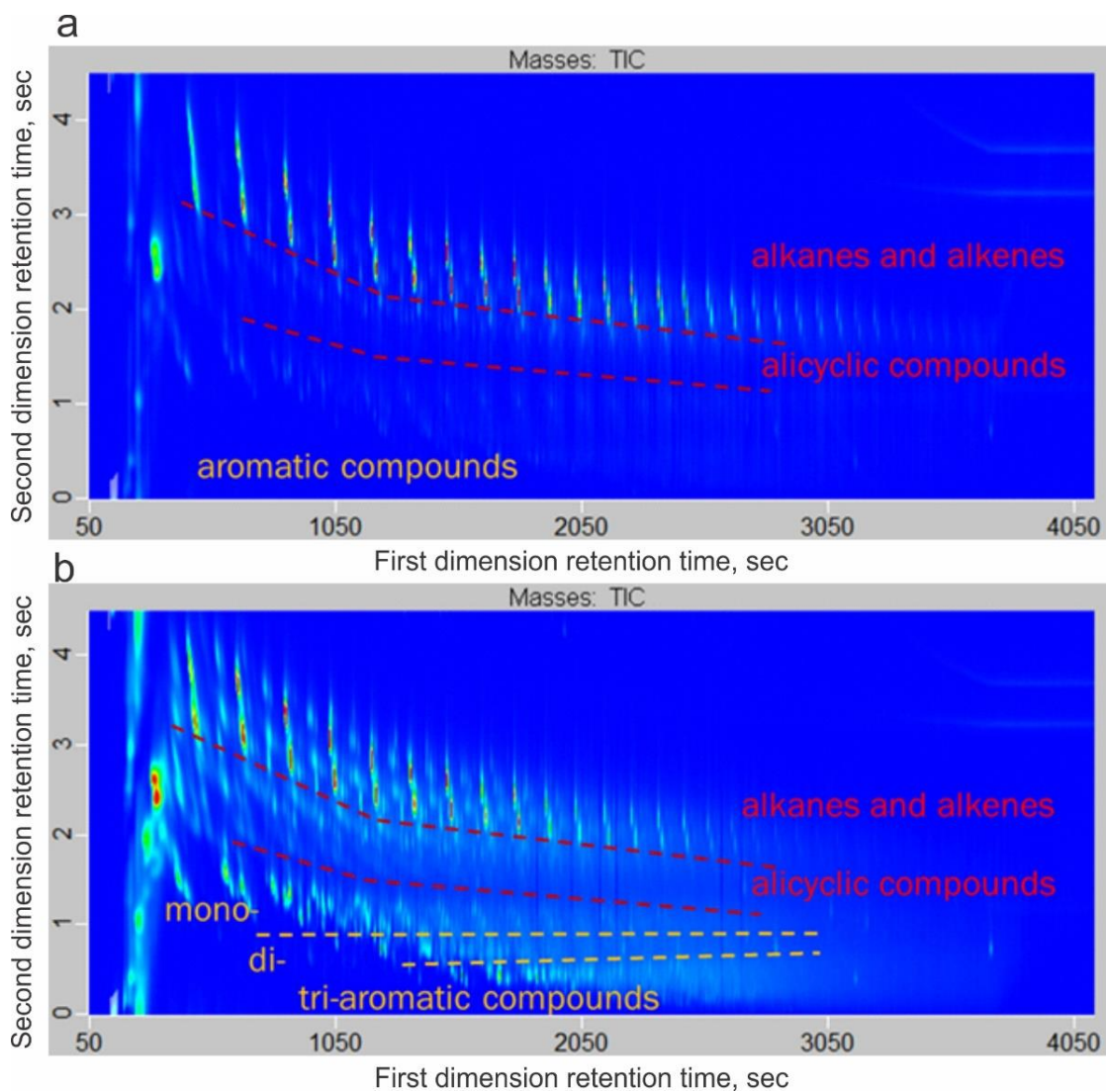


Figure 5.7.1. Two-dimensional total ion chromatograms (TIC) of kerogen cracking products (500°C) for the alginite-rich layers (a) and host rocks (b)

Table 5.7.1. Distribution of HC classes from Pyro-GC×GC-TOF MS/FID for the alginite-rich layers and host rocks

| Hydrocarbon Classes (% w/w)             | Well S-O 128 |                     | Well V-I 301 |                     |
|---|--------------|---------------------|--------------|---------------------|
|   | Host rock    | Alginite-rich layer | Host rock    | Alginite-rich layer |
| Light HC C <sub>1</sub> -C <sub>7</sub> | 7            | 6                   | 19           | 8                   |
| n-Alkanes C <sub>8-40</sub>             | 8            | 25                  | 25           | 33                  |
| Unsaturated HC and naphthenes           | 37           | 64                  | 29           | 53                  |
| Mono-aromatic compounds                 | 21           | 4                   | 19           | 4                   |
| Di-aromatic compounds                   | 15           | 1                   | 7            | 1                   |
| Tri- and poly-aromatic compounds        | 12           | 0                   | 1            | 1                   |
| Aliphatic/Aromatic                      | 52/48        | 95/5                | 73/27        | 94/6                |

The abundance of aliphatic compounds in the pyrolysis products of type I kerogen are in good agreement with the FTIR data and high H/C ratios and suggest the generation of light crude oils.

## 5.8 C, N and S isotope composition of whole rock samples

Among geochemical data, the isotope composition of carbon, nitrogen, and sulfur in rocks enables the genesis estimation of organic matter. Table 5.8.1 shows the results of stable isotope studies of carbon, nitrogen and sulfur.

Table 5.8.1. Bulk C, N and S elemental and isotope composition for the alginite-rich layers and host rocks

| Type of sample       | Sample | $C_{org}/N_{tot}$ | $C_{org}$ , wt. % | $\delta^{13}C_{org}$ , ‰ PDB | $N_{tot}$ , wt. % | $\delta^{15}N_{tot}$ , ‰ AIR | $S_{tot}$ , wt. % | $\delta^{34}S_{tot}$ , ‰ CDT |
|----------------------|--------|-------------------|-------------------|------------------------------|-------------------|------------------------------|-------------------|------------------------------|
| Alginite-rich layers | 21     | 93.37             | 19.57             | -31.5                        | 0.21              | 5.9                          | 2.31              | -6.0                         |
|                      | 14     | 103.28            | 11.85             | -31.8                        | 0.11              | 7.7                          | 1.61              | -18.5                        |
|                      | 13     | 109.57            | 7.67              | -31.8                        | 0.07              | 17.5                         | 2.75              | -11.2                        |
|                      | 11     | 155.50            | 23.33             | -31.1                        | 0.15              | 25.7                         | 1.37              | -9.3                         |
|                      | 18     | 76.83             | 16.14             | -31.9                        | 0.21              | 13.0                         | 2.10              | -7.1                         |
|                      | 22     | 193.35            | 50.27             | -31.2                        | 0.26              | 4.9                          | 4.37              | -12.0                        |
|                      | 16     | 81.91             | 27.85             | -31.5                        | 0.34              | 4.5                          | 3.43              | -6.9                         |
|                      | 27     | 119.10            | 23.82             | -31.3                        | 0.20              | 4.2                          | 2.28              | -10.2                        |
| 24                   | 107.36 | 15.03             | -31.4             | 0.14                         | 6.4               | 2.31                         | -13.5             |                              |
| Host rocks           | 58     | 43.84             | 17.81             | -31.4                        | 0.37              | 0.9                          | 4.36              | -17.3                        |
|                      | 57     | 23.36             | 7.71              | -31.8                        | 0.33              | 3.5                          | 2.95              | -21.8                        |
|                      | 59     | 43.54             | 12.30             | -30.5                        | 0.34              | 3.2                          | 3.71              | -34.9                        |
|                      | 52     | 42.23             | 11.03             | -31.9                        | 0.24              | 5.4                          | 4.18              | -26.0                        |
|                      | 60     | 47.66             | 13.64             | -31.8                        | 0.29              | 3.6                          | 2.93              | -21.6                        |
|                      | 61     | 45.42             | 12.83             | -32.2                        | 0.28              | 3.8                          | 3.12              | -29.0                        |

The isotope composition of carbon in the kerogen of the alginite-rich layers and the host rocks is characterized by a similar concentration of the  $^{13}C$  carbon isotope (Figure 5.8.1a). The  $\delta^{13}C_{org}$  varies from  $-31.1$  to  $-31.9$ ‰ for the alginite-rich layers and from  $-30.5$  to  $-32.2$ ‰ for the host rocks. These values are typical of the initial marine organic matter that formed the kerogen in the Bazhenov Formation (Kontorovich et al., 2019). The carbon isotope composition for the alginite-rich layers varies in the range from  $-31.1$  to  $-31.9$ ‰, while for the host rocks  $\delta^{13}C_{org}$  it varies from  $-30.5$  to  $-31.9$ ‰.

The nitrogen concentration in the alginite-rich layers and the host rocks ranges from 0.07 to 0.37 wt %; for all samples from the alginite-rich layers, we recorded lower values compared to the host rocks (in 1.5–2 times). The values of  $\delta^{15}N_{tot}$  vary from 0.9 to 5.4‰ for the host rocks at a nitrogen concentration from 0.24 to 0.37 wt %. The alginite-rich layers have  $^{15}N$  enrichment, e.g., the values of  $\delta^{15}N_{tot}$  are 5.9–25.7‰ at a nitrogen concentration from 0.07 to 0.21 wt %. The C/N ratios correlate directly with increased heaviness of nitrogen isotope composition (Figure 5.8.1b). The alginite-rich layers has very low N content compared to carbon, this suggests diagenetic changes. Nitrogen and other easily degradable organic compounds were utilized by bacteria,

whereas the refractory organic carbon was preserved. The wide range of  $\delta^{15}\text{N}_{\text{tot}}$  values, probably, indicates diagenetic changes alternating in different localities, related to bacterial activity.

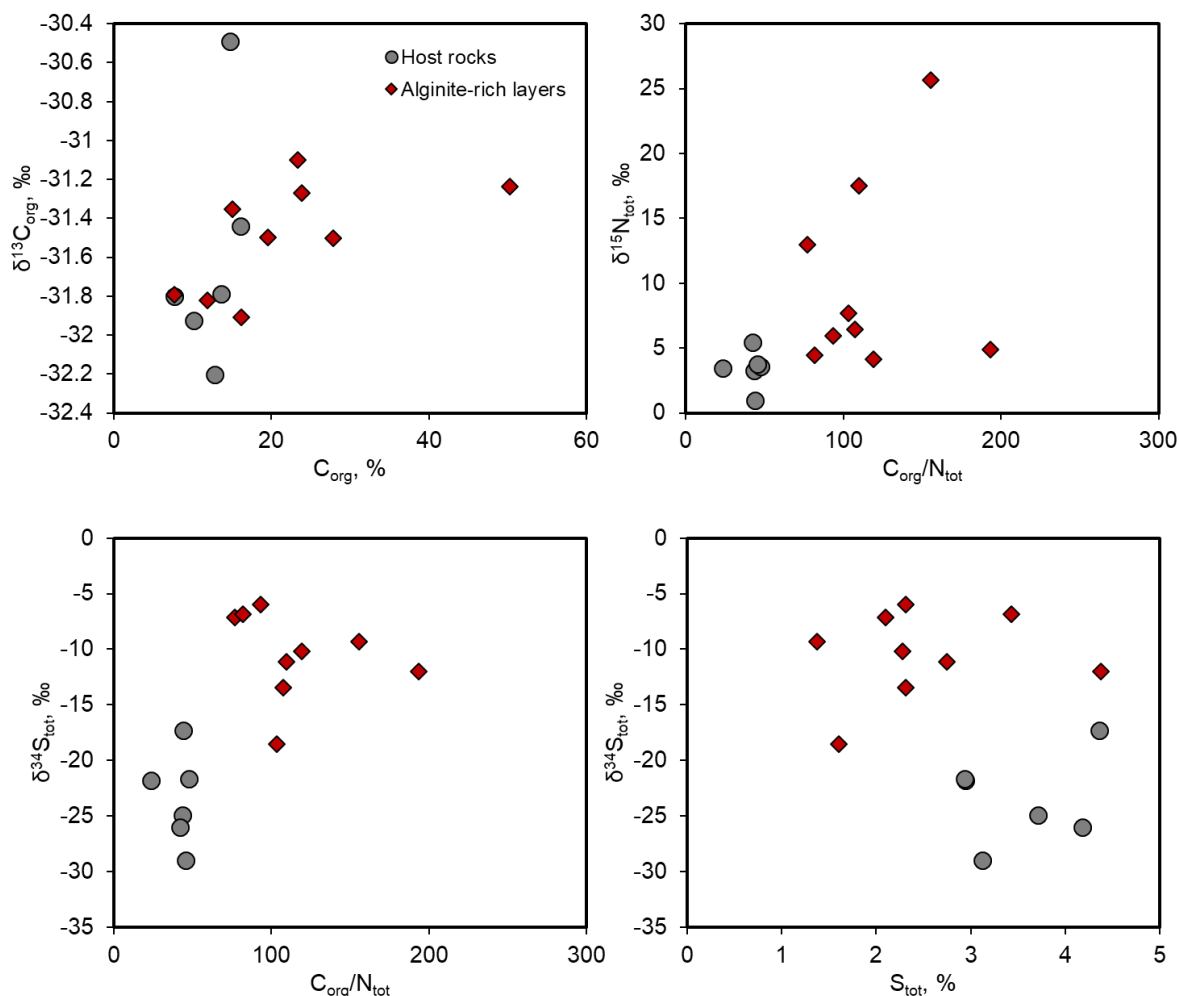


Figure 5.8.1. Plots of (a)  $\delta^{13}\text{C}_{\text{org}}-\text{C}_{\text{org}}$ , (b)  $\delta^{15}\text{N}_{\text{tot}}-\text{C}_{\text{org}}/\text{N}_{\text{tot}}$ , (c)  $\delta^{34}\text{S}_{\text{org}}-\text{C}_{\text{org}}/\text{N}_{\text{tot}}$ , and (d)  $\delta^{34}\text{S}_{\text{tot}}-\text{S}_{\text{tot}}$  for studied samples

The  $\delta^{15}\text{N}$  values are exceptionally high compared to other lacustrine and marine depositional environments (Figure 5.8.2). The most important biogeochemical processes that can fractionate nitrogen isotopes are: nitrification ( $\text{NH}_4^+$  to  $\text{NO}_2^-$  and further to  $\text{NO}_3^-$ ), denitrification ( $\text{NO}_3^-$  to  $\text{N}_2$ ), assimilation of  $\text{NH}_4^+$ , dissociation ( $\text{NH}_4^+$  to  $\text{NH}_3$ ) and volatilization of  $\text{NH}_3$  gas (Ryabenko, 2013). Denitrification and  $\text{NH}_3$  volatilization lead to a strong positive excursion of  $\delta^{15}\text{N}$  values and nitrogen loss. However, both processes cannot be strictly distinguished from each other only based on  $\delta^{15}\text{N}$  values. Thus, we can assume that the microbial biomass of the Bazhenov alginite-rich sediments was prone to strong denitrification and/or  $\text{NH}_3$  volatilization. This contributed to the outstanding isotopic and geochemical composition of type I kerogen in the Bazhenov Formation.

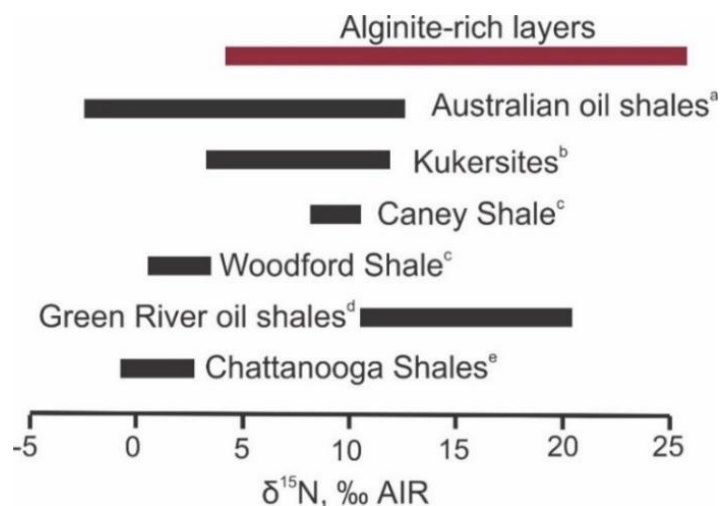


Figure 5.8.2. Ranges of measured  $\delta^{15}\text{N}$  values for a different shale samples

(a) from Rigby and Batts 1986; (b) from Kiipli and Kiipli 2013; (c) from Quan et al. 2013; (d) from Tuttle M.L. 1973; (e) from Tuite, Williford, and Macko 2019



The content and isotope composition of total sulfur are also different in the alginite-rich layers and the host deposits. For the alginite-rich layers, the values of  $\delta^{34}\text{S}_{\text{tot}}$  vary from  $-6.0$  to  $-18.5\text{‰}$  at a total sulfur concentration from 1.37 to 2.75 wt % (Figure 5.8.1c, d). The host rocks showed the dominance of light-weight sulfur, while  $\delta^{34}\text{S}_{\text{tot}}$  varied from  $-17.3$  to  $-29.0\text{‰}$  at  $\text{S}_{\text{tot}}$  ranging from 3.71 to 4.36 wt %. The alginite-rich layers are characterized by the heavier values of  $\delta^{34}\text{S}_{\text{tot}}$ , which reflects, probably, their more oxidizing depositional environments compared to the host rocks.

Thereby, the algae grew and was subjected to the early diagenesis in oxic waters and after burial the diagenesis continued in the anoxic environment.

## 5.9 CSIA of individual n-alkanes

The CSIA of n-alkanes provides unique information about hydrocarbons. The n-alkanes of the studied extracts mainly has a fairly light isotopic carbon composition, the  $\delta^{13}\text{C}$  values of individual alkanes lie mainly in the range of  $-30.0$  to  $-32.0\text{‰}$  and typically for marine OM of the Bazhenov Formation (Table 5.9.1; Figure 5.9.1). Normal alkanes from  $\text{C}_{17}$  to  $\text{C}_{22}$  are commonly depleted in  $^{13}\text{C}$ . For homologues in the n- $\text{C}_{23}$  to n- $\text{C}_{30}$  range has the irregular slope in the n- $\text{C}_{25}$  to n- $\text{C}_{31}$  region.

For the oil sample,  $\delta^{13}\text{C}$  values are in the range of  $-27.49$  to  $-32.02\text{‰}$ . The oil sample has a negatively sloping curve up to n- $\text{C}_{26}$  and an irregular positive slope for n-alkanes with longer chain lengths.

The carbon isotope ratios of short-chain n-alkanes in the Bazhenov oil are higher than those in extracts of the alginite-rich layers and host rock. The increasing of the  $\delta^{13}\text{C}$  values of n-alkanes

in the oil in comparison to the extracts is apparently due to the staged of hydrocarbon generation. Hydrocarbon fluids of the first generation usually are enriched in isotopically light carbon. This is due to it taking slightly less energy to break bonds between the lightest (and most commonly occurring) isotopes; for example, the  $^{12}\text{C}-^{12}\text{C}$  bond is weaker than the  $^{12}\text{C}-^{13}\text{C}$  bond.

Table 5.9.1. Individual carbon isotopic compositions and standard deviation of n-alkanes for extracts and oil

| n-alkane          | Alginite-rich layers extracts  |          |                                |          | Host rock extract              |          | Bazhenov oil                   |          |
|-------------------|--------------------------------|----------|--------------------------------|----------|--------------------------------|----------|--------------------------------|----------|
|                   | 7                              |          | 12                             |          | 62                             |          | P218                           |          |
|                   | $\delta^{13}\text{C}$ , ‰ VPDB | Std.dev. |
| n-C <sub>13</sub> | -                              | -        | -                              | -        | -27.49                         | 0.17     | -                              | -        |
| n-C <sub>14</sub> | -                              | -        | -                              | -        | -30.31                         | 0.48     | -                              | -        |
| n-C <sub>15</sub> | -                              | -        | -                              | -        | -31.16                         | 0.15     | -                              | -        |
| n-C <sub>16</sub> | -                              | -        | -30.08                         | 0.11     | -31.37                         | 0.39     | -                              | -        |
| n-C <sub>17</sub> | -                              | -        | -31.02                         | 0.41     | -31.52                         | 0.25     | -                              | -        |
| n-C <sub>18</sub> | -30.96                         | 0.65     | -31.11                         | 0.17     | -31.74                         | 0.23     | -29.08                         | 0.05     |
| n-C <sub>19</sub> | -31.49                         | 0.10     | -31.55                         | 0.17     | -31.72                         | 0.42     | -29.47                         | 0.22     |
| n-C <sub>20</sub> | -31.74                         | 0.02     | -31.61                         | 0.17     | -31.81                         | 0.42     | -30.28                         | 0.41     |
| n-C <sub>21</sub> | -31.40                         | 0.42     | -31.38                         | 0.60     | -31.84                         | 0.39     | -30.14                         | 1.13     |
| n-C <sub>22</sub> | -31.45                         | 0.01     | -31.36                         | 0.46     | -31.53                         | 0.32     | -30.03                         | 0.03     |
| n-C <sub>23</sub> | -30.64                         | 0.59     | -30.68                         | 1.04     | -31.79                         | 0.11     | -30.56                         | 0.09     |
| n-C <sub>24</sub> | -30.74                         | 0.58     | -31.33                         | 0.01     | -32.02                         | 0.12     | -30.69                         | 0.07     |
| n-C <sub>25</sub> | -30.40                         | 0.59     | -31.61                         | 0.60     | -31.16                         | 0.29     | -30.50                         | 0.10     |
| n-C <sub>26</sub> | -31.01                         | 0.30     | -31.22                         | 0.63     | -31.02                         | 0.29     | -31.01                         | 0.30     |
| n-C <sub>27</sub> | -30.07                         | 0.73     | -29.77                         | 1.97     | -30.27                         | 0.50     | -30.81                         | 0.04     |
| n-C <sub>28</sub> | -29.13                         | 1.45     | -30.54                         | 0.64     | -30.50                         | 0.22     | -29.93                         | 0.30     |
| n-C <sub>29</sub> | -29.27                         | 1.19     | -30.11                         | 0.20     | -30.08                         | 0.78     | -30.50                         | 0.54     |
| n-C <sub>30</sub> | -30.66                         | 0.89     | -30.54                         | 0.033    | -30.74                         | 0.41     | -29.78                         | 0.98     |
| n-C <sub>31</sub> | -29.64                         | 0.46     | -30.71                         | 1.03     | -30.05                         | 1.51     | -31.35                         | 0.80     |

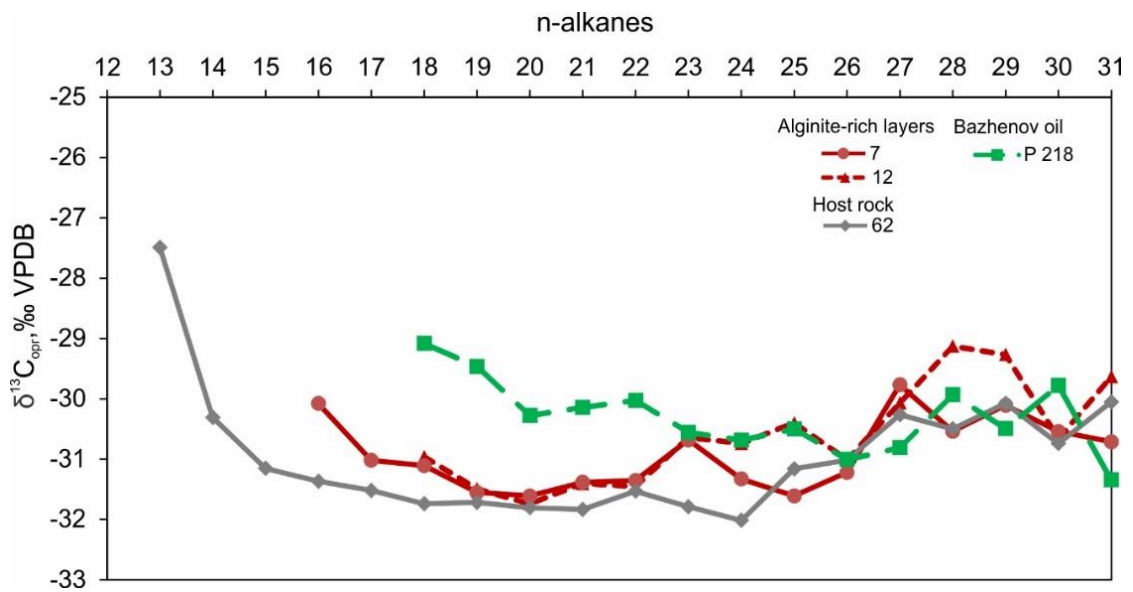


Figure 5.9.1. Curves of n-alkane carbon isotopes

According to published data, for the Bazhenov oils are common negative  $\delta^{13}\text{C}$  values from -31.41 to -33.88 ‰ and a positive slope curve (Liu et al., 2016). Stable isotopes of the n-alkanes in oils with a small contribution from the Tyumen source rocks show  $^{13}\text{C}$ -rich values compared to oils from the Bazhenov Formation. Therefore, the studied Bazhenov oil sample (P218) also possibly has some contribution from the Tyumen source rocks.

#### 5.10 Depositional environment and origin

The obtained results indicate the algal nature of the studied luminescent alginite-rich layers of the Bazhenov Formation. Geochemical studies confirm the presence in these layers of "pure" type I kerogen, which is "diluted" by type II during the transition to the host silicites of the Bazhenov Formation.

The most widely known alginite-contain deposits are lacustrine sapropels. In addition to typical lacustrine sapropels, there are examples of saltwater marine basins (for example, the Black and Mediterranean Seas), but in them, sapropel sediments are associated with stagnant hydrogen sulfide conditions, which is typical for the entire Bazhenov basin and does not explain the concentrated interlayers of type I kerogen.

High bioproductivity, development and accumulation of sapropelic matter are possible in areas of deep water upwelling. Due to the rise of cold waters from the depth, intensive development of phytoplankton, its death and fossilization occur. However, the upwelling proposal is contradicted by the wide areal distribution and "simultaneity" of the described layers, as well as confinement to the central parts of the paleobasin.

Another possible scenario for the formation of the alginite-rich layers can be outbreaks of phytoplankton development on nutrient from aeolian transport. In the south and southwest of the Bazhenov paleosea, a semi-arid climate is dominated by the development of coastal deserts. The episodic removal of desert material into the basin by sandstorms ensured the supply of clay minerals, humus, microelements, and detrital quartz to the central parts of the basin and the warming of the upper layers of water as a result of the spread of warm air masses. The quartz of the alginite layers has a specific morphology, is not found in other rocks of the Bazhenov Formation, and has similar shapes to the clastic material of eolian rafting (Khotylev et al., 2019). The supply of nutrients could provoke outbreaks of phytoplankton development – algal blooms, which quickly faded due to the depletion of the supply of introduced nutrients.

The formation of alginite-rich layers can also be associated with the activity of paleovolcanoes. The presence of pyroclastics in the rocks of the Bazhenov formation was repeatedly indicated in many works (Van and Kazanskiy, 1985; Bulatov et al., 2017; Panchenko et al., 2021). Volcanic ash can be a nutrient medium for the development of various cyanobionts

and symbiotic algal colonies (Fujimura et al., 2011). The oddly shaped quartz particles present in the layers appear to be crystallized volcanic glass.

Also, the supply of a large amount of nutrients may be associated with an actively developing marine transgression. Marine transgression leading to sea level rise and expansion of the Bazhenov epicontinental sea. The rapid flooding of coastal areas could lead to a sharp increase in the content of nutrients in the water, ensuring the prosperity of marine biota. Member 4 of the Bazhenov Formation where alginite-rich layers were found represents the maximum of the marine transgression during Jurassic-Cretaceous. The central part of Western Siberia in the Tithonian was the deepest part of the sea (Figure 5.10.1).

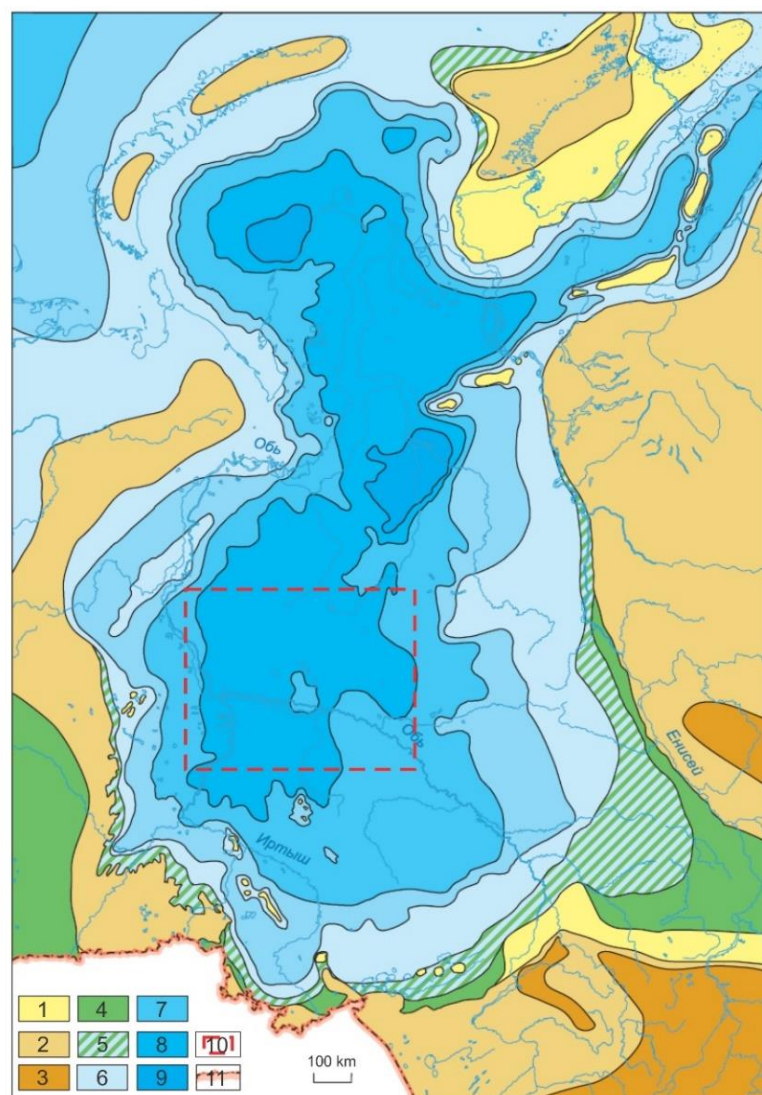


Figure 5.10.1. Paleogeography of West Siberia in the Tithonian (Kontorovich et al., 2013)  
 Paleogeographic areas: Areas of continental deposition: (1) erosional-depositional plain; (2) elevated plain (erosional land); (3) low mountains; (4) low-lying depositional plain (channel, floodplain, and lacustrine facies). Transitional areas: (5) coastal plain, periodically inundated by the sea (floodplain, swampy-lacustrine, channel, deltaic, barrier bar, beach facies). Areas of marine deposition: (6) shallow sea, up to 25 m in depth; (7) shallow sea, up to 25–100 m in depth; (8) deep sea, 200–400 m in depth; (9) deep sea with depths exceeding 400 m. (10) studied area; (11) state border

In any case, the sedimentation of algal matter on the bottom of the sea basin, judging by the relatively small thickness of the alginite-rich layers, is an instantaneous event on the scale of geological time and represents an algal bloom. As the concentration of nutrients decreases, the amount of algae in seawater decreases, and their material begins to mix with other producers and siliceous sediment in the bottom nepheloid water layer. Therefore, the lower contacts of the alginite layers are sharp, with signs of microdiscontinuities, while the upper ones often have gradation layering.

### 5.11 Summary

Alginite-rich layers contain oil-prone type I kerogen and have much better hydrocarbon generation potential than host rocks. Alginite-rich layers are categorized from thermally immature (PC3) to early to middle mature (MC1-2), despite high  $T_{max}$  (up to 454 °C). The maceral composition is dominated by alginite. According to FTIR spectroscopy data, the aliphatic bonds of type I kerogen are greater than type II kerogen. The distribution spectrum of  $E_a$  is very narrow and consist of sing  $E_a=53$  kcal/mol. Luminescence of the alginite-rich layers is decreased and disappeared with thermal maturation due to conversion of organic matter into more aromatics and less aliphatics.

Molecular parameters show that organic matter of the alginite-rich layers and the host rocks are characterized by similar values. Both alginite-rich layers and host rocks have been deposited under reducing marine environment ( $Pr/Ph < 1$ ;  $n-C_{27}/n-C_{17} < 1$ ; lower concentrations of  $C_{29}$  sterane and greater relative abundances of  $C_{27}$  and  $C_{28}$  steranes). Thermal maturation parameters indicate immature organic matter. The abundant of aliphatic compounds in the pyrolysis products of type I kerogen are in good agreement with the FTIR data and high H/C ratio, which demonstrate higher aliphatic compound.

The isotope composition of carbon in the kerogen of the alginite-rich layers and the host rocks is characterized by a similar values of  $\delta^{13}C_{org}$  from -30.5 to -32.2 ‰, which in range of marine organic matter of the Bazhenov Formation. The high C/N ratio and enrichment of  $^{15}N$  of the alginite-rich layers are associated with denitrification and/or  $NH_3$  volatilization. The relative higher values of  $\delta^{34}S_{tot}$  of the alginite-rich layers likely corresponds to their more oxidizing depositional environments compared to the host rocks.

The obtained data indicate algal bloom events during Upper Jurassic – Lower Cretaceous in the Bazhenov paleosea, which led to the formation of the alginite-rich layers. The required condition for the formation of the alginite-rich layers is the supply of nutrients from various sources.

## CHAPTER 6. MODELING OF THERMAL MATURATION AND HYDROCARBON GENERATION OF THE TYPE I KEROGEN

### 6.1 Artificial maturation in open system

The thermal evolution of OM, accompanied by the generation, migration and accumulation of hydrocarbons, is a long and important process in the geological history of the development of petroleum basins. Reconstruction of the stages of thermal transformation of kerogen in the oil window and determination of the maximum generation of hydrocarbons are necessary data both for basin modeling and forecasting of oil and gas potential and for selecting the most optimal methods for enhanced oil recovery. The ongoing studies of thermal effects on high-carbon rocks make it possible to move from experimental pyrolysis temperatures to reservoir ones.

The most representative samples of the Bazhenov formation were taken as objects for modeling, characterized by thermally weakly transformed (PC3 stage) type II kerogen and type I kerogen (Table 6.1.1). The calculated kinetic spectra of the samples before thermal exposure are presented in Figure 6.1.1.

Table 6.1.1. Rock-Eval pyrolysis data for initial samples

| Sample | Type                  | S0+S1,<br>mg HC/g<br>rock | S2,<br>mg HC/g<br>rock | TOC,<br>wt. % | T <sub>max</sub> ,<br>°C | HI,<br>mg HC/g<br>TOC | K <sub>goc</sub> ,<br>% | CC,<br>wt.<br>% | Type of<br>kerogen |
|--------|-----------------------|---------------------------|------------------------|---------------|--------------------------|-----------------------|-------------------------|-----------------|--------------------|
| SE12   | Organic-rich silicite | 7.33                      | 69.32                  | 10.38         | 428                      | 658                   | 62                      | 3.01            | II                 |
| M184   | Alginite-rich layer   | 0.86                      | 306.69                 | 29.09         | 454                      | 1054                  | 90                      | 0.48            | I                  |

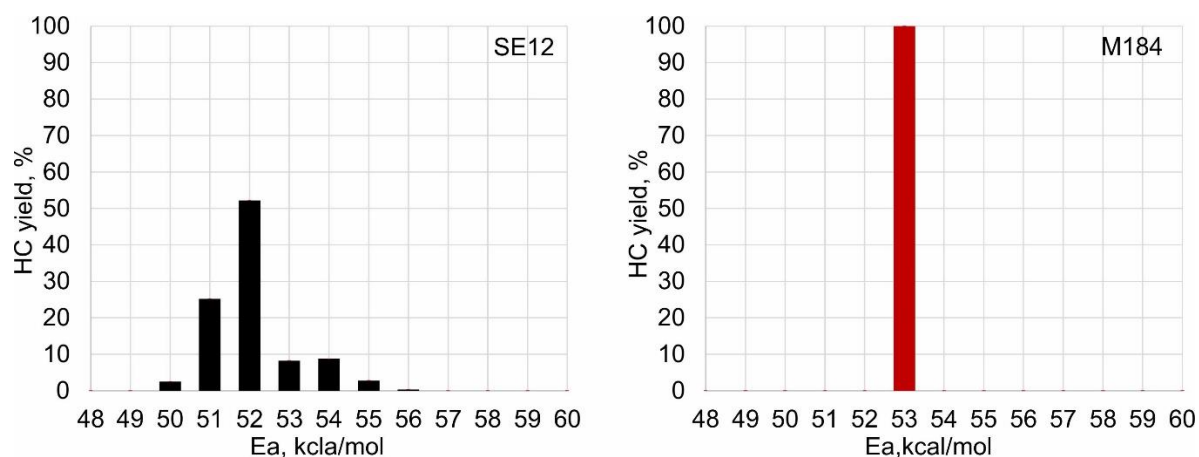


Figure 6.1.1. The distribution of Ea for studied initial samples.  
For all spectra, the frequency factor  $A=1 \times 10^{14} \text{ s}^{-1}$

These samples were subjected to temperature exposure (300-450 °C) in an open system for 30 minutes in an inert helium atmosphere with a step-by-step determination of pyrolysis characteristics and kinetic parameters. The results of the experiments are presented in Table 6.1.2.

Table 6.1.2. Rock-Eval pyrolysis data for matured samples in open system

| Sample | T, °C | S <sub>2</sub> ,<br>mg HC/g rock | TOC,<br>wt. % | T <sub>max</sub> ,<br>°C | HI,<br>mg HC/g TOC | K <sub>goc</sub> ,<br>% | TR*,<br>% |
|--------|-------|----------------------------------|---------------|--------------------------|--------------------|-------------------------|-----------|
| SE12   | 300   | 63.5                             | 9.82          | 428                      | 646                | 58                      | 6.6       |
|        | 325   | 61.21                            | 9.74          | 430                      | 628                | 54                      | 12.2      |
|        | 350   | 58.15                            | 9.40          | 431                      | 618                | 54                      | 13.6      |
|        | 375   | 47.36                            | 8.56          | 433                      | 553                | 48                      | 22.7      |
|        | 400   | 26.02                            | 6.36          | 437                      | 409                | 36                      | 42.8      |
|        | 425   | 6.39                             | 5.71          | 450                      | 111                | 11                      | 84.5      |
|        | 450   | 1.34                             | 4.93          | 471                      | 27                 | 4                       | 96.2      |
| M184   | 300   | 306.20                           | 29.57         | 454                      | 1035               | 88                      | 5.9       |
|        | 325   | 297.35                           | 28.76         | 451                      | 1034               | 88                      | 6.0       |
|        | 350   | 295.83                           | 28.67         | 454                      | 1032               | 88                      | 6.2       |
|        | 375   | 255.65                           | 25.52         | 452                      | 1001               | 85                      | 9.0       |
|        | 400   | 199.83                           | 21.85         | 449                      | 914                | 78                      | 16.9      |
|        | 425   | 41.34                            | 8.67          | 447                      | 476                | 41                      | 56.7      |
|        | 450   | 0.76                             | 5.15          | 527                      | 14                 | 3                       | 98.7      |

\*TR- transformation ratio,  $TR = (HI_0 - HI) / HI_0 \times 100\%$  [Jarvie D.M., 2012].  $HI_0$  for the SE12 is 715 mg HC/g TOC, for M184 is 1100 mg HC/g TOC

The results indicate a decrease in the generation potential of the OM with an increase in the exposure temperature. In the SE12 sample, containing type II kerogen, there are practically no significant changes up to an exposure temperature of 350 °C, and after heating at a temperature of 375-400 °C, a sharp jump in the change pyrolysis parameters is noted. The HI values are reduced by 30-60%, and K<sub>goc</sub> is reduced by an average of 20-50% (Figure 6.1.2). When the sample heated to 400-450 °C, kerogen is characterized by almost complete depletion of the oil generation potential (TR=96.2%).

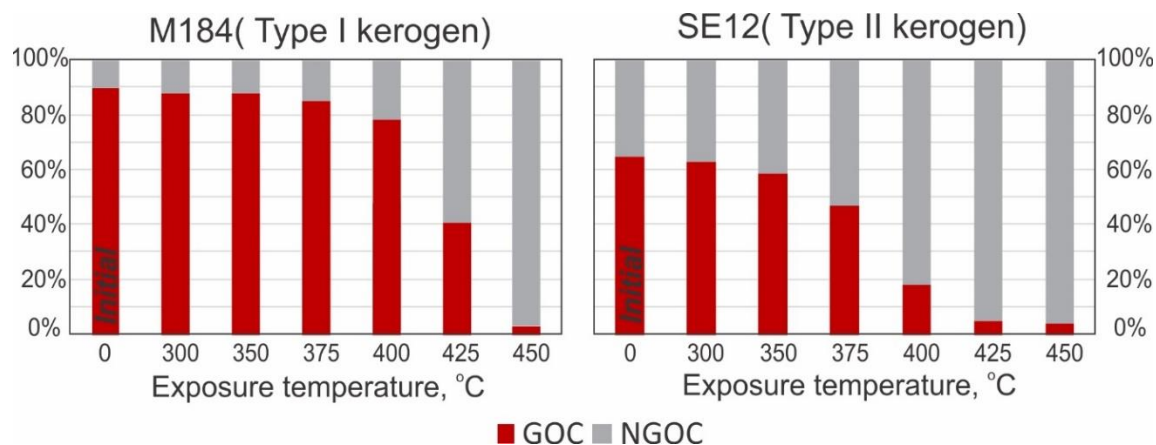


Figure 6.1.2. Change in the ratio of GOC and NGOC during artificial maturation

For sample M184, containing type I kerogen, the generation potential values are initially significantly higher than for the sample SE12. As the pyrolytic parameters for type II kerogen decrease significantly with increasing thermal exposure to 375-400 °C, type I kerogen still retains its high oil generation potential (Table 6.1.2; Figure 6.1.2). At an exposure temperature of 300–400 °C, the HI values decrease only to 13%. Only when exposed to a temperature of 425–450 °C, the generation potential is significantly depleted (TR=98.7%).

Based on the nature of the behavior of the line of change in HI and  $T_{max}$ , we can confidently say that the simulation performed well reproduces the geological process of thermal maturation of OM, both type II and type I kerogen (Figure 6.1.3). The differences in the initial  $T_{max}$  of kerogens for complete transformation give rise to a different maturation path.

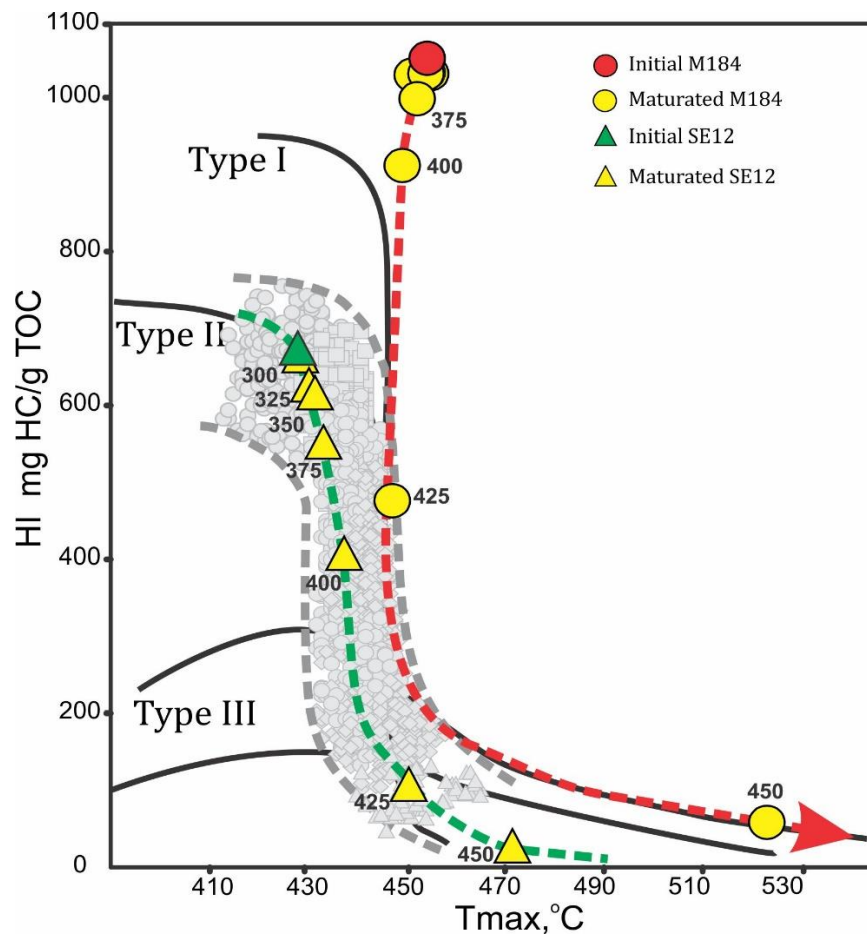


Figure 6.1.3. The HI- $T_{max}$  plot for the initial and matured samples

The obtained value points for a type II kerogen sample after thermal exposure do not go beyond the maturation pathway determined from the HI- $T_{max}$  plot for samples of the Bazhenov Formation of various degrees of maturity. Type I kerogen after thermal exposure also falls on the line characterizing thermal maturation.

The conducted kinetic studies show the nature of the change in the shape of the activation energy distribution spectrum at each stage of thermal exposure (Figure 6.1.4).

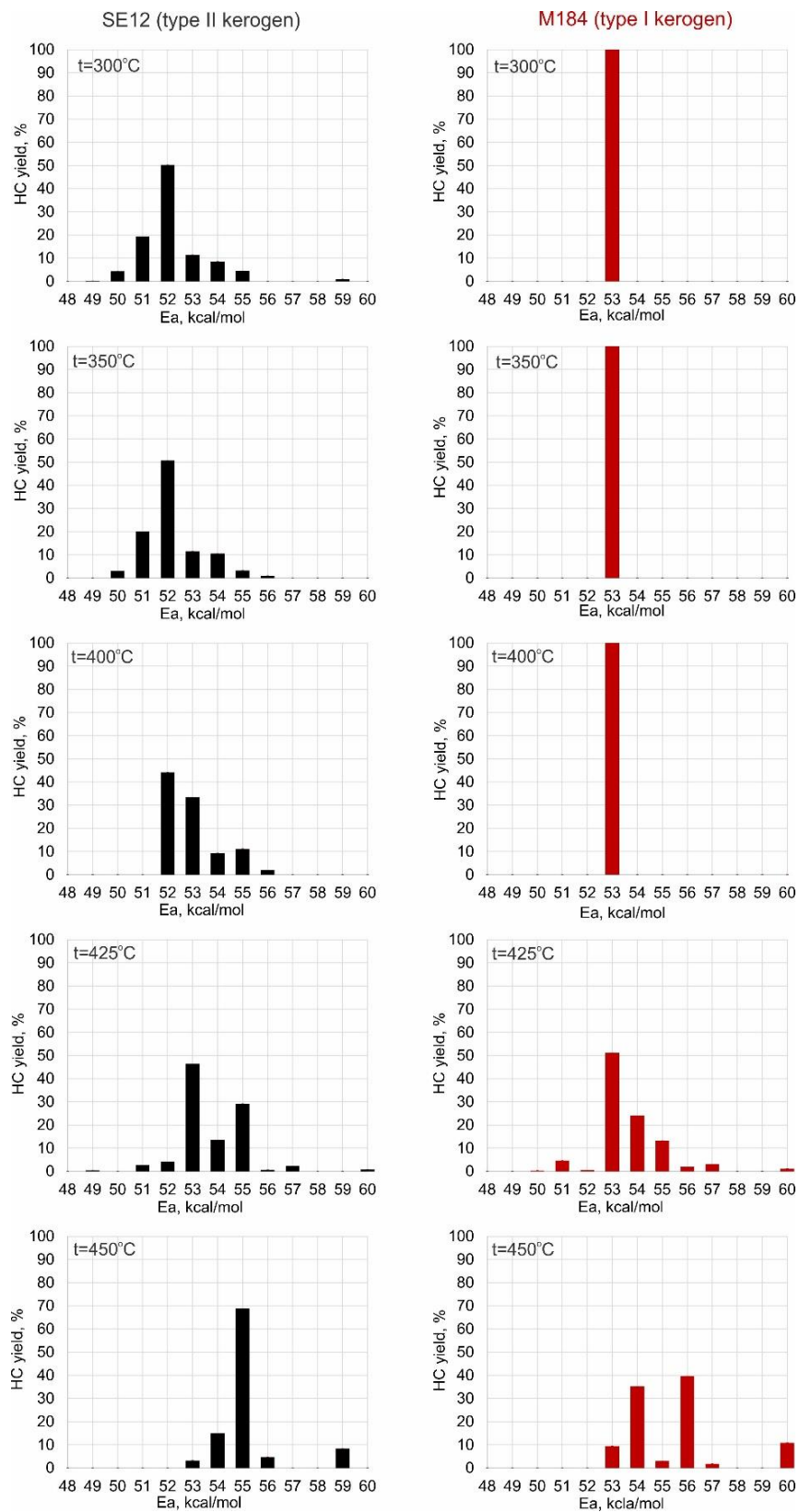


Figure 6.1.4. The Ea distribution for matured samples in open system. For all spectra, the frequency factor  $A=1 \times 10^{14} \text{ s}^{-1}$ .

An increase in the exposure temperature is gradually reflected in the shape of the spectra of type II kerogen. Up to a temperature of 350 °C, the kinetic spectra practically do not undergo significant changes. When exposed to temperatures from 375-400 °C, the hydrocarbon yield almost completely disappears at energies of 50-51 kcal/mol, and the spectrum maximum shifts towards higher energies. Apparently, this is due to the fact that, as the stage of catagenesis increases, the realization of the generation potential begins with reactions with low activation energies. For type I kerogen, the change in the kinetic spectrum begins only after exposure to a temperature of 425-450 °C – there is a "decay" of the primary narrow spectrum and an increase in the interval of activation energies.

The presence of alginite-rich layers containing type I kerogen in the rocks of the Bazhenov formation significantly increases the oil generation potential of the entire stratum. When type II kerogen exhausts its oil generation potential at high thermal maturity levels, type I kerogen still retains it and at later stages begins to actively generate light hydrocarbons due to its high aliphaticity. Thus, the compositional kinetic spectrum of type I kerogen showed that, as a result of thermal destruction, the generation products are predominantly normal alkanes of the composition C<sub>7</sub>-C<sub>15</sub> (Figure 6.1.5). Thus, the OM of alginite layers, upon reaching its oil window, will be a source of high-quality light oils.

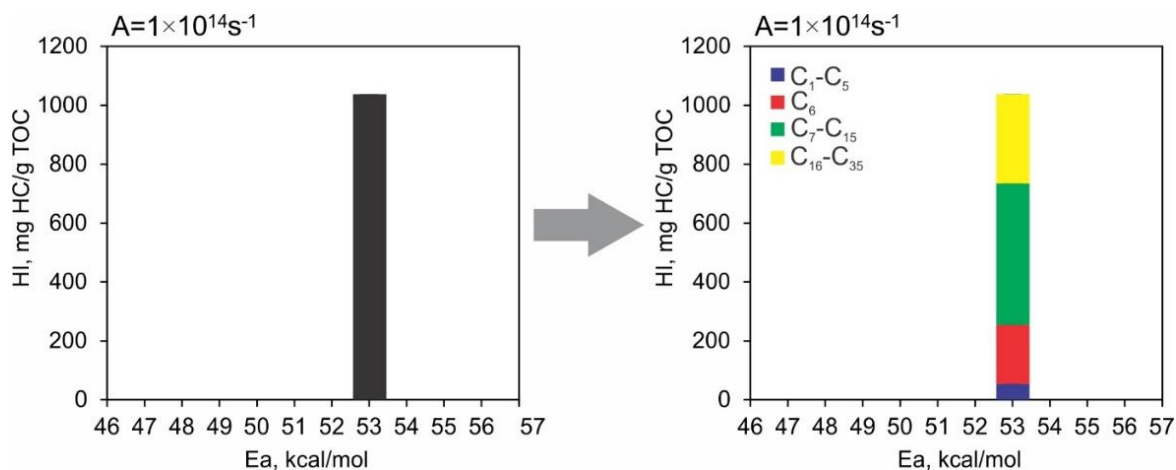


Figure 6.1.5. The bulk and compositional kinetic spectra of the type I kerogen in the Bazhenov Formation

Kerogens having different kinetics will respond differently to a given thermal history [Tissot B.P., Welte D.H., 1984]. In other words, different types of organic matter require different burial and thermal conditions to reach the onset of petroleum generation due to the wide spectrum of  $E_a$  from (48 to 60 kcal/mol). All basin-modelling software programs (PetroMod, BasinMod and others) supply a basic set of at least three default kerogen types with their appropriate  $E_a$

distributions for the chemical kinetics [Burnham A.K., 2017; Galushkin Y.I., 2007]. Type I kerogen have the highest  $E_a$  and narrow distribution, while type II have lower  $E_a$  and wider spectrum. Ideally, however, the kinetics parameters of the particular interest should always be used.

## 6.2 The amount of generated hydrocarbons

The obtained data on the thermal maturation of kerogens gives a qualitative assessment of generated hydrocarbons but does not provide reliable information about their amount. To determine the amount of hydrocarbons generated by kerogens, it is necessary to know their initial characteristics.

In (Magoon and Dow, 1994) it is proposed to determine, the total mass of generated hydrocarbons (HGG, t HC) will be calculated by the equation:

$$HGG = \frac{TOC}{100} \times \rho \times S \times h \times (HI_0 - HI) \times 10^{-3}$$

To determine the mass of organic carbon (M, kg TOC), contained in the source rock unit, it is proposed to calculate by the equation:

$$M = \frac{TOC}{100} \times \rho \times S \times h, \text{ where}$$

TOC – average organic carbon content (wt. %) is divided by 100 to convert from percent abundance to fractional abundance;  $\rho$  – average density, t/m<sup>3</sup>; S – square of the unit, m<sup>2</sup>; h – thickness of the unit, m.

Since the consumption of TOC in the process of maturation is quite high for sapropel OM, the initial TOC (TOC<sub>0</sub>) is used in the equation. The TOC<sub>0</sub> for sample SE12 was calculated based on (Jarvie, 2012). For sample M184, TOC<sub>0</sub> was used relatively higher, due to resistance of type I kerogen on the early stages of catagenesis.

The mass of hydrocarbons (R, kg HC/t rock) generated per gram TOC is expressed through the equation:

$$R = HI_0 - HI, \text{ where}$$

HI<sub>0</sub>, HI – initial and present-day values of hydrogen index, respectively, kg HC/t TOC.

The value of HI<sub>0</sub> is established based on the Rock-Eval pyrolysis data of many samples from the Bazhenov Formation, characterized by immature organic matter. It is also worth considering the facies variability of the Bazhenov horizon since for the Golchikhinskaya, Yanovstanskaya, and Maryanovskaya Formations HI<sub>0</sub> values will be lower than for the Bazhenov

Formation from central part of the Western Siberia (Goncharov et al., 2021). Approximating the obtained Rock-Eval pyrolysis data to the minimum level of catagenetic transformation of OM, it can be established with sufficient confidence that for the studied samples of the Bazhenov rocks (type II kerogen), the initial values of  $HI_0$  is about 715 kg HC/t rock. For the alginite-rich layers,  $HI_0$  approximately is 1100 kg HC/t rock. The average density is 2.5 t/m<sup>3</sup>.

Thus, the total mass of generated hydrocarbons (HGG, t HC) will be calculated by the equation:

$$HGG = \frac{TOC_0}{100} \times \rho \times S \times h \times (HI_0 - HI) \times 10^{-3}$$

In the present day, both the alginite-rich layer and host rocks have generated a small amount of hydrocarbons. The maximum amount of generated hydrocarbons by the alginite-rich layers per 1 m<sup>3</sup> can be up to 0.790 tones of hydrocarbons, while for the Bazhenov rocks can be 0.179 tones (Table 6.2.1).

Table 6.2.1. Estimation of the total mass of generated hydrocarbons

| Sample                          | Type of kerogen | TOC, wt. % | TOC <sub>0</sub> , wt. % | HI, kg HC/t TOC | HI <sub>0</sub> , kg HC/t TOC | HGG, t HC |
|---------------------------------|-----------------|------------|--------------------------|-----------------|-------------------------------|-----------|
| <i>TR ~ 6.0 % (present day)</i> |                 |            |                          |                 |                               |           |
| SE12                            | II              | 10.38      | 11.60                    | 658             | 715                           | 0.016     |
| M184                            | I               | 29.09      | 29.10                    | 1054            | 1100                          | 0.033     |
| <i>TR &gt; 96.0 %</i>           |                 |            |                          |                 |                               |           |
| SE12                            | II              | 4.93       | 11.6                     | 27              | 715                           | 0.179     |
| M184                            | I               | 5.15       | 29.1                     | 14              | 1100                          | 0.790     |

### 6.3 Summary

Artificial maturation of type I kerogen was performed under isothermal open system in the temperature range from 300 to 450 °C with time of 30 min. Results show that active hydrocarbon generation stage start from exposure temperature of 425 °C, while for type II kerogen its start from 375-400 °C. These differences are observed due to different kinetics. Type I kerogen with different generation kinetics result in non-synchronous timing of onset of the petroleum generation. According to compositional kinetics, type I kerogen in the Bazhenov Formation generate mostly light hydrocarbons starting from high thermal maturity levels (from MC2 and above), while type II kerogen by this time has exhausted its generation potential by half.

Calculations showed that the amount of generated hydrocarbons by type I kerogen in the alginite-rich layers can exceeds the amount of generated hydrocarbons by type II kerogen in the Bazhenov rocks. However, the total thickness of the alginite-rich layers usually do not exceeds 1-5% from the whole cross-section of the Bazhenov Formation. But if the thickness of the alginite-rich layers somewhere is over 1-2 meters, then they can generate oil in enormous amounts.

## CONCLUSIONS

In the present study, type I kerogen was discovered in the specific luminescent layers within the Bazhenov sequence contains predominantly type II kerogen. Due to the abundance of alginite (40–50 vol.%) in composition, we called these layers “alginite-rich layers”. A number of advanced methods and techniques were used to determine their distinguishing characteristics.

Alginite-rich layers were identified in 27 wells out of 60 examined and located in the central part of the West Siberian Petroleum Basin. The layers were sampled based on their bright yellow and orange luminescence under UV light and visual lithological features. The alginite-rich layers are situated in the Member 4 of the Upper part of the Bazhenov Formation. The thicknesses of the individual alginite-rich layers vary from 1 to 50 mm, and the total thickness is up to 1 m in the cross-section.

Integrated lithological and geochemical methods showed the differences between the alginite-rich layers and surrounding host rocks.

Based on XRD data, thin section petrographical description and SEM analysis, the alginite-rich layers composed mostly of organic matter and quartz grains. Inorganic chemical composition revealed that the alginite-rich layers are characterized by relatively low total REE (9.6–93.4 ppm) compared to the total REE abundance of the host rocks (74.3–186.8 ppm).

According to Rock-Eval pyrolysis and elemental analysis, the alginite-rich layers are characterized by exceptionally high initial hydrogen index ( $HI_0$  up to 1100 mg HC/g TOC) and H/C ratio (up to 1.88) typical for type I kerogen. The high  $K_{goc}$  (up to 90 %) and  $T_{max}$  (higher by 6–14 °C) are also distinguish the alginite-rich layers from host rocks. The high hydrogen concentrations are in good accordance with FTIR spectroscopy data indicating the highly aliphatic structure of the kerogen. Type I kerogen of the alginite-rich layers shows narrow energies distribution with dominant  $E_a$  of 53 kcal/mol according to kinetic analysis. Pyrolysis products suggest generation of light crude oils with predominance of normal alkanes  $C_7$ – $C_{15}$ . The  $\delta^{15}N$  values (5.9–25.7‰) and C/N ratio (76.8–193.4) of the alginite-rich layers are exceptionally high compared to the host rocks.

The enrichment of deposits with type I kerogen is due to the high bioproductivity of the basins. The formation of such sediments occurred in various territories and under various sedimentary facies conditions, including marine basins, large lakes and swamps, under certain conditions due to the accumulation of high-lipid organic matter. An important condition for the formation of such sediments is the additional supply of a large number of nutrients to the sedimentation basin from various sources.

The obtained data indicate algal bloom events during Upper Jurassic – Lower Cretaceous in the Bazhenov paleosea, which led to the formation of the alginite-rich layers. The required condition for the formation of the alginite-rich layers is the supply of nutrients from sources, including aeolian transport, volcanic eruptions or marine transgression. Based on geochemical parameters ( $\text{Pr/Ph} < 1$  and relatively high  $\delta^{34}\text{S}_{\text{tot}}$  from  $-6.0$  to  $-18.5\%$ ), the alginite-rich layers were deposited in anoxic conditions but were more oxidizing compared to the host rocks. During the deposition, the lipid-rich organic matter had undergone extensive bacterial reworking in a reducing environment according to high  $\delta^{15}\text{N}$  values and low nitrogen content.

The wide distribution on the territory of the central part of Western Siberia (more than 0.5 million  $\text{km}^2$ ) allows using the alginite-rich layers as marker horizons for stratification of the Bazhenov sequence.

Luminescence of the alginite-rich layers can be used to confirm the thermal maturity parameters of Rock-Eval pyrolysis or biomarker analysis of the Bazhenov deposits from immature conditions (PC3) to the early to the middle mature stage (MC1-2). Generally, the luminescent colors of the alginite-rich layers change from a greenish-yellow color to a bright yellow and orange under UV light before luminescence is mostly extinguished at the middle oil window (MC2).

Since different types of kerogen require different burial and thermal conditions to reach the onset of petroleum generation, the type of kerogen and its kinetics parameters should always be used in basin modelling. Different generation kinetic of type I and type II kerogen lead to different stages of petroleum generation. The alginite-rich layers will generate more aliphatic crude oils during the peak of the oil window and above due to type I kerogen properties while the hydrocarbon generation potential of type II kerogen of the host rocks will be exhausted. Hence, the proportion of type I kerogen in the Bazhenov Formation may determine the source rock quality and provide valuable information related to the prediction of expelled fluid properties.

The present study provides new insight into the nature and depositional conditions of organic matter in the Bazhenov Formation. The comprehensive study of organic matter of the Bazhenov Formation is important for both paleoenvironmental studies and petroleum exploration.

#### *Recommendations for future work*

The Re-Os isotope analysis is proposed for direct age determination of the alginite-rich layers to confirm their isochronous behavior and for independent (from biostratigraphic methods) dating to choose the position of the Jurassic-Cretaceous boundary.

Artificial maturation in a closed system to clarify the kinetics and pyrolysis products of type I kerogen.

Of special interest is the compound-specific isotope analysis of n-alkanes of generated hydrocarbons from artificial maturation of the alginite-rich layers and the Bazhenov oils, which

can prove the contribution of the type I kerogen into the productivity in the late stage of the oil window.

Analysis of the Upper Jurassic – Lower Cretaceous source rocks to make inter-basinal and global correlations.

## REFERENCES

1. A.V. Van, Kazanskiy Y.P. Volcanoclastic material in sediments and sedimentary rocks. Novosibirsk: Nauka, 1985. 128 p.
2. Amon E.O. et al. Stratigraphy and paleogeography of the Mesozoic-Cenozoic Sedimentary Cover of the Shaim Oil and Gas Region (Western Siberia). Ekaterinburg: UGGU, 2010. 257 p.
3. Bazhenova O.K. Geology and geochemistry of oil and gas. Moscow: MSU, 2000. 384 p.
4. Behar F., Beaumont V., Penteado H.D.B. Rock-Eval 6 Technology: Performances and Developments. Oil Gas Sci. Technol. Rev. IFP 2001, 56, 111–134.
5. Bertrand P., Pittion J.S., Bernaud C. Fluorescence of sedimentary organic matter in relation to its chemical composition // Org. Geochem. 1986. Vol. 10. No 1–3. pp. 641–647.
6. Birdwell J.E. et al. Geological, geochemical, and reservoir characterization of the Uteland Butte Member of the Green River Formation, Uinta Basin, Utah // Hydrocarbon source rocks Unconv. Play. Rocky Mt. Reg. 2016. pp. 352–378.
7. Bradley W.H. Origin and microfossils of the oil shale of the Green River formation of Colorado and Utah // Geol. Surv. 1931. Vol. 168. pp. 1–91.
8. Bulatov T.D. et al. Tuffaceous interlayers in the deposits of the Bazhenov formation in the central part of Western Siberia // XXI scientific-practical conference “Ways to realize the oil and gas potential of Khanty-Mansiyski Autonomous Okrug – Yugra”. Khanty-Mansiysk: IzdatNaukServis, 2017. pp. 189–198.
9. Burnham A.K. Global Chemical Kinetics of Fossil Fuels. 2017. 315 p.
10. Collister J.W. et al. Partial resolution of sources of n-alkanes in the saline portion of the Parachute Creek Member, Green River Formation (Piceance Creek Basin, Colorado) // Org. Geochem. 1994. Vol. 21. No 6–7. pp. 645–659.
11. Dembicki H. Three common source rock evaluation errors made by geologists during prospect or play appraisals // Am. Assoc. Pet. Geol. Bull. 2009. Vol. 93. No 3. pp. 341–356.
12. Drits A. V. et al. Does Zooplankton Control Phytoplankton Development in White Sea Coastal Waters in Spring? // Oceanology. 2018. T. 58. № 4. pp. 558–572.
13. Foster C.B., Wicander R., Reed J.D. Gloeocapsomorpha prisca Zalessky, 1917: A new study part II: Origin of Kukersite, a new interpretation // Geobios. 1990. Vol. 23. No 2. pp. 133–140.
14. French K.L., Birdwell J.E., Berg M.D. Vanden. Biomarker similarities between the saline lacustrine Eocene Green River and the Paleoproterozoic Barney Creek Formations // Geochim. Cosmochim. Acta. 2020. Vol. 274. pp. 228–245.

15. Fuhrmann A. et al. Organic facies, depositional environment and petroleum generating characteristics of the lacustrine Shahejie Formation, ES4 member, Western Depression, Liaohe Basin (NE China) // *J. Pet. Geol.* 2004. Vol. 27. No 1. pp. 27–46.
16. Fujimura R. et al. Analysis of early bacterial communities on volcanic deposits on the island of Miyake (Miyake-jima), Japan: A 6-year study at a fixed site // *Microbes Environ.* 2011. Vol. 27. No 1. pp. 19–29.
17. Galimov E. M. *Geochemistry of stable carbon isotopes.* Moscow: Nedra, 1968. 226 p.
18. Galushkin Y.I. *Sedimentary basins modelling and assessment their oil-gas generation.* Moscow: Scientific World, 2007. 456 p.
19. Gerschel H. et al. Lignite oxidation under the influence of glacially derived groundwater: The pyropissite deposits of Zeitz-Weißenfels (Germany) // *Int. J. Coal Geol.* 2018. Vol. 189. pp. 50–67.
20. Goncharov I.V. *Geochemistry of oils in Western Siberia.* Moscow: Nedra, 1987. 181 p.
21. Goncharov I.V. et al. Types of organic matter and catagenesis of the Bazhenov formation and its same-aged analogues // *Neft. Khozyaystvo - Oil Ind.* 2016. Vol. 10. pp. 20–25.
22. Goncharov I.V. et al. Petroleum generation and migration in the southern Tyumen region, Western Siberia Basin, Russia // *Org. Geochem.* 2021. Vol. 152. pp. 104178.
23. Gonzales-Vila F.J. Alkane biomarkers. Geochemical significance and application in oil shale geochemistry // *Compos. Geochemistry Convers. Oil Shales.* 1995. pp. 51–68.
24. Hackley P.C., Cardott B.J. Application of organic petrography in North American shale petroleum systems: A review // *Int. J. Coal Geol.* 2016. Vol. 163. pp. 8–51.
25. He W. et al. Organic geochemical characteristics of the Upper Cretaceous Qingshankou formation oil shales in the Fuyu oilfield, Songliao Basin, China: Implications for oil-generation potential and depositional environment // *Energies.* 2019. Vol. 12. No 24.
26. Holba A. G. et al. Application of tetracyclic polyprenoids as indicators of input from fresh-brackish water environments // *Org. Geochem.* 2003. Vol. 34. No 3. pp. 441–469.
27. Horsfield B. Practical criteria for classifying kerogens: Some observations from pyrolysis-gas chromatography // *Geochim. Cosmochim. Acta.* 1989. Vol. 53. No 4. pp. 891–901.
28. Horsfield B. et al. Organic geochemistry of freshwater and alkaline lacustrine sediments in the Green River Formation of the Washakie Basin, Wyoming, U.S.A. // *Org. Geochem.* 1994. Vol. 22. No 3–5. pp. 415–440.
29. Huc A. Y. *Geochemistry of fossil fuels, from conventional to unconventional hydrocarbon systems.* TECHNIP, 2013. 254 p.

30. Jarvie D.M. Shale resource systems for oil and gas: Part 1—shale-gas resource systems // AAPG Mem. 2012. Vol. 97. pp. 69–87.
31. Kalkreuth W. et al. Fluorescence properties of alginite-rich oil shales from the Stellarton Basin, Canada // Fuel. 1990. Vol. 69. No 2. pp. 139–144.
32. Kalmykov A.G. et al. The effect of catagenetic maturity on the formation of reservoirs with organic porosity in the Bazhenov formation and peculiarities of their extension // Georesources. 2019. Vol. 21. No 2. pp. 159–171.
33. Karnyshina E.E. Siliceous rocks of the Bazhenov Formation of the Krasnoleninsky Arch (Western Siberia) // Moscow Univ. Geol. Bull. 2003. Vol. 6. pp. 19–27.
34. Khotylev O.V. et al. The model of accumulation radiolarite layers in the bazhenov formation of West Siberia // Moscow Univ. Geol. Bull. 2019. Vol. 1. pp. 2–7.
35. Kiipli E., Kiipli T. Nitrogen isotopes in kukersite and black shale implying ordovician-silurian seawater redox conditions // Oil Shale. 2013. Vol. 30. No 1. pp. 60–75.
36. Killips S.D., Killips V.J. Introduction to Organic Chemistry. : Blackwell Publishing, 2005. 393 p.
37. Kisilev E.A. Government report on the state and use of mineral and raw resources of the russian federation in 2019. Moscow: 2020. 494 p.
38. Kontorovich A. E. et al. Geology of oil and gas in Western Siberia. Moscow: Nedra, 1975. 680 p.
39. Kontorovich A.E. et al. Geochemistry and catagenetic transformation of kerogen from the Bazhenov horizon // Geokhimiya. 2019. Vol. 64. No 6. pp. 585–593.
40. Kontorovich E.A. et al. Jurassic paleogeography of the West Siberian sedimentary basin // Russ. Geol. Geophys. 2013. Vol. 54. No 8. pp. 747–779.
41. Kozlova E.V., Fadeeva N.P., Kalmykov G.A., Balushkina N.S., Pronina N.V., Poludetkina E.N., Kostenko O.V., Yurchenko A.Y., Borisov R.S., Bychkov A.Y. et al. Geochemical technique of organic matter research in deposits enrich in kerogen (the Bazhenov Formation, West Siberia). Mosc. Univ. Geol. Bull. 2015, 70, 409–418.
42. Lee R.F., Hagen W., Kattner G. Lipid storage in marine zooplankton // Mar. Ecol. Prog. Ser. 2006. Vol. 307. No 1863. pp. 273–306.
43. Leushina E., Mikhaylova P., Kozlova E., Polyakov V., Morozov N., Spasennykh M. The effect of organic matter maturity on kinetics and product distribution during kerogen thermal decomposition: the Bazhenov Formation case study // Journal of Petroleum Science and Engineering, 2021, Vol. 204.

44. Li S. et al. Geochemistry of petroleum systems in the Niuzhuang South Slope of Bohai Bay Basin: Part 3. Estimating hydrocarbon expulsion from the Shahejie formation // *Org. Geochem.* 2005. Vol. 36. No 4. pp. 497–510.
45. Liu Z. et al. Oil families and mixed oil of the North-Central West Siberian basin, Russia // *Am. Assoc. Pet. Geol. Bull.* 2016. Vol. 100. No 3. pp. 319–343.
46. Lopatin N.V., Emec T.P. Pyrolysis in oil and gas geochemistry. Moscow: Nauka, 1987. 144 p.
47. Magoon L.B., Dow W.G. The petroleum system: From source to trap: AAPG Memoir 60. Tulsa: The American Association of Petroleum Geologist, 1994. 639 p.
48. Martínez-Tarazona R.M., Martínez-Alonso A., Tascón J. M. D. Characterization of common lignite, xylitic lignite and pyropissite varieties of low-rank coals // *Fuel.* 1994. Vol. 73. No 11. pp. 1723–1728.
49. Mastalerz M. et al. Chemical and isotopic properties of kukersites from Iowa and Estonia // *Org. Geochem.* 2003. Vol. 34. No 10. pp. 1419–1427.
50. Maxwell J.R. Studies in Organic Geochemistry, 1967, Ph.D. Thesis, University of Glasgow.
51. Maende A., Weldon W.D. Pyrolysis and TOC Identification of Tight Oil Sweet Spots. In Proceedings of the Unconventional Resources Technology Conference, Denver, CO, USA, 12–14 August 2013, pp. 2573–2583.
52. Najdek M., Puskaric S., Bochdanský A.B. Contribution of zooplankton lipids to the flux of organic matter in the northern Adriatic Sea // *Mar. Ecol. Prog. Ser.* 1994. Vol. 111. No 3. pp. 241–250.
53. Oksenoyd E.E. et al. № 5, 2017 // *Oil Gas.* 2017. Vol. 5. pp. 34–43.
54. Orr W.L. Kerogen/asphaltene/sulfur relationships in sulfur-rich Monterey oils // *Org. Geochem.* 1986. T. 10. Vol 1–3. pp. 499–516.
55. Panchenko I.V. et al. Stratification and detailed correlation of the Bazhenov horizon in the central part of the Western Siberia according to lithological and paleontological core analysis and well logging // *Oil gas Geol.* 2016. Vol. 6. pp. 22–34.
56. Panchenko I.V. et al. Volcanic Tuffs and Tuffites at the Jurassic-Cretaceous Boundary Beds (Volgian–Ryazanian Stages) of Western Siberia // *Lithol. Miner. Resour.* 2021. No 2. pp. 144–183.
57. Pedentchouk N., Turich C. No Title // *Geol. Soc. London, Spec. Publ.* 2018. Vol. 468. No 1. pp. 105–125. 
58. Peters K. E., Walters C.C., Moldowan J.M. The biomarker guide. Volume 2. Cambridge: Cambridge University Press, 2005. 1156 c.

59. Pickel W. et al. Classification of liptinite – ICCP System 1994 // *Int. J. Coal Geol.* 2017. Vol. 169. pp. 40–61.
60. Quan T. M. и et al. Evaluating nitrogen isotopes as proxies for depositional environmental conditions in shales: Comparing Caney and Woodford Shales in the Arkoma Basin, Oklahoma // *Chem. Geol.* 2013. Vol. 360–361. pp. 231–240.
61. Revill A.T. et al. Hydrocarbon biomarkers, thermal maturity, and depositional setting of tasmanite oil shales from Tasmania, Australia // *Geochim. Cosmochim. Acta.* 1994. Vol. 58. No 18. pp. 3803–3822.
62. Rigby D., Batts B. D. The isotopic composition of nitrogen in Australian coals and oil shales // *Chem. Geol. Isot. Geosci. Sect.* 1986. Vol. 58. No 3. pp. 273–282.
63. Romankevich E.A. Geochemistry of organic matter in the ocean. Moscow: Nauka, 1977. 256 p.
64. Ryabenko E. Stable isotope methods for the study of the nitrogen cycle // *Top. Oceanography.* 2013. pp. 1–40.
65. Shaldybin M. V. et al. The nature, origin and significance of luminescent layers in the Bazhenov Shale Formation of West Siberia, Russia // *Mar. Pet. Geol.* 2019. Vol. 100. pp. 358–375.
66. Shpilman V.I., Zmanovsky N.I., Podsosova L.L. Tectonic map of the central part of the West Siberian Plate. Tyumen. 1998.
67. Simonei B.R.T. et al. Unusual carbon isotope compositions of biomarker hydrocarbons in a Permian tasmanite // *Geochim. Cosmochim. Acta.* 1993. Vol. 57. No 17. pp. 4205–4211.
68. Sinninghe Damste J.S. et al. Characterization of Tertiary Catalan lacustrine oil shales: Discovery of extremely organic sulphur-rich type I kerogens // *Geochim. Cosmochim. Acta.* 1993. Vol. 57. No 2. pp. 389–415.
69. Smith W. D. et al. Composition and depositional environment of major eastern Canadian oil shales // *Int. J. Coal Geol.* 1991. Vol. 19. No 1–4. pp. 385–438.
70. Spasennykh M. et al. Geochemical trends reflecting hydrocarbon generation, migration and accumulation in unconventional reservoirs based on pyrolysis data (On the example of the bazhenov formation) // *Geosciences.* 2021. Vol. 11. No 8.
71. Speight J. Origin and properties of oil shale. 2020. pp. 671–714.
72. Sýkorová I. et al. Classification of huminite - ICCP System 1994 // *Int. J. Coal Geol.* 2005. Vol. 62. No 1-2 SPEC. ISS. pp. 85–106.
73. Karamov T.I. et al. Maturation : study on the example of the Bazhenov Formation // 2021. pp. 1–2.

74. Taylor S.R., McLennan S.M. The Continental Crust: Its Composition and Evolution. 1985. 312 p.
75. Tissot B.P., Pelet R., Ungerer Ph. Thermal history of sedimentary basins, maturation indices, and kinetics of oil and gas generation // Am. Assoc. Pet. Geol. Bull. 1987. Vol. 71. No 12. pp. 1445–1466.
76. Tissot B.P., Welte D.H. Petroleum Formation and Occurrence. 1984. Springer. 700 p.
77. Tuite M. L., Williford K. H., Macko S. A. From greenhouse to icehouse: Nitrogen biogeochemistry of an Epeiric sea in the context of the oxygenation of the Late Devonian atmosphere/ocean system // Palaeogeogr. Palaeoclimatol. Palaeoecol. 2019. T. 531. pp. 1–13.
78. Tuttle M.L. Geochemical, Biochemical, and Sedimentological Studies of the Green River Formation, Wyoming, Utah, and Colorado. 1973.
79. Vassoevich N.B. Geochemistry of organic matter. Moscow: Nauka, 1986. 368 p.
80. Vtorushina E., Bulatov T., Kozlov I., Vtorushin M. The advanced technique for determination of pyrolysis parameters of rocks // Russian Oil and Gas Geology, 2018, No. 2, pp. 71–77.
81. Xie X. et al. Geochemical characteristics of expelled and residual oil from artificial thermal maturation of an Early Permian tasmanite shale, Australia // Energies. 2021. Vol. 14. No 21.
82. Zhang P. et al. Sequence stratigraphy and geochemistry of oil shale deposits in the upper cretaceous Qingshankou Formation of the Songliao Basin, NE China: Implications for the geological optimization of in situ oil shale conversion processing // Energies. 2020. Vol. 13. No 11.